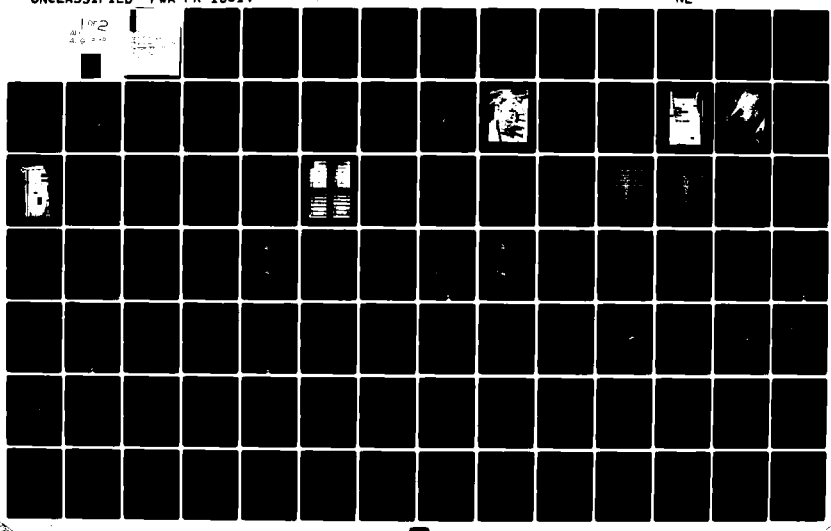


AD-A091 378 PRATT AND WHITNEY AIRCRAFT GROUP WEST PALM BEACH FL G--ETC F/G 20/4
SUPERCRITICAL AIRFOIL TECHNOLOGY PROGRAM WAKE EXPERIMENTS AND M--ETC(U)
SEP 80 D E HOBBS, J H WAGNER N00019-79-C-0229
UNCLASSIFIED NL PMA-FR-13514



AD A091028

SECTION III

WAKE EXPERIMENT

SELECTION OF AIRFOILS AND TEST CONFIGURATION

Detailed wake flow measurements were desired for a new fore-loaded supercritical design and a conventional aft-loaded multiple circular arc design. The supercritical airfoil design chosen was the fan exit guide vane mean section tested under a previous NASC contract (NASC N00019-77-C-0546). The conventional airfoil was a design which was later tested for a transonic wind tunnel investigation. These two airfoils were selected because they had been tested at the same chord Reynolds number.

UNCLASSIFIED

SECURITY CLASSIFICATION OF THIS PAGE (When Data Entered)

REPORT DOCUMENTATION PAGE		READ INSTRUCTIONS BEFORE COMPLETING FORM
1. Report Number	2. Govt Accession No.	3. Recipient's Catalog Number
4. Title (and Subtitle) SUPERCritical AIRFOIL TECHNOLOGY PROGRAM Wake Experiments and Modeling for Fore- and Aft-Loaded Compressor Cascades		5. Type of Report & Period Covered Final Report
6. Author(s)	7. Authors D. E. Hobbs A. H. Wagner J. F. Dannenhoffer R. P. Dring Joe	8. Performing Org. Report Number FR-13514
9. Performing Organization Name and Address United Technologies Corporation Pratt & Whitney Aircraft Group Government Products Division P.O. Box 2691, West Palm Beach, FL	10. Program Element, Project, Task Area & Work Unit Numbers 123	
11. Controlling Office Name and Address Department of the Navy Naval Air Systems Command Washington, D.C. 20361 ATTN: Code AIR-810, AIR-954	12. Report Date Sept 1980	
14. Monitoring Agency Name & Address (if different from Controlling Office)	13. Number of Pages 120	
	15. Security Class. (of this report) Unclassified	
	15a. Declassification/Downgrading Schedule	
16. Distribution Statement (of this Report) Approved for public release; distribution unlimited.		
17. Distribution Statement (of the abstract entered in Block 20, if different from Report)		
18. Supplementary Notes		
19. Key Words (Continue on reverse side if necessary and identify by block number) Shockless Airfoils, Supercritical Airfoil, Cascade Tunnel, Airfoil Design, Compressor, Turbulent Boundary Layer, Turbulent Wake, Vortex Shedding, Potential Flow		
20. Abstract (Continue on reverse side if necessary and identify by block number) Pratt & Whitney Aircraft has developed a procedure for designing supercritical cascade airfoils satisfying practical aerodynamic and structural requirements. The purpose of the research reported herein is to improve the calculation of flow turning and profile loss for these airfoils through the use of a model of the viscous wake. Wakes were measured in a large-scale, low-speed facility for two cascades. The first cascade configuration was a fore-loaded supercritical design; the second was a conventional aft-loaded design. The experimental results were used to analytically model the viscous wake in an inviscid potential flow calculation.		

ACKNOWLEDGEMENTS

The principal experimental investigator was Mr. Joel H. Wagner. Mr. John Horan provided many helpful suggestions in the design of the cascade test section and also assisted in the analytical wake modeling study. The authors are especially indebted to Miss Diane Rodimon for her programming skills and data reduction and to Mr. David Potash for the cascade construction and data acquisition.

Accession For	
NTIS GRA&I	<input checked="" type="checkbox"/>
DDC TAB	<input type="checkbox"/>
Unannounced	<input type="checkbox"/>
Justification	
By _____	
Distribution/	
Available Codes	
Dist.	Avail and/or special
A	

TABLE OF CONTENTS

<u>Section</u>	<u>Page</u>
I Introduction	1
General Background	1
Compressor Cascade Design System	1
II Design System Development	5
Prediction of Turning and Profile Loss	5
III Wake Experiment	9
Selection of Airfoils and Test Configuration	9
Test Facility	13
Instrumentation	16
Measurement Locations	20
Data Acquisition	23
Data Reduction	23
IV Experimental Results	25
Cascade Test Conditions	25
Two-Dimensionality and Periodicity	25
Upstream Uniformity	27
Low Speed-High Speed Flow Similarity	30
Far Wakes	30
Boundary Layers and Near Wakes	35
Turbulence and Wake Shedding Frequency	40
Wake Velocity Profile Similarity and Integral Parameters	44
V Analytical Wake Models	59
Wake Models	59
Profile Loss	61
Flow Turning	65
VI Conclusions	67
APPENDIX - Tables of Experimental Results	69
References	115
List of Symbols	117
Distribution List	119

LIST OF ILLUSTRATIONS

<u>Figure</u>		<u>Page</u>
1.	Supercritical Airfoil Aerodynamic Design Requirements	4
2.	Comparison of Test and Analytical Surface Mach Number Distribution	7
3.	Supercritical Fore-Loaded Cascade - Build I	10
4.	Standard Multiple Circular Arc Aft-Loaded Cascade - Build II	10
5.	Compressible Pressure Distribution for Builds I and II	12
6.	Large-Scale Cascade	14
7.	Large-Scale Cascade Test Section	15
8.	Schematic of Test Section	17
9.	Cascade Inlet	18
10.	Cascade Endwalls - Corner Slots and Slider Bars	19
11.	Traverse Probes	21
12.	Tuft Flow Visualization - Build I	26
13.	Tuft Flow Visualization - Build II	26
14.	Airfoil Surface Static Pressures - Builds I and II	28
15.	Kiel Total Pressure Results - Build I	31
16.	Kiel Total Pressure Results - Build II	32
17.	Five-Hole Total Pressure and Velocity Results - Build I	33
18.	Five-Hole Total Pressure and Velocity Results - Build II	34
19.	Boundary Layer Profiles - Build I	36
20.	Boundary Layer Profiles - Build II	37
21.	Boundary Layer and Near Wake Velocity Profile - Builds I and II	38
22.	Boundary Layer and Near Wake Hot-Film Velocity Deficit - Builds I and II	39

<u>Figure</u>	<u>Page</u>
23. Turbulence Intensity Profiles - Build I and II	41
24. Near Wake Hot-Film Local Turbulence Intensity - Builds I and II	43
25. Wake Nomenclature	45
26. Frequency Spectrum Profiles - Builds I and II	46
27. Universal Wake Profile (Five-Hole Probe Data) - Builds I and II	47
28. Universal Wake Profiles (Hot-Film Probe Data) - Builds I and II	49
29. Boundary Layer and Wake Integral Parameters - Builds I and II	53
30. Wake Location - Build I	57
31. Wake Location - Build II	58
32. Measured Data Wake Model and Pressure Distribution	60
33. Constructed Initial Wake Model and Pressure Distribution	62
34. Computed Displacement Thickness for Boundary Layer and Wake	63
35. Computed Momentum Thickness for Boundary Layer and Wake	63
36. Constructed Final Wake Model and Pressure Distribution	64

LIST OF TABLES

	<u>Page</u>
1. Cascade Geometry Test Conditions	11
2. Measurement Locations and Estimated Probe Placement Accuracies	22
3. Airfoil Surface Static Pressures - Builds I and II	29
4. Tabulation of Five-Hole Traverse Data - Build I	70
5. Tabulation of Kiel Traverse Data - Build I	74
6. Tabulation of Hot-Film Traverse Data - Build I	77
7. Tabulation of Five-Hole Traverse Data - Build II	90
8. Tabulation of Kiel Traverse Data - Build II	95
9. Tabulation of Hot-Film Traverse Data - Build II	98
10. Wake and Boundary Layer Integral Parameters - Build I	110
11. Wake and Boundary Layer Integral Parameters - Build II	112

SECTION I

INTRODUCTION

GENERAL

This report discusses the results of two compressor cascade airfoil wake experiments directed toward obtaining information necessary to model wakes in a compressor airfoil design system. The experiments include extensive measurements of the near and far wakes, trailing-edge boundary layers, and airfoil surface static pressures. The measured wake displacement surface and computed boundary layers were used in conjunction with a potential cascade flow solver to demonstrate the feasibility of modeling the viscous aspects of cascade flow. With this flow model and a generalized control volume mixing calculation, the computed uniform downstream flow angle and total pressure loss coefficient were shown to be consistent with the measurements downstream of the cascade.

BACKGROUND

Compressor Cascade Design Systems

Compressor airfoil sections of current production compressors and many advanced compressors are derived from related families of airfoils such as the NACA 65 series, the NACA 400 series, and the double circular arc series. Extensive plane cascade tests have been conducted on these families of cascade sections, and the performance of these cascades has been correlated as a function of their specific geometry, Mach number, and inlet air angle. The cascade correlations for exit air angle are formulated in terms of a "deviation angle" from some geometric reference angle such as the trailing-edge mean camber line angle. These correlations, modified to include actual compressor experience, are employed in current design systems that accurately predict the performance of compressors using standard series airfoil sections.

In the past 10 years, compressor cascade technology has advanced to the point where mathematically defined airfoils can be designed for given aerodynamic and structural requirements. These airfoils possess

optimum surface pressure distributions and boundary layer characteristics, and offer aerodynamic performance superior to the standard airfoil sections currently in use. One very important example of this type of designed airfoil is the "supercritical" cascade airfoil.

Supercritical airfoils are transonic airfoils which operate with subsonic inlet and exit flow velocities and with embedded regions of supersonic flow adjacent to the airfoil surface. The term "supercritical" refers to the presence of velocities in the flowfield which are above the "critical", or sonic speed. Historically, progress in the design methods for transonic airfoils severely lagged methods used to design fully subsonic or supersonic airfoils. The lag results primarily from mathematical difficulties in solving the inviscid flow equations which model the transonic flow field. Without the fundamental ability to compute the velocities on the airfoil surface, the well-developed, low-speed isolated airfoil design techniques employing boundary layer viscous flow theory have been of no practical value.

The early knowledge of airfoils in the transonic regime was derived from wind tunnel experiments on subsonic or supersonic designs. This type of experimentation provided an understanding that the aerodynamic deficiencies of these designs were caused by the strong normal shocks which terminated the embedded supersonic region. For isolated airfoils, this shock caused a rapid increase in drag and a reduction of lift as the approach Mach number increased through the high subsonic range. In cascades, this shock produced the analogous effects of increased total pressure loss and reduced flow turning. Typical features of this transonic flow field for a NACA 65 series cascade were shown in the schlieren photographs in the work of Dunavant et. al., (Reference 1).

In 1965, a resurgence of interest in developing improved supercritical design methods resulted from Whitcomb's now-famous supercritical isolated airfoil experiment at NASA Langley. Whitcomb's experimentally developed airfoil demonstrated the existence of shockless supercritical flowfields (Reference 2). The shockless feature made the flow entirely irrotational outside the boundary layer and wake and, thus, amenable to modeling with the potential equation.

Subsequently, Garabedian, Korn, and Bauer (References 3, 4, and 5) of New York University developed a complex hodograph solution satisfying the two-dimensional potential equation for supercritical flows over isolated airfoils. By using this hodograph technique, an isolated semi-infinite displacement body containing the airfoil, plus boundary layer and wake displacement thickness, could be determined from a specified shockless surface velocity distribution. The final airfoil design program, including viscous boundary layer considerations necessary to extract the airfoil shape from the displacement body, was delivered to NASA in 1974, and has been used to design airfoils for a variety of applications. In the same year, Korn (Reference 6) developed a similar shockless supercritical cascade airfoil design system. In a cooperative program with Pratt & Whitney Aircraft (P&WA), a supercritical cascade was designed in 1974 by Korn, and tested in 1976 in the transonic cascade facility of the Deutsche Forschung and Versuchsanstalt fur Luft und Raumfahrt (DFVLR) in Cologne, West Germany. The results of these tests, reported by Stephens (Reference 7), substantiated the performance improvements predicted for this newly designed cascade airfoil.

During 1976 and 1977, these test results provided the motivation for the development by P&WA of a new transonic cascade design procedure suitable for compressor application. This new design system incorporated a set of aerodynamic design point features for the airfoil surface Mach number distribution and boundary layer characteristics required to achieve efficient shockless cascade flow. A schematic of these features is shown in Figure 1. This new design system also reduced the cascade spacing restriction of the original Korn design method and introduced quasi three-dimensional effects necessary for compressor airfoil design. The new method permitted the selection of airfoil geometric characteristics which satisfied structural and foreign object damage resistance requirements. The design system was based on an analysis method developed by Ives and Liutermozza (References 8 and 9).

The advantages of a practical supercritical airfoil were then demonstrated experimentally in the DFVLR cascade facility under Naval Air Systems Command (NASC) Contract N00019-77-C-0546. These results are reported by Stephens and Hobbs (Reference 10). Based on these results

and further P&WA tests, an airfoil design system is currently under development which is intended to have general applicability beyond the range of available experimental results.

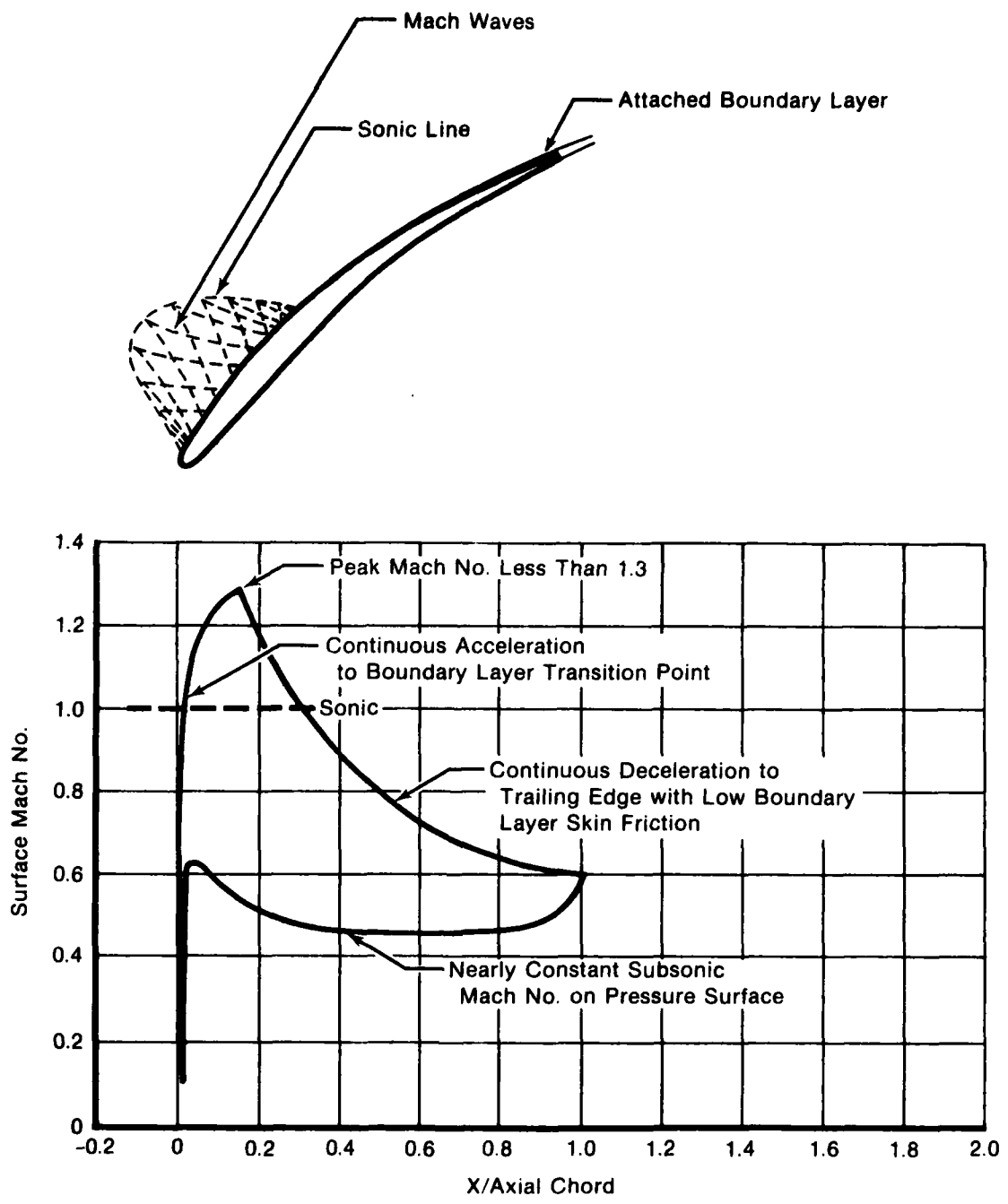


FIGURE 1
SUPERCRITICAL AIRFOIL AERODYNAMIC DESIGN REQUIREMENTS

FD 197984

SECTION II

DESIGN SYSTEM DEVELOPMENT

PREDICTION OF TURNING AND PROFILE LOSS

An accurate prediction of flow turning angle is necessary in compressor designs to ensure that the required rotor and stator pressure ratios are obtained, and that the optimum incidence is provided to the successive rows of airfoils. The supercritical airfoil data acquired to date have indicated that the turning angle and the profile total pressure loss of designed airfoil cascades are not predicted accurately by data correlations currently employed for standard airfoil series. This appears to be due to the attached boundary layer behavior which is a specific design requirement for these new airfoils. Also, because of the many geometric degrees of freedom, it is difficult to pursue a geometrically based cascade correlation to develop a deviation and loss system for designed airfoils. For designed airfoils, the correlation approach would require a large number of tests and become excessively expensive.

The approach to this design problem, which currently seems most cost effective and technically promising under the circumstances of attached boundary layers, is an analytical prediction which includes an accurate wake model and a control volume mixing calculation. The mixing calculation would be similar to the well-known method of Stewart (Reference 11), or would be generalized to use variable aerodynamic conditions on the airfoil trailing-edge boundary of the control volume. The choice of mixing calculations depends on the amount of flow nonuniformity in the cascade exit plane. The conditions would be taken from the inviscid analysis of the flow, coupled with adjustments for the viscous boundary layer and wake. The approach is similar to that proposed by Hansen, Serovy, and Sockol (Reference 12). The current problem with this approach centers on the modeling of wakes of relatively thick, blunt trailing edges of typical compressor airfoils.

Mathematical techniques for design and analysis are now available that closely model the aerodynamics of cascades, except in the immediate region of the thick, blunt trailing edge. In this region, current inviscid cascade flow calculations are inadequate, even with boundary

layer adjustments to the airfoil surface because they do not model the airfoil wake. The wake modeling deficiency presents two major problems, as discussed in the following paragraphs.

The first problem arises because surface velocity distribution cannot be computed accurately without accounting for viscous effects. When the wake is not modeled, a stagnation point not existing in the real viscous flow is computed on the airfoil surface at the trailing edge which affects the pressure distribution over the last 10 to 15 percent of the airfoil surface. The effect is shown in Figure 2 by comparing data with a calculation for the NASC supercritical airfoil from Reference 10. The methods currently used to correct these inaccuracies in the trailing edge flow are based on past experience with standard series airfoils. These methods lack the sound physical basis that would permit their general use for designed airfoils. Subsequently, if the velocity distribution is not corrected properly, errors in the calculated boundary layer may result, possibly masking separation prior to the trailing edge. Perhaps, more importantly, the errors in the trailing-edge region also make it difficult to apply a viscous trailing-edge condition to determine the downstream flow angle. A recent discussion of this problem is provided by Klein (Reference 13).

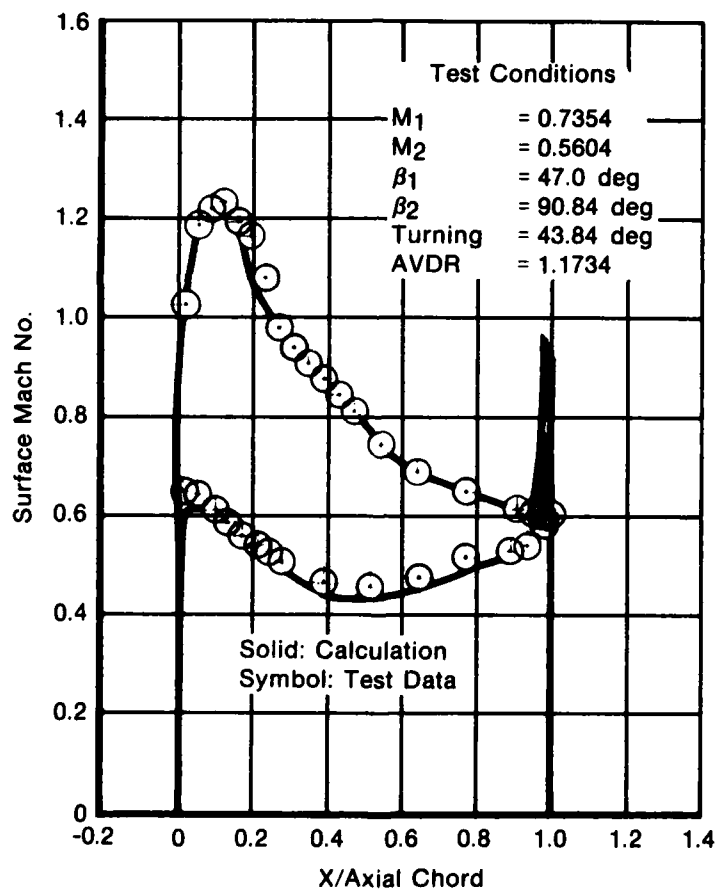
The second problem involves inaccuracies throughout the entire trailing-edge region. The large velocity variations at the airfoil trailing edge create an artificial disturbance which may propagate across the entire pitch. This leads to errors in the calculation of the downstream flow properties when wake mixing calculations are used.

Since a mixing calculation can be used for the accurate prediction of the far downstream cascade total pressure loss and gas angle for designed airfoils, the current approach is to provide the mixing calculation with the correct trailing-edge flow properties in the boundary layer and free stream. The problem can be solved through a physically based model of the cascade wake which can be used in conjunction with inviscid cascade and boundary layer calculations.

Unfortunately, very little detailed aerodynamic data exists to guide the development of such a wake model for cascades of airfoils with thick, blunt trailing edges. The present work is intended to fill this need and, hopefully, suggest the type of modeling which would be

adequate to achieve the design goal to predicting turning and loss. The goal of this experiment is to measure the wake flow of an airfoil operating in a periodic, two-dimensional cascade flow. Specifically, it is desired to determine the local time-mean velocities in the wake so that the trajectory of the wake centerline and wake parameters can be computed. To make use of this wake information in developing the design methods, the aerodynamic conditions far upstream and downstream of the cascade, static pressures on the airfoil surface, and the boundary layers at the airfoil trailing edge are also required.

The succeeding sections of this report discuss the cascade wake experiment and the application of the results to wake modeling.



FD 197995

FIGURE 2
COMPARISON OF TEST AND ANALYTICAL SURFACE MACH NO. DISTRIBUTION

SECTION III

WAKE EXPERIMENT

SELECTION OF AIRFOILS AND TEST CONFIGURATION

Detailed wake flow measurements were desired for a new fore-loaded supercritical design and a conventional aft-loaded multiple circular arc design. The supercritical airfoil design chosen was the fan exit guide vane mean section tested under a previous NASC contract (NASC N00019-77-C-0546). The conventional airfoil was a design which was later tested for comparison with the supercritical design. These two cascades are shown in Figures 3 and 4. Significant differences in these designs include the shape of the suction surface static pressure distributions, the thickness of the airfoil leading and trailing edges, and the pitch to chord ratio. The cascade geometry is listed in Table 1.

Required near and far wake flow measurements include velocities, pressures, turbulence levels, and flow angles. To achieve acceptable measurement accuracy near the airfoil trailing edge with reasonably reliable probes, a large-scale, low-speed experiment was required. The scale-speed combination was chosen to retain dynamic similitude in the wake by holding the airfoil chord Reynolds number within the correct range. Also, to achieve the desired high-speed static pressure coefficient distribution shape on the airfoil surface at a low Mach number, the upstream flow angle of the airfoil was altered so that the cascades operated at -5° incidence, relative to the original high-speed design conditions. The resulting distributions are shown in Figure 5. Both of the airfoils tested in this experiment have undergone extensive high-speed testing in the DFVLR transonic cascade tunnel. The results of these experiments show no significant change in cascade performance with inlet Mach numbers below a value of 0.70, except near the cascade choking condition at -10° of incidence.

Another important consideration in the design of this experiment was the requirement for a two-dimensional flow. This was achieved by measuring on the cascade centerline and controlling the endwall boundary layer flows sufficiently to achieve an overall midspan axial velocity-density ratio near 1.0. Reducing the axial velocity ratio from the design value of 1.15 to 1.0 increased the cascade loading

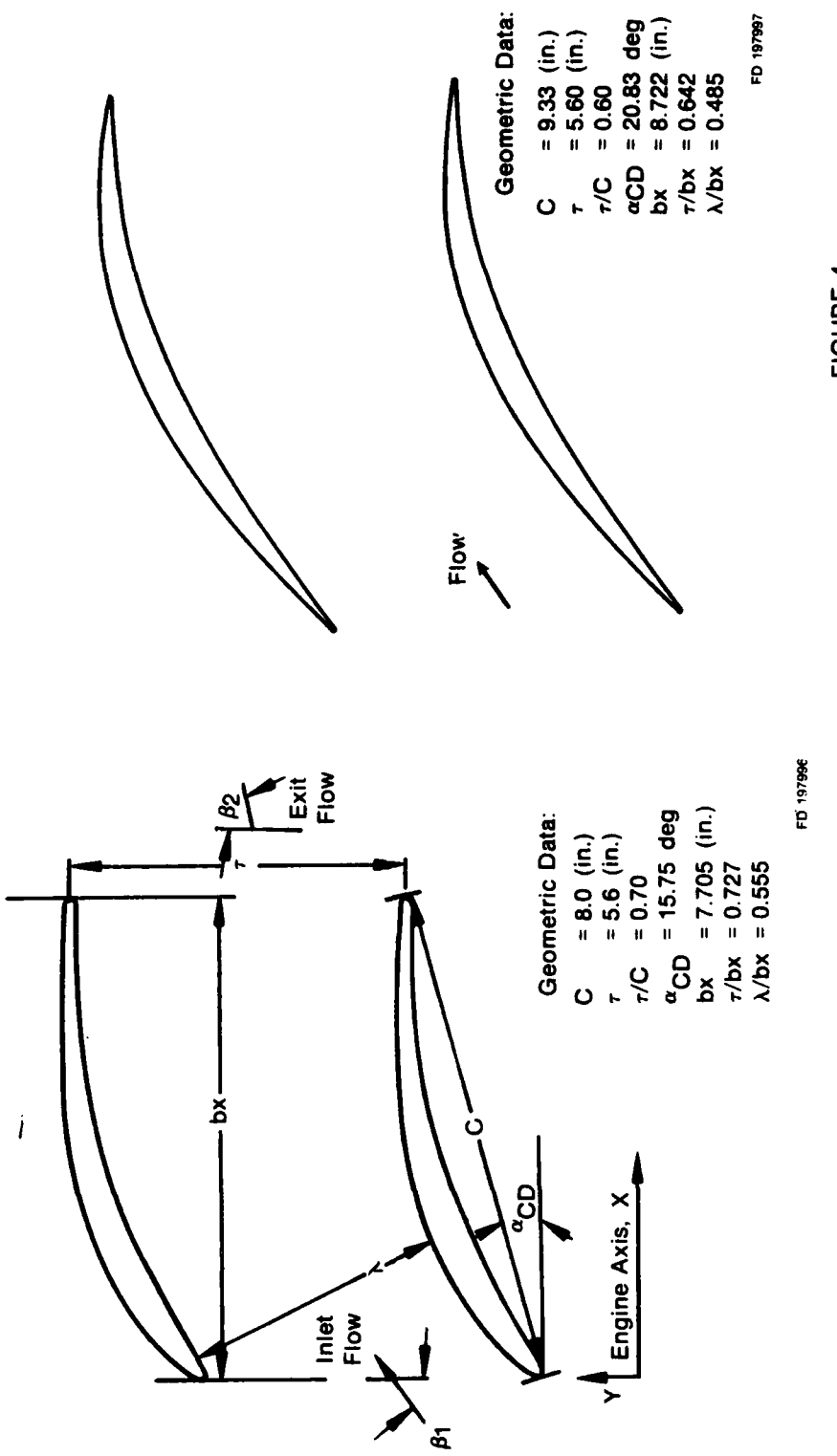


FIGURE 4
STANDARD MULTIPLE CIRCULAR ARC AFT -
LOADED CASCADE - BUILD II

FIGURE 3
SUPERCritical FORE-LOADED CASCADE - BUILD I

TABLE I. CASCADE GEOMETRY AND TEST CONDITIONS

<u>Cascade Geometry</u>	<u>Build I</u>	<u>Build II</u>
Pitch/Chord	0.70	0.60
Aspect Ratio (Span/Chord)	1.525	1.307
Pitch	142.24mm (5.600 inches)	142.24mm (5.600 inches)
Axial Chord	195.58mm (7.700 inches)	221.64mm (8.726 inches)
Chord	203.20mm (8.000 inches)	237.11mm (9.335 inches)
Trailing edge diameter	3.6068mm (0.142 inches)	1.3208mm (0.052 inches)
<u>Test Conditions</u>	<u>Build I</u>	<u>Build II</u>
Inlet Flow Angle (degrees from tangential)	52	50.5
Exit Flow Angle (degrees from tangential)	87.1	87.1
Flow Turning (degrees)	35.1	36.6
Inlet Mach Number	0.1132	0.1162
Exit Mach Number	0.0912	0.0928
AVDR	1.023	1.037
Profile Loss (ω)	0.017	0.0175
Reynolds Number	4.78 (10^5)	5.88 (10^5)

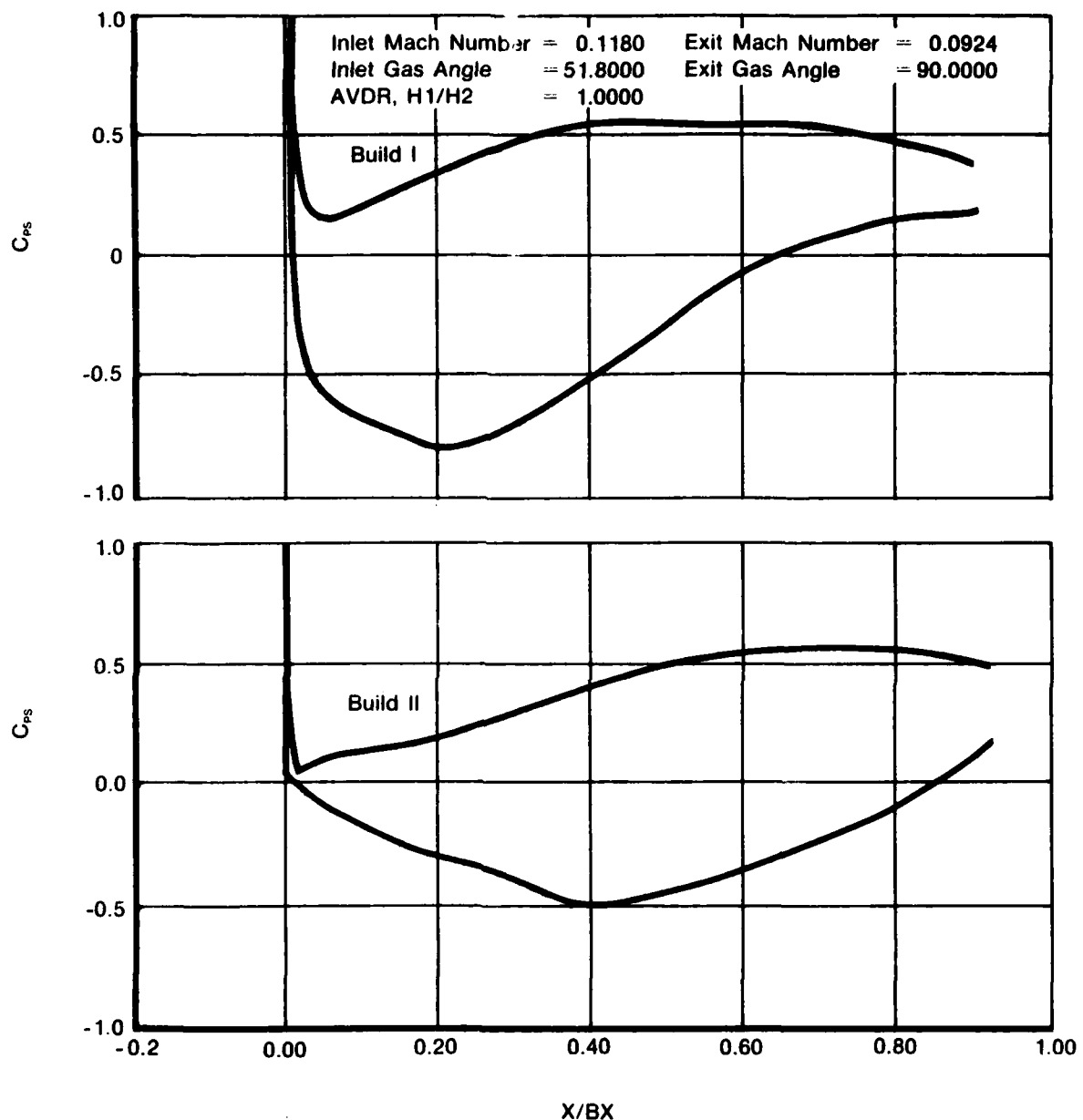


FIGURE 5
COMPRESSIBLE PRESSURE DISTRIBUTION - CP vs X/BX

and countered the decrease in loading resulting from the -5° incidence change. The approximately axial cascade outlet flow angle was also optimum for eliminating the effect of any remaining local axial velocity ratio variations on the mean flow angle in the flow downstream of the trailing edge.

TEST FACILITY

The facility used for these experiments was the United Technologies Research Center's Large-Scale Cascade (LSC). The cascade tunnel, as shown in Figure 6, is an open-loop type, receiving and exhausting air within a single test cell. The upstream air supply section consists of a double inlet, double-width fan, a perforated plate, honeycomb and screens, and an adjustable contraction. The test section attaches to the contraction and holds the cascade of seven airfoils with a 310 mm (12.2 in.) span.

The fan is a radial flow, squirrel cage design, belt-driven with a 37.3 kw (50 hp) electric motor. Flowrate is controlled by simultaneously adjusting two vortex valves located at the fan inlets. The fan is capable of producing a flow of 450 kliters/min. (16,000 cfm) with a 21 mm Hg (11 in. of water) pressure rise and 750 kliters/min (26,500 cfm) at no pressure rise. For typical cascades, this gives a maximum inlet test section velocity of approximately 43 m/sec (140 ft/sec), or a typical Reynolds number range of about 5.0×10^5 to 1.0×10^6 .

Perforated plate, honeycomb, and screen were carefully selected to obtain a minimum amount of total pressure distortion at the test section inlet. Screens were selected to minimize distortion due to screen non-uniformity and maximize flow distortion attenuation. Inlet distortion was less than $\pm 1\%$ of the inlet dynamic head (Q_0).

As shown in Figure 6, the test section is mounted on rollers and is easily attached or removed from the contraction of the upstream section. The endwall disks rest on rollers to allow changing the cascade setting angle. For this test, the airfoils were attached to both endwalls, one metal and the other clear plexiglass. A view of the cascade through the plexiglass wall is shown in Figure 7.

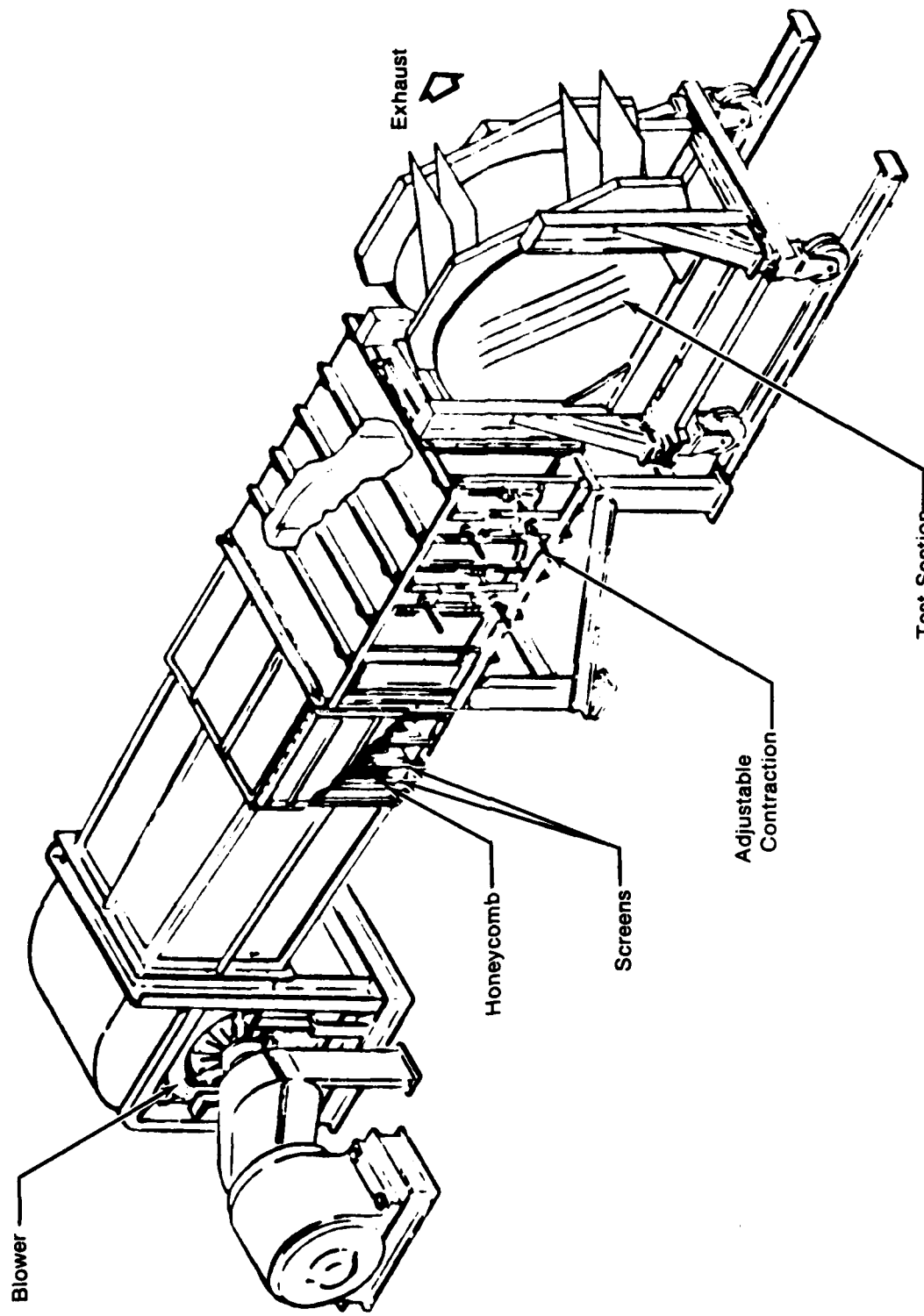
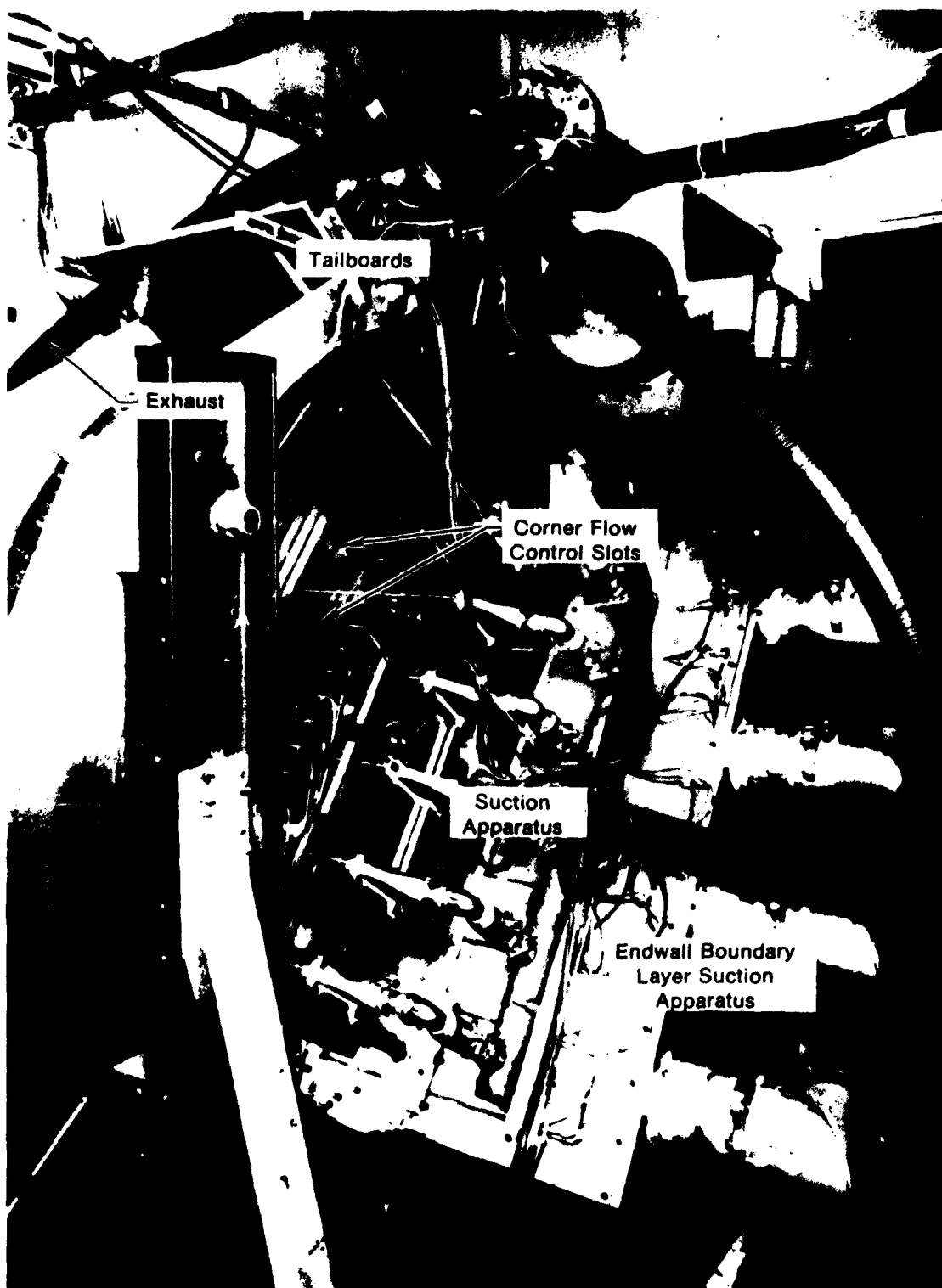


FIGURE 6
LARGE-SCALE CASCADE

FD 19799

FIGURE 7
LARGE-SCALE CASCADE TEST SECTION



FD 195942
R00707

Two suction systems and movable tailboards were used to obtain two-dimensional, periodic flow in the cascade test section. The locations of the various controls are shown schematically in Figure 8.

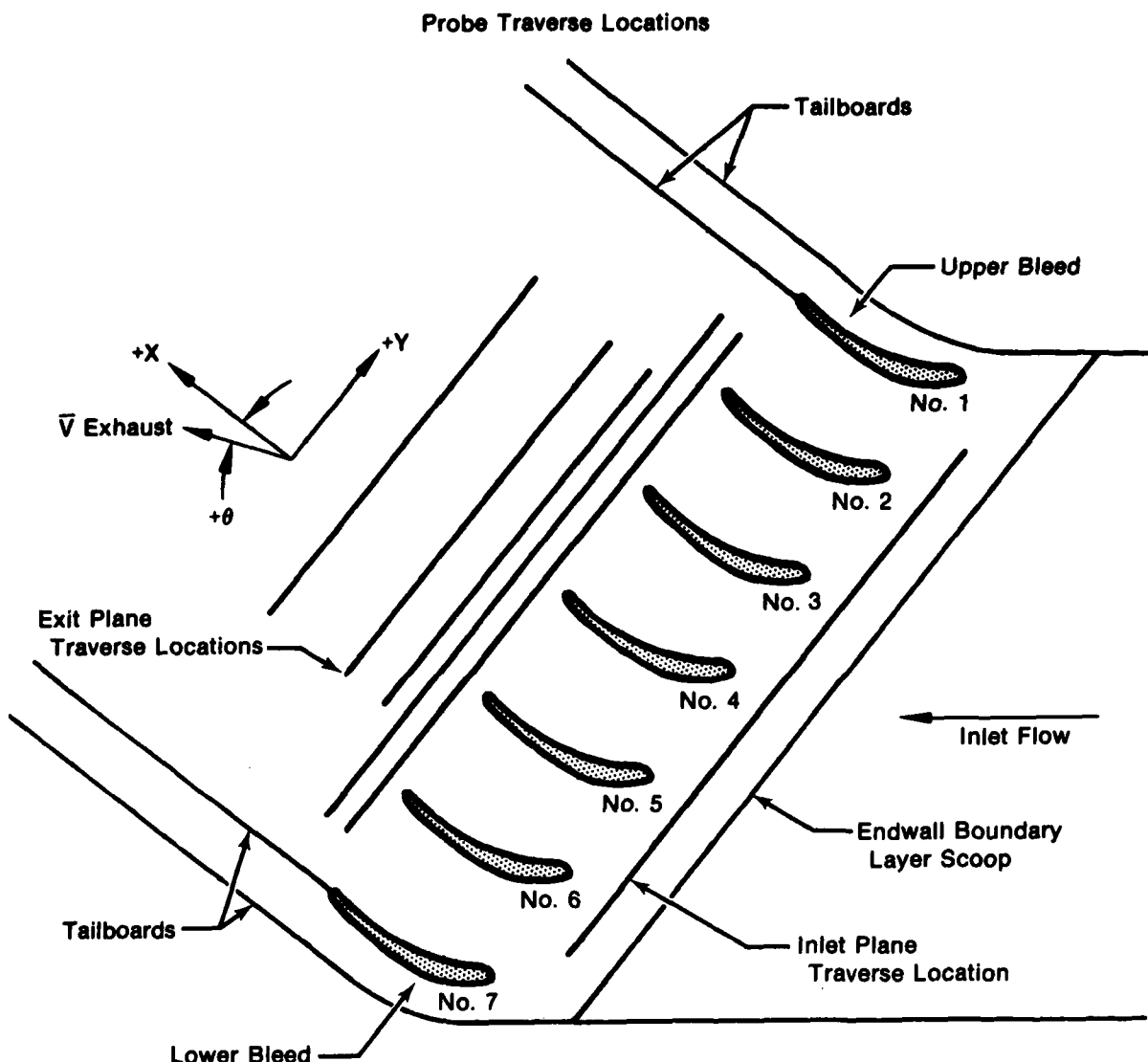
The endwall boundary layer scoops are located upstream of the cascade to remove the boundary layer on the endwalls as shown in Figure 9. The upper and lower bleeds were used to remove the boundary layers formed on the ceiling and floor of the cascade inlet section. A second suction system was used to remove the corner endwall secondary flow on the suction side of each airfoil. These corner flow control slots are shown in Figure 10. The effectiveness of corner slots in eliminating cascade secondary flow is shown by Peacock (Reference 14). The final adjustment for controlling the periodicity of cascade flow was the system of tailboards shown in Figures 7 and 8. All four tailboards are independently adjustable.

INSTRUMENTATION

Measurements were made of total and static pressure, velocity, turbulence, temperature, as well as pitch and yaw flow angles. Pressure was measured with either a miniature Kiel probe, a five-hole combination probe, or surface static taps. Velocity was measured with a single-element hot-film probe. Kiel and five-hole combination probes were used for the far wake traverses, whereas only a single-element hot-film probe was used in the near wake. All the probes used are shown in Figure 11 with a cross section of the trailing edges of Build 1 and Build 2 shown for comparison. Temperature was measured with a chromel-alumel thermocouple or a mercury thermometer.

The Kiel probe was used to measure the total pressure downstream of the cascade. The Kiel is a standard United Sensor miniature, 1.5 mm (0.060 in.) in diameter, probe supported in a 6.3 mm (0.25 in.) stainless steel tube. The Kiel acceptance angle was found to be $\pm 45^\circ$.

The five-hole probe is a standard United Sensor probe with five pressure taps on an ogival tip of 2.4 mm (0.093 in. diameter). With calibration curves, it is possible to determine total and static pressure, as well as yaw and pitch angles.



FD 198000

FIGURE 8
SCHEMATIC OF TEST SECTION

FIGURE 9
CASCADE INLET

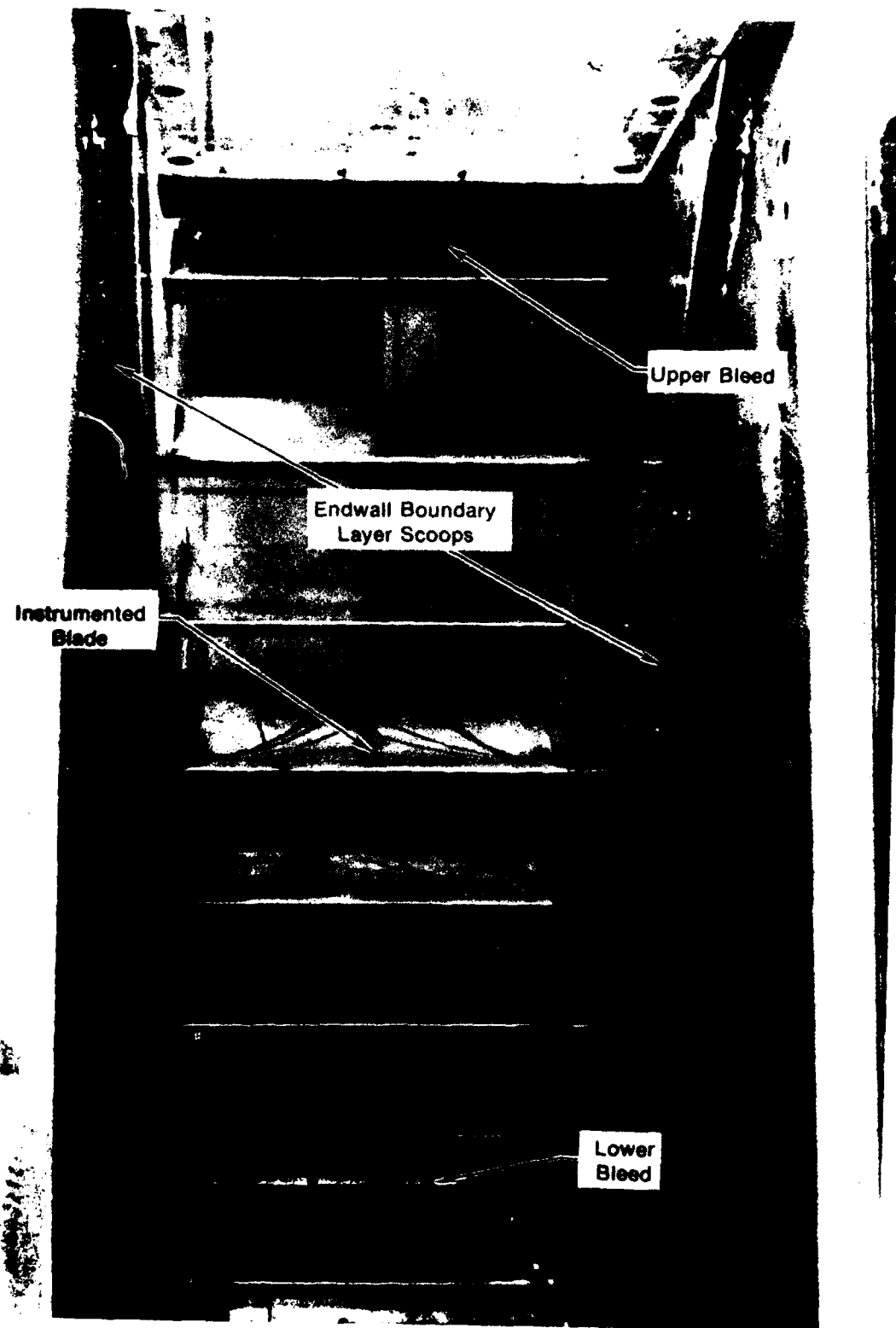
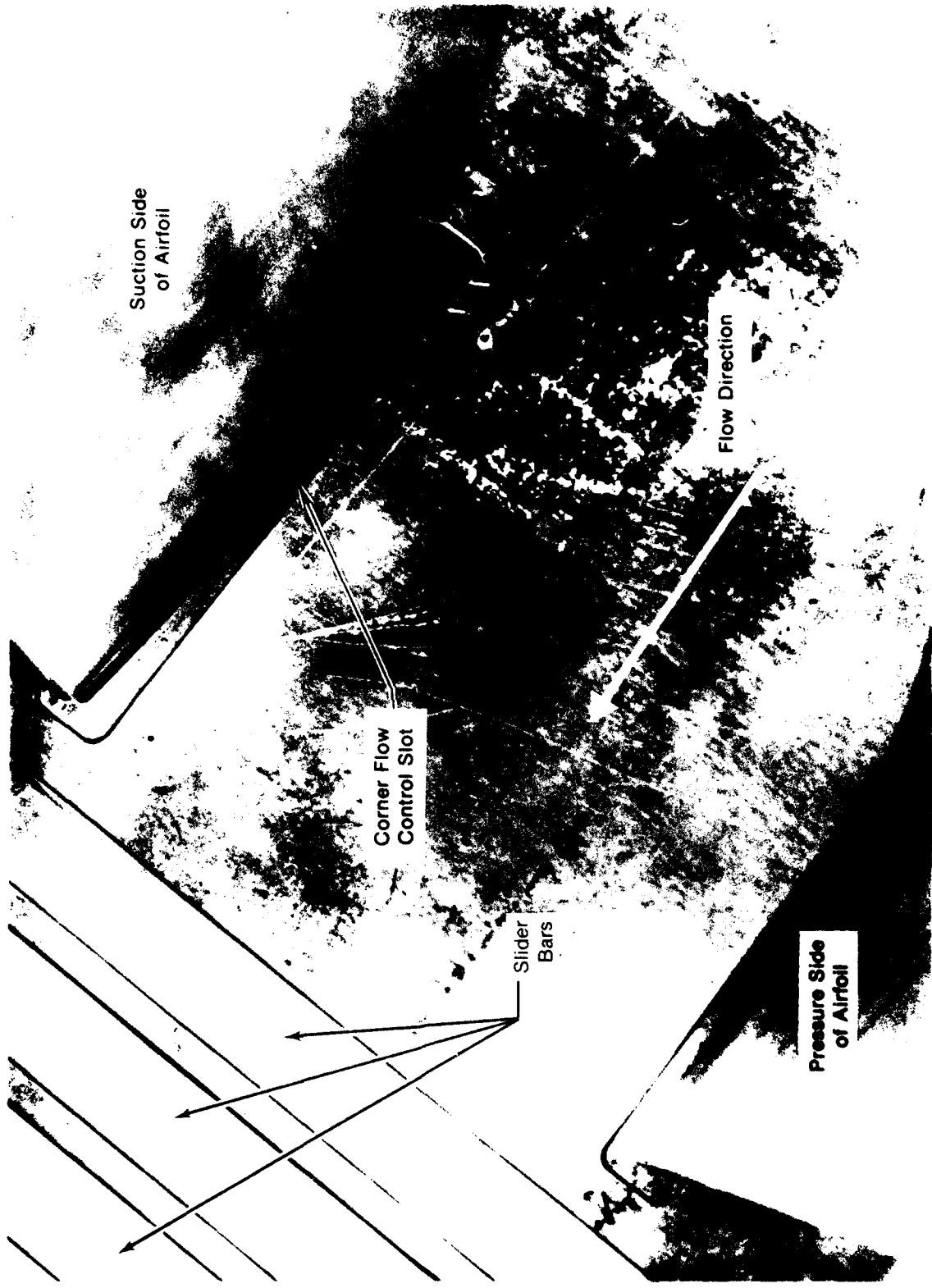


FIGURE 10
CASCADE ENDWALLS - CORNER SLOTS AND SLIDER BARS



F D 19594
8010-0-

The hot-film probe used to measure flow velocity and turbulence is a single-element type with a 0.025 mm (0.001 in.) diameter sensing portion. The sensing element is supported on 6.3 mm (0.25 in) long needles which are attached to a 100 mm (4 in.), 1.5mm (0.060 in.) diameter tube. A special probe holder, shown in Figure 11, was designed to allow probe tip axial locations other than the mechanical probe slider positions in the endwall.

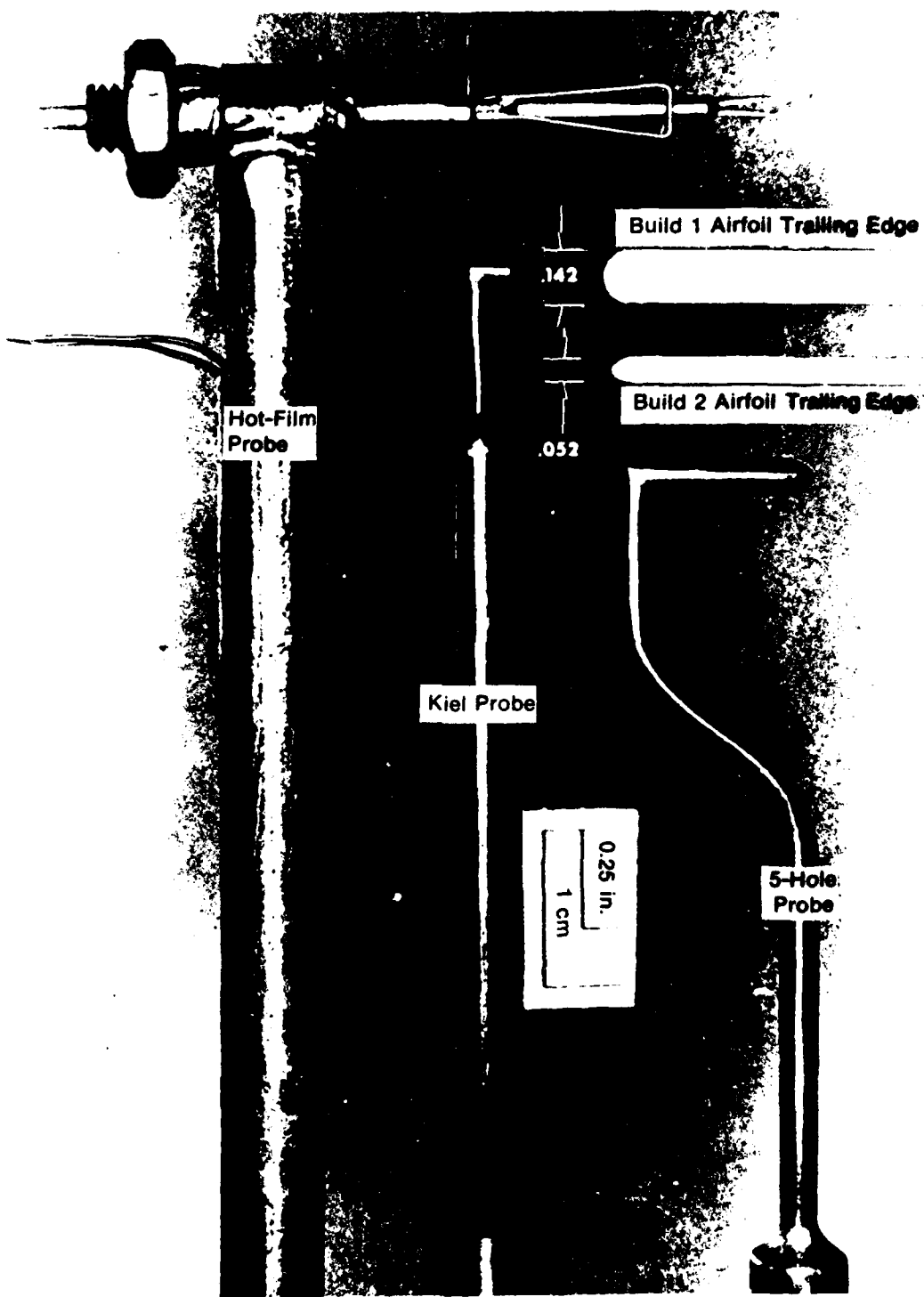
All the airfoils used in the investigation were instrumented with static pressure taps, primarily at midspan. The center airfoils were more heavily instrumented than the surrounding airfoils with a concentration of taps near the trailing edge and eight taps located spanwise at two-chord locations. The instrumented airfoils can be seen in Figure 9.

MEASUREMENT LOCATIONS

Seven airfoils were used in each cascade, numbered as shown in Figure 8. The coordinate system used to locate the measurements for both builds originated at the trailing edge along the mean camber line of the center airfoil. The positive x-direction is in the direction of flow normal to the cascade plane, while the positive y-direction is parallel to the cascade plane and pointing away from the pressure side of the airfoil surface. Angles are measured counterclockwise from the x-axis. See Figure 8.

The probe traverse system, mounted on the metal endwall, consists of a motor-driven worm gear on a threaded rod attached to a precision traverse table. The probe traverse table moves parallel to the cascade trailing-edge plane, i.e., in the y-direction. The platform has probe traverse mounting slots directly corresponding to sliding bars in the metal endwall. A partial view of these bars can be seen in Figure 10. There are five probe traverse locations downstream of the blade and one upstream, as shown in Figure 8. Axial placement of the Kiel and five-hole probes was limited to the fixed axial traverse locations, while the hot-film probe could be placed at any axial location desired. The same axial traverse locations were used for both builds. Listed in Table 2 are the traverse locations and the type of probe used. Table 2 also includes estimates of the probe location accuracy.

FIGURE 11
TRAVERSE PROBES



FD 195945
800707

TABLE 2. PROBE MEASUREMENT LOCATIONS AND ESTIMATED PROBE PLACEMENT ACCURACIES

Measurement Locations

X (mm)	X (in.)	X/TED		KIEL	FIVE-HOLE	HOT-FILM
		Build I	Build II			
-241.0	-9.50				X	
- 6.4	-0.25	-1.76	-4.81			X
- 0.8	-0.031	-0.22	-0.60			X
0.8	0.031	0.22	0.60			X
2.4	0.094	0.66	1.81			X
4.0	0.156	1.10	3.00			X
6.4	0.25	1.76	4.81			X
12.7	0.50	3.52	6.92	*		X
25.4	1.00	7.04	19.23	*		X
50.8	2.00		38.46	X		**
76.2	3.00			X	X	
127.0	5.00			X	X	
228.6	9.00			X	X	

* BUILD I only

** Build II only

Estimated Probe Placement Accuracies

Probe Position

X-Direction

Five-hole and Kiel ± 1.27 mm ($\pm .050$ in.)

Hot-Film ± 0.38 mm ($\pm .015$ in.)

Y-Direction

Relative $\pm .02$ mm ($\pm .001$ in.)

Absolute $\pm .84$ mm ($\pm .030$ in.)

Angles $\pm .5$ degrees 22

DATA ACQUISITION

The basic data acquisition system is comprised of probe traversing controls, transducers, water manometers, and the Colog recording system. Anemometry and spectrum equipment and various digital voltmeters were used for hot-film measurements. All probe traversing and rotation was controlled from the control room. Probe position was determined with a calibrated linear potentiometer.

Pressure measurements were made either with the Scanivalve/Colog system or read manually on water manometer boards. The Scanivalve is a forty-eight port model incorporating a 45 mm Hg (24 in. H₂O) Druck transducer. The first eight ports were dedicated to measuring four calibration pressures from the transducer calibration system. The remaining port assignments were either probe pressures or airfoil surface static pressures. The transducer calibration system is a secondary standard system consisting of four water columns calibrated with a Meriam micromanometer. When the Colog system is activated, the Scanivalve is automatically stepped every 4 sec. The signal is smoothed with a low frequency filter for 3 sec and read during the fourth. The data is converted into a digital signal and stored in Colog memory. After all the ports are sampled, the data is punched on paper tape and processed later on a Univac 1110 computer.

The hot-film velocity acquisition system consists of a TSI 1050 anemometer, 1052 linearizer, and a 1047 averaging circuit. Linearized anemometer voltages were read with Kiehly model 177 and Hewlett Packard 3466A digital voltmeters with dc and true rms capabilities. Linearized anemometer output was also input to a Spectral Dynamics model SD340 spectrum analyzer capable of analyzing frequencies up to 20 kHz.

The estimated accuracy of the data acquisition system for pressure measurements is +1% of the upstream reference dynamic head, Q_o. The estimated accuracy for velocities is +2% of the local velocity.

DATA REDUCTION

A computer program was developed to reduce and plot the data for comparison with analytical results and with other data.

The reduction program, used for all the probe traverse data, accepts raw Kiel, five-hole, and hot-film data and reduces it to engineering units. Mass averaging was done over one pitch, while wake integral parameters were found by integrating only the wake data, as shown in the data tables (between the asterisks). The wake edge was defined as the location of the velocity deficit, which was 99% of the nearest free stream level.

Because the cascade tunnel cannot be operated at a strictly constant temperature, the hot-film probe was operated at a fixed operating resistance, or essentially a fixed sensor temperature. The anemometer output was linearized to simplify the determination of turbulence and velocity. The reduction of the hot-film velocity data was performed with a simple temperature correction for the small variations of temperature in the rig, as suggested by the TSI General System Information Manual (Reference 15).

SECTION IV

EXPERIMENTAL RESULTS

The results of this experimental investigation are divided into four sections: (1) cascade test conditions, (2) far wake Kiel and five-hole total pressure and velocity measurements, (3) boundary layers and near wake hot-film velocity measurements, and (4) wake similarity fits, mass averaged and integrated wake parameters, and wake centerline location. All data are tabulated in the Appendix.

CASCADE TEST CONDITIONS

The measurements of cascade two-dimensionality, periodicity, and inlet uniformity confirmed that the desired aerodynamic cascade conditions were achieved for the wake experiment. Surface pressure distributions and boundary layer behavior of both airfoils provided airfoil trailing-edge conditions similar to the viscous trailing-edge flow at high speed. Cascade test conditions are listed in Table 1.

Two-Dimensionality and Periodicity

Flow visualization and airfoil surface static pressures were used to determine the extent of two-dimensionality and periodicity. Figures 12 and 13 show the cascade test section for each build with yarn tufts installed. The pictures with and without corner suction show the effectiveness of the corner flow slots in preventing endwall boundary layers from flowing toward the cascade midspan on the airfoil suction side. Note the tufts point inward with no suction and straight backward with suction. The tufts also indicated that the Build II configuration had less stable suction side boundary layer which occasionally separated at about 75% chord. Another method of flow visualization used was ammonia gas injected on airfoil and endwall surfaces covered with Ozalid paper. The ammonia traces show the surface flows in Build I to be two-dimensional over essentially the full span, while Build II was two-dimensional over the center 40% of the airfoil span.

The two-dimensionality of the midspan flow is shown in Figure 14 by a comparison of the measured airfoil surface pressures with the two-dimensional analysis of Caspar (Reference 16) using the aerodynamic

FIGURE 12
TUFT FLOW VISUALIZATION - BUILD I

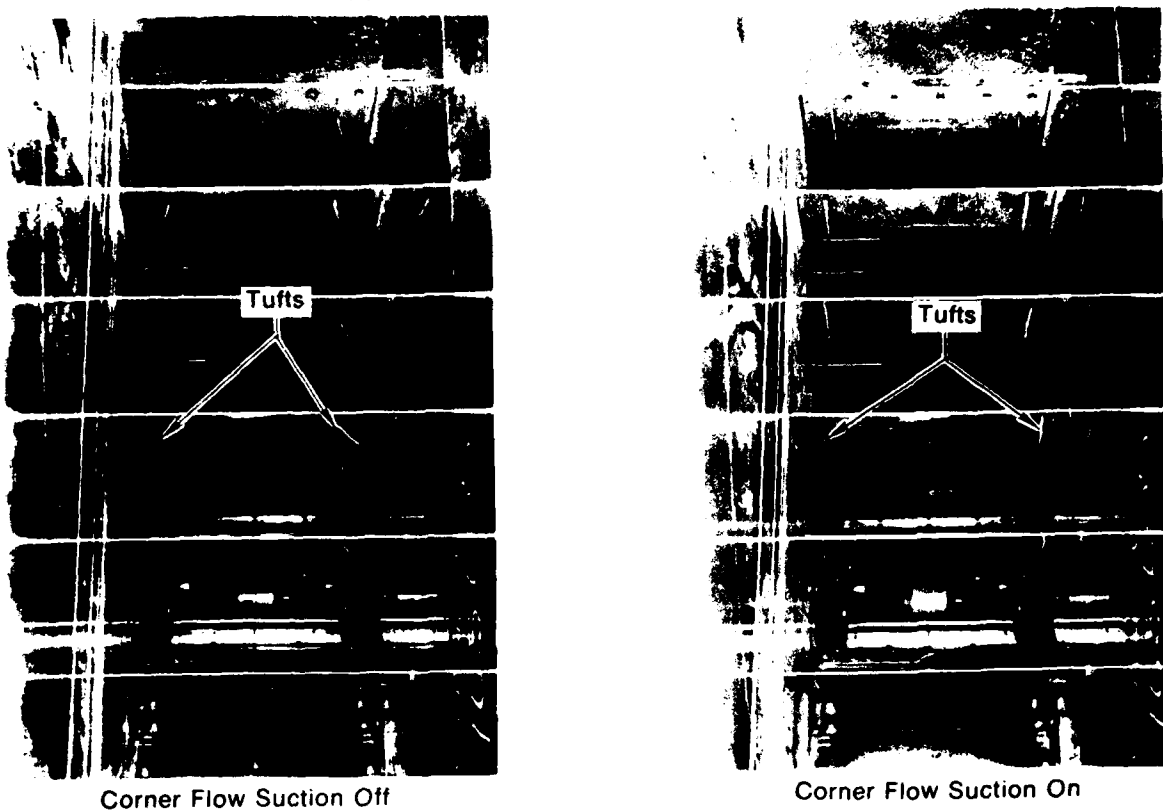
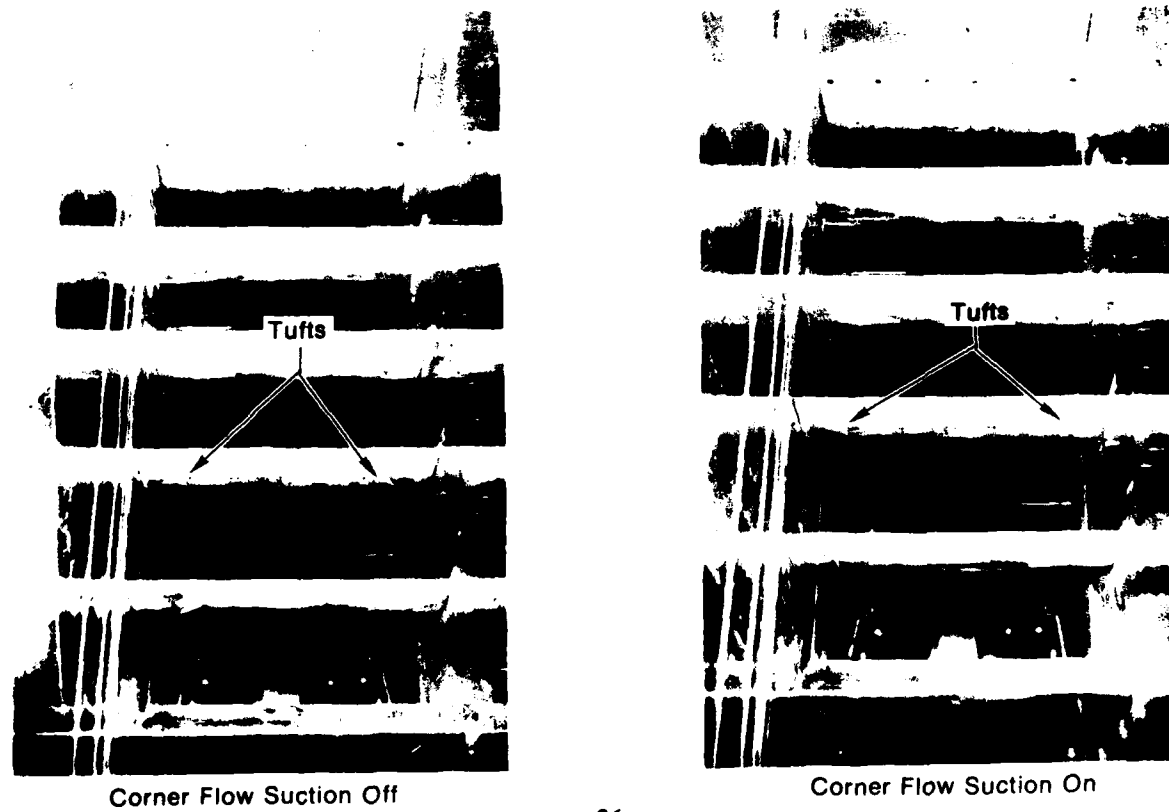


FIGURE 13
TUFT FLOW VISUALIZATION - BUILD II



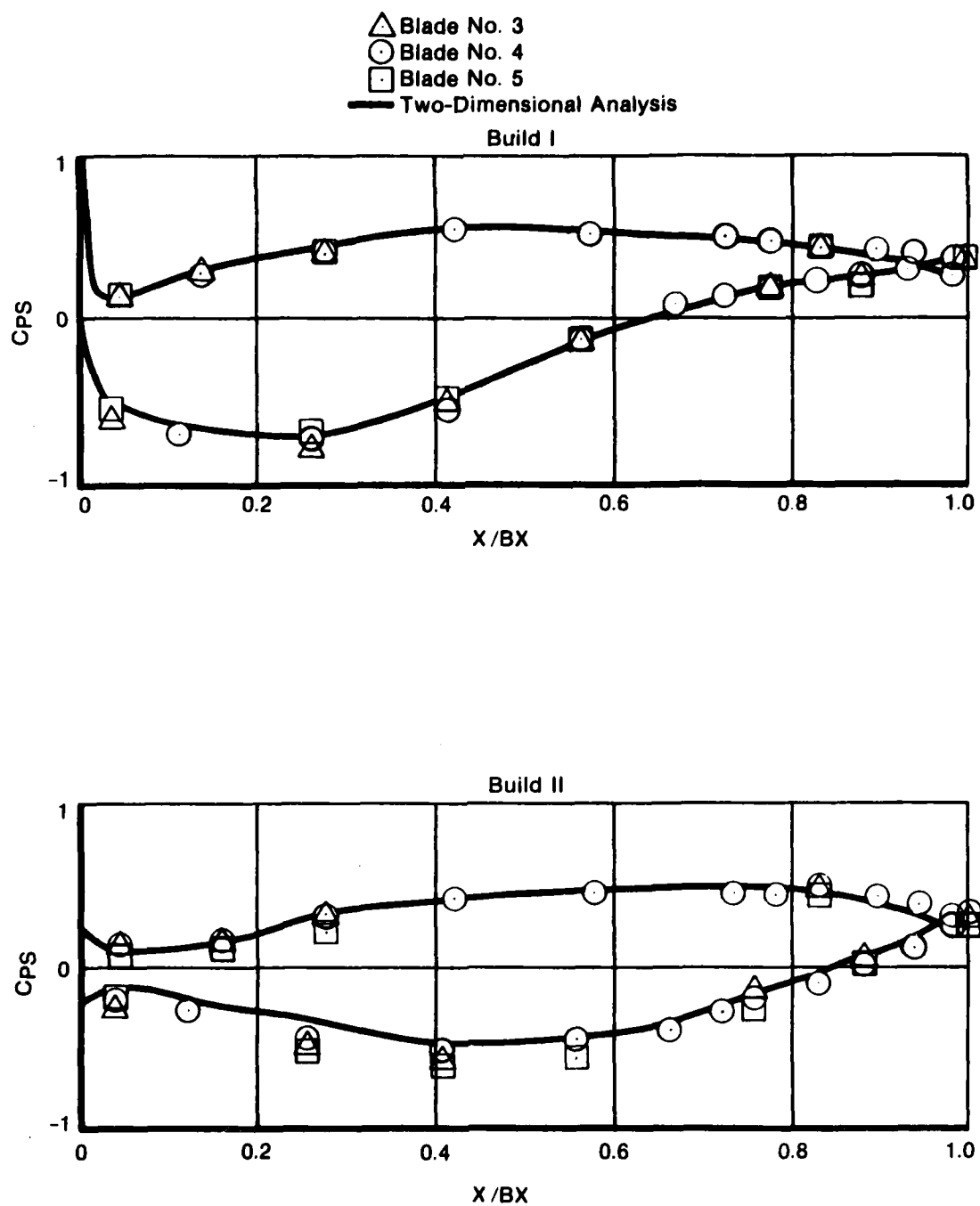
conditions in Table 1. Excellent cascade periodicity is shown for both builds in Figure 14 for the central three cascade passages by the close agreement of airfoil surface static pressures.

Build I static pressures did not vary with span. Build II spanwise static pressure data displayed weak spanwise gradients due to the secondary flow phenomena seen by the tufts and ammonia traces near the quarter span locations. The center airfoil static pressures are tabulated in Table 3 in terms of pressure coefficient, C_{ps}, versus chord location.

Excellent periodicity was also shown for the wakes of the center three airfoils by the far downstream, midspan measurements. Traverses for both Builds I and II showed the center three blades to have nearly identical, periodic wakes. Downstream distortion of static pressure and flow angle were minimal. Pressures measured between wakes far downstream varied by less than 1% of the inlet referenced dynamic head, Q_o.

Upstream Uniformity

The two builds had acceptable inlet uniformity for total pressure, static pressure, and flow angle. Upstream five-hole probe measurements were made to check inlet uniformity. Sparse traverse locations at approximately 0.15 axial chords upstream of the leading edge were selected over the entire inlet in the y-direction. For both builds the inlet total pressure distortion was less than $\pm 1\%$ of inlet Q_o, while static pressure results showed a $\pm 5\%$ variation in inlet static pressure with a 5 to 7% decrease in the mass average static pressure from the reference probe located further upstream. The variation in static pressure was primarily caused by blade-to-blade potential flow variations since the axial location of the measurements was close to the leading edge. The decrease in the mass averaged static pressure is caused by a streamtube contraction, due to insufficient removal of flow through the boundary layer scoops and, possibly, the corner slots. Upstream yaw angle non-uniformity was $\pm 1^\circ$ and $\pm 1.5^\circ$ for Builds I and II respectively. There was a 2° difference in the measured mass average inlet yaw angle between the two builds.



FD 201751

FIGURE 14
AIRFOIL SURFACE STATIC PRESSURES - BUILD I AND II
Blade Static Pressures

TABLE 3. TABULATION OF BLADE STATIC PRESSURE DATA

BUILD I

SUCTION SIDE DATA

X	CPS
.404	-.589
1.192	-.782
2.407	-.718
3.597	-.552
4.813	-.167
5.602	.011
6.055	.073
6.375	.125
6.797	.182
7.197	.219
7.597	.243
7.942	.255
7.980	.268

PRESSURE SIDE DATA

X	CPS
.403	.099
1.196	.244
2.397	.405
3.589	.511
4.800	.493
5.987	.466
6.398	.437
6.784	.405
7.196	.376
7.592	.327
7.905	.252
7.952	.270
7.991	.271

BUILD II

SUCTION SIDE DATA

X	CPS
.430	-.189
1.318	-.261
2.867	-.407
4.266	-.603
5.763	-.490
6.682	-.411
7.154	-.279
7.381	-.211
8.048	-.080
8.481	.036
8.870	.169
9.270	.306
9.322	.316

PRESSURE SIDE DATA

X	CPS
.524	.109
1.441	.131
2.828	.229
4.235	.421
5.661	.482
7.072	.501
7.540	.490
7.991	.494
8.485	.463
8.888	.432
9.258	.307
9.288	.302
9.340	.326

1. These dimensions are in inches

2. X is true chord dimension from leading edge.

Low Speed-High Speed Flow Similarity

Overall cascade test conditions are listed for Builds I and II in Table 1. For comparison, the relevant high-speed data for the supercritical design can be found in the data summary of Reference 10, test points 30-32. The profile loss of the low-speed test follows the smooth, nearly constant trend with inlet Mach number established by the DFVLR high-speed results for Mach numbers between 0.43 and 0.70. Flow turning in the low-speed test was lower than the high-speed test. This is primarily due to the approximately 10% lower AVDR of the low-speed test. The low-high speed performance comparison for the Build II cascade was similar. Low-speed pressure distributions were also similar in shape to the desired high-speed distributions. The Build I fore-loaded suction side distribution peaked at approximately 20% axial chord, while Build II aft-loaded pressure distribution peaked at approximately 50% axial chord. The combination of similar surface pressure distributions and Reynolds numbers implies that the trailing-edge boundary layers will also be similar to the high-speed counterparts. This is partially confirmed by the similar profile losses. Thus, it can be concluded in this instance that the low-speed test can be used to model the viscous effects present in shockless high-speed cascade flow.

FAR WAKES

Far downstream Kiel and five-hole traverse results are shown in Figures 15 through 18. Results are presented in terms of pressure coefficients and nondimensional velocity ratios. Downstream static pressure varied by less than 1% of inlet Q_0 and is not plotted here. Angles are also not shown because of the excellent exit flow uniformity. The five-hole probe did indicate yaw angle variations due to the shear flow in the wakes. These apparent yaw angle variations are probably not actually present in the flow. Kiel total pressure results (Figures 15 and 16) compare closely to the five-hole total pressure data (Figure 17 and 18).

The five-hole results in Figures 17 and 18 for the two builds show several phenomena. Both builds produced a gradual decrease in wake depth and increase in wake width with increasing distance downstream. At a fixed axial location, the Build II wake is more attenuated than

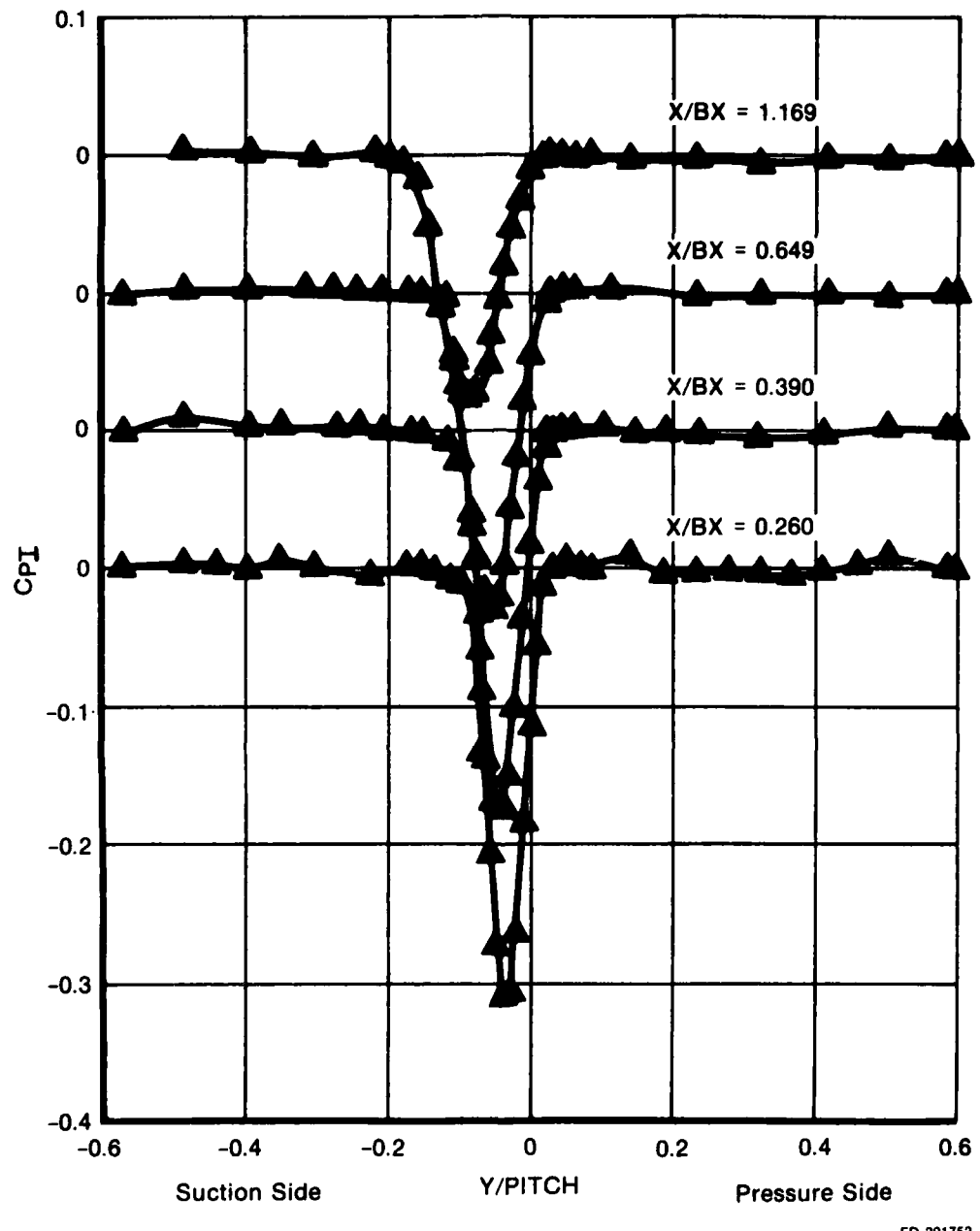


FIGURE 15
KIEL TOTAL PRESSURE RESULTS - BUILD I

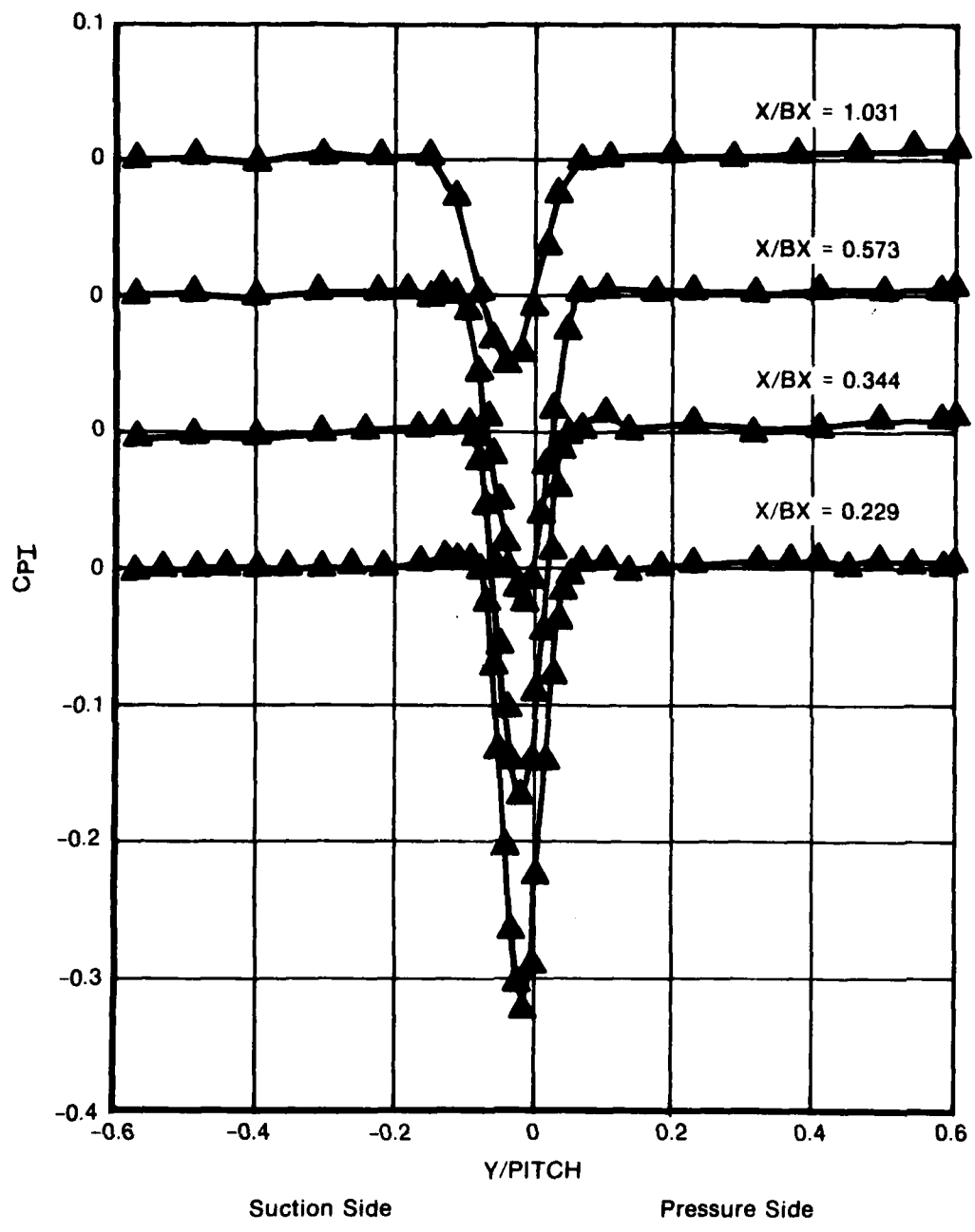


FIGURE 16
KIEL TOTAL PRESSURE RESULTS - BUILD II

FD 201753

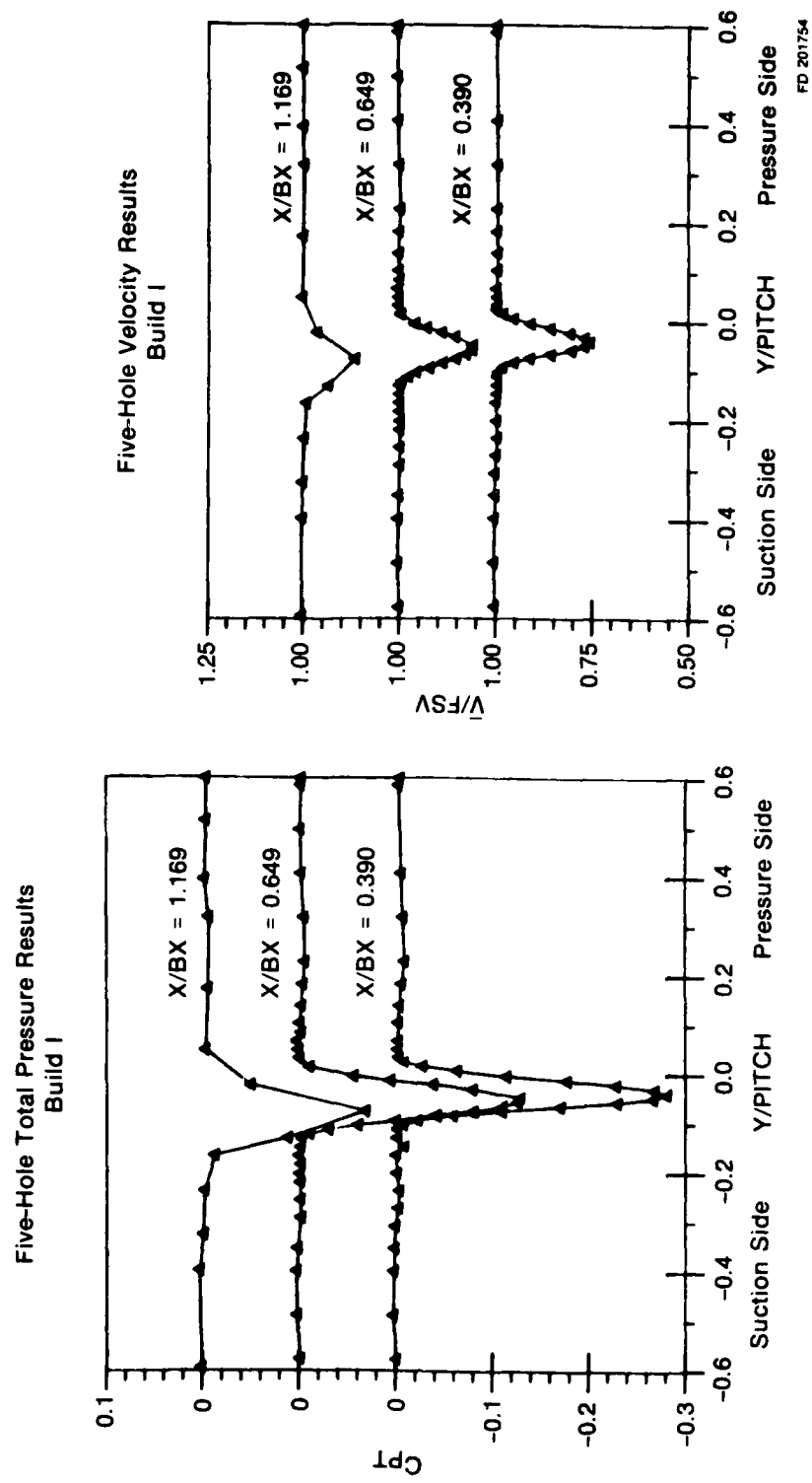


FIGURE 17
FIVE-HOLE TOTAL PRESSURE AND VELOCITY RESULTS - BUILD I
FD 2017s4

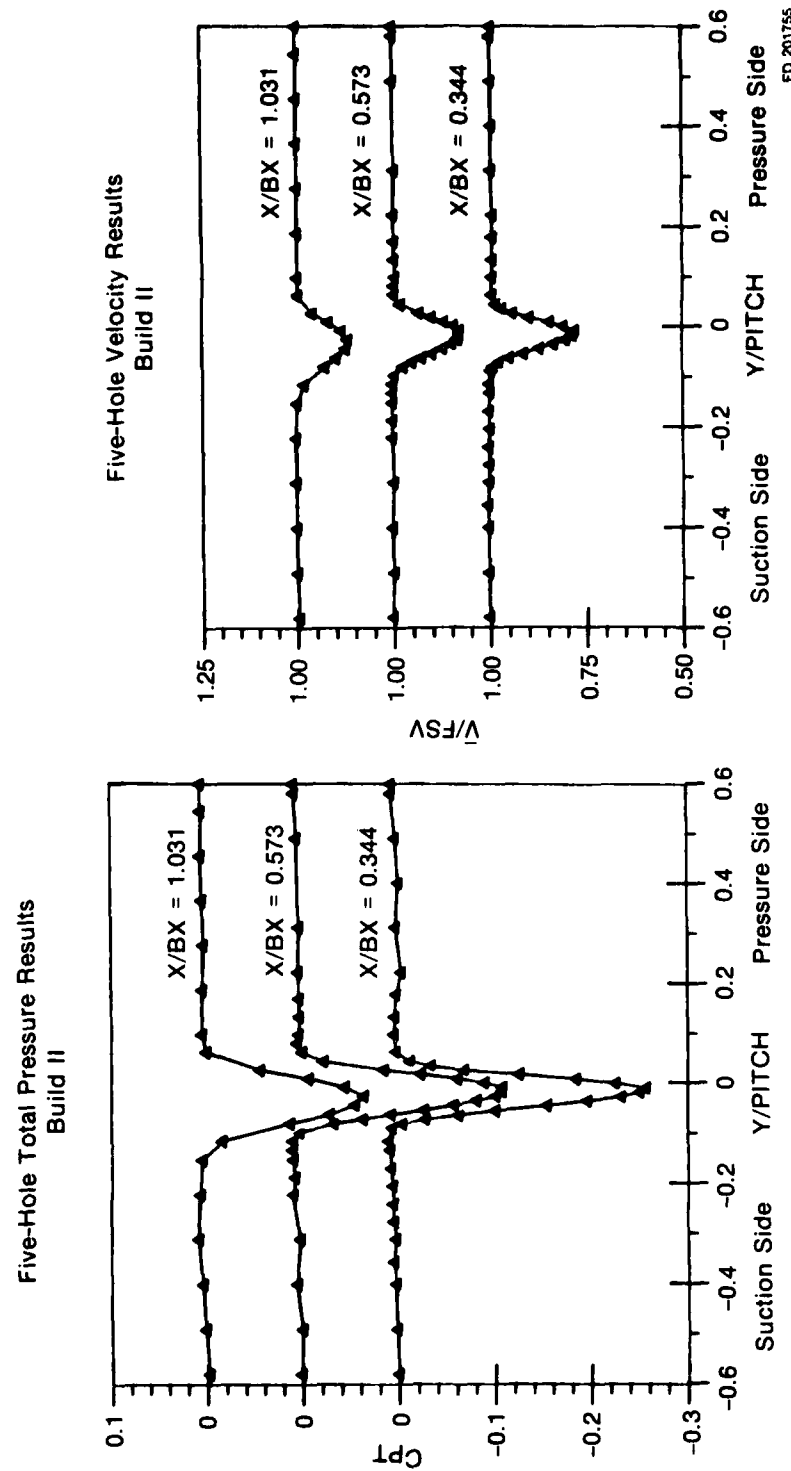


FIGURE 18
FIVE-HOLE TOTAL PRESSURE AND VELOCITY RESULTS - BUILD II

the Build I wake. This is evidenced by shallower wake depths. The angle of the wake minimum velocity trajectory for Build I was approximately one degree higher than the measured exit air angle. For Build II, the wake trajectory was at an angle slightly more than two degrees.

BOUNDARY LAYERS AND NEAR WAKES

Boundary layers from both builds measured at the $X = -6.35$ mm (0.25 in.) position are presented in Figures 19 and 20. Both pressure and suction side profiles are shown. Curves plotted in U^+ and Y^+ coordinates are from a Scharnhorst et. al., (Reference 18) three parameter boundary layer fit. Two general observations can be made. The pressure surface universal profiles have favorable pressure gradient profile shapes (see Figure 14), while the suction side data shows large adverse pressure gradient shapes. The boundary layer thickness on the pressure side of Build II is twice as large as that on the Build I airfoil. Further comparisons will be made with the integrated data results in the following section.

Boundary layer and mean velocity defect profile results in the near wake are shown in Figures 21 and 22. Again, Build I profiles show much more wake shifting in the y -direction than Build II. The Build I traverse data shows a region of nearly constant low velocity in the very near wake at X/BX locations of 0.004, 0.012, and 0.020. This low velocity region increases in apparent velocity with increasing X/BX which seems to rule out steady reversed flow as its cause. The Build II wakes do not show such a low velocity region. For Build I, these first three traverses ($X/BX = 0.004, 0.012, \text{ and } 0.020$) were made within a distance 1.25 trailing-edge diameters aft of the airfoil. For Build II, however, only one traverse was made within this relative distance. This was due to the much thinner trailing-edge diameter of Build II. The fact that the low velocity region observed in the near wake of Build I was not observed in Build II at a corresponding relative distance aft of the airfoil (X/TED) suggest that the ratio of the trailing-edge diameter to total boundary layer size may play a role in determining the nature of the near wake.

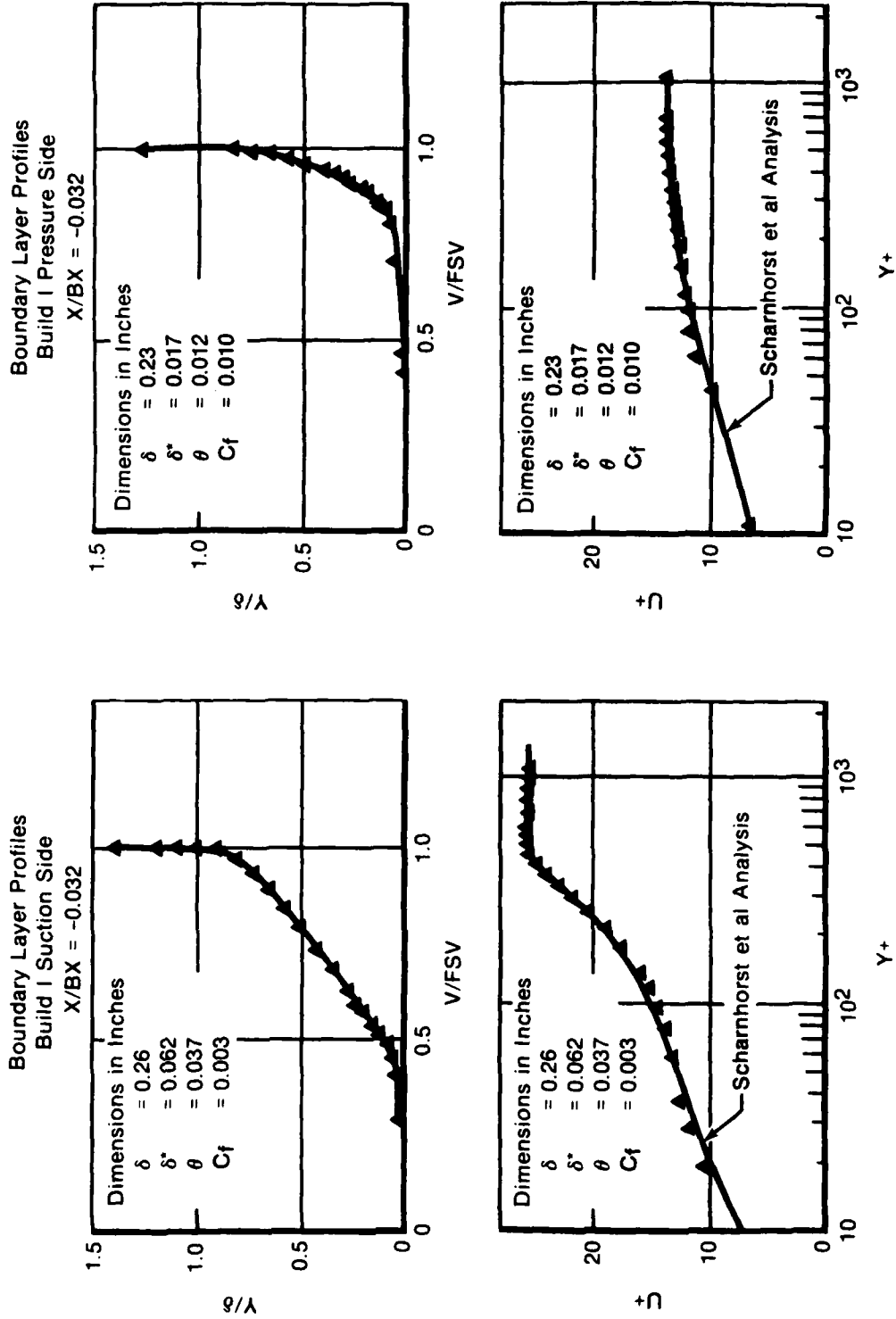


FIGURE 19
BOUNDARY LAYER PROFILES - BUILD I

FD 201756

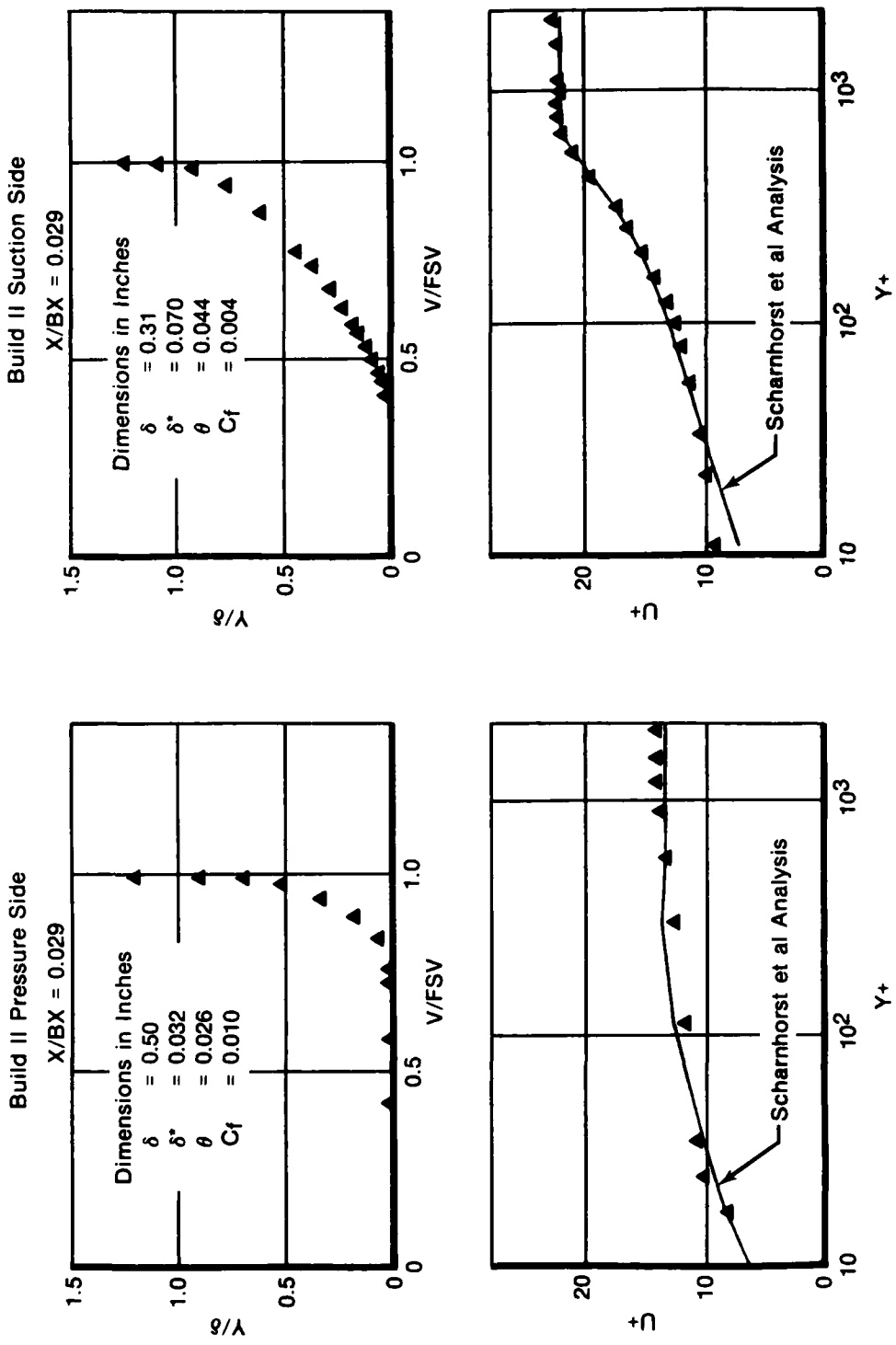
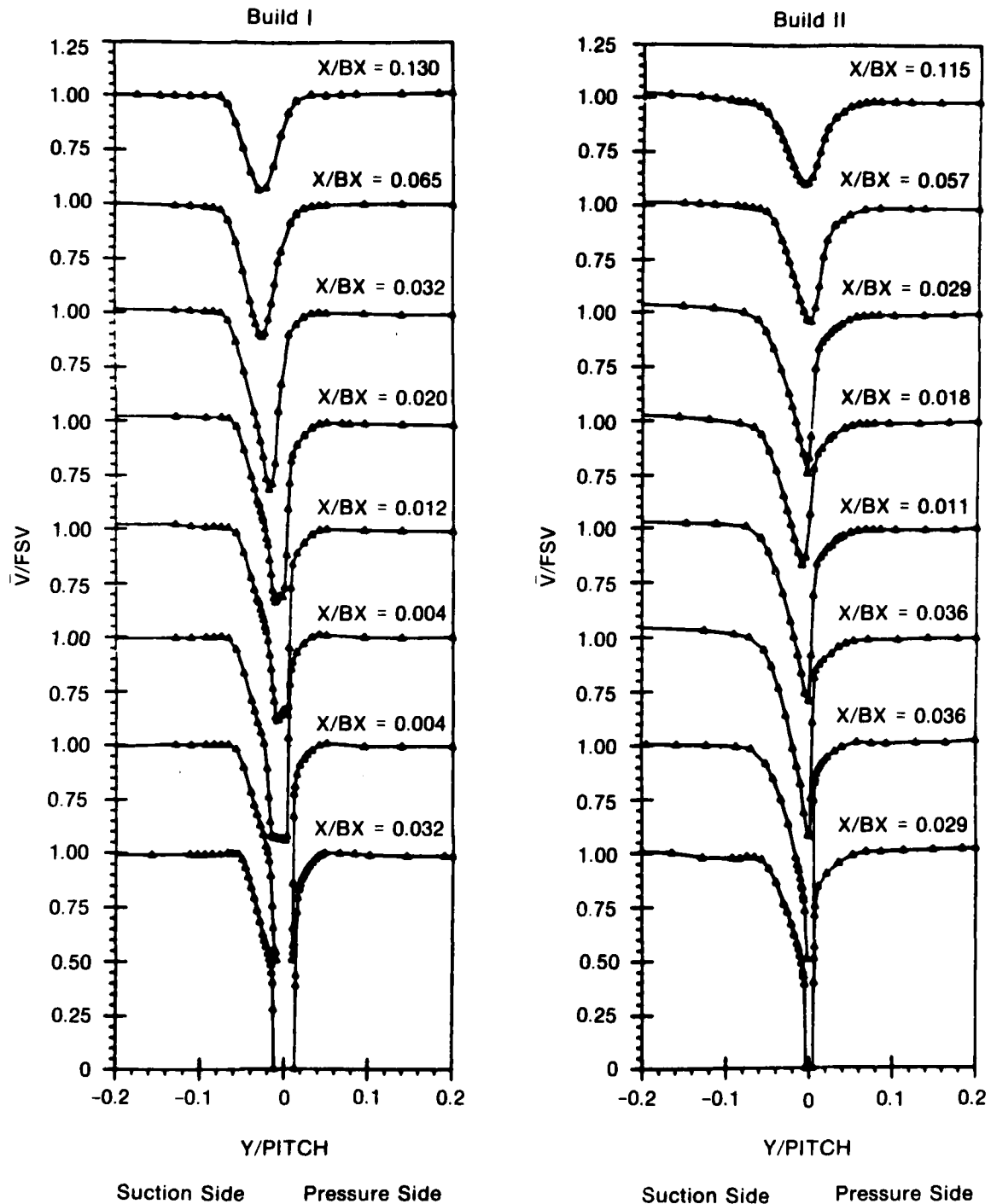


FIGURE 20
BOUNDARY LAYER PROFILES - BUILD II

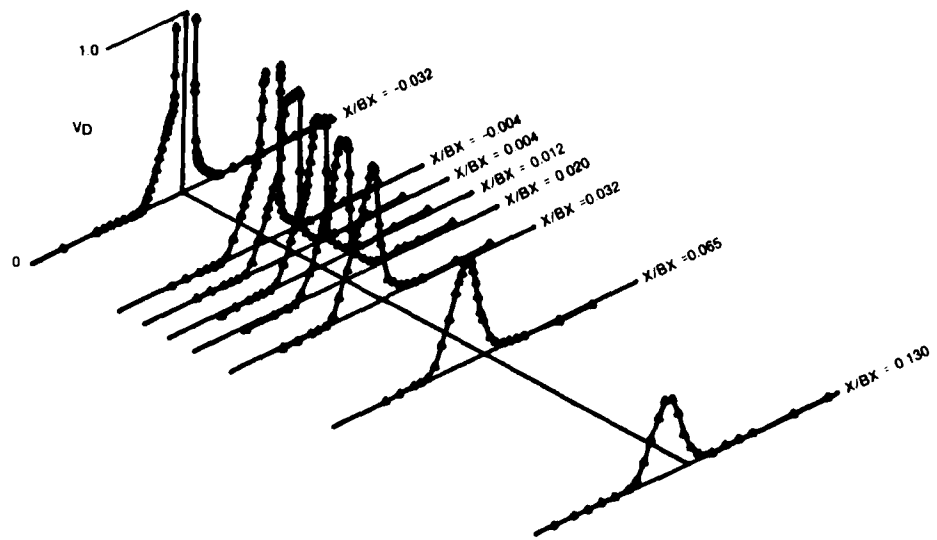
Boundary Layer and Near Wake Velocity Profiles



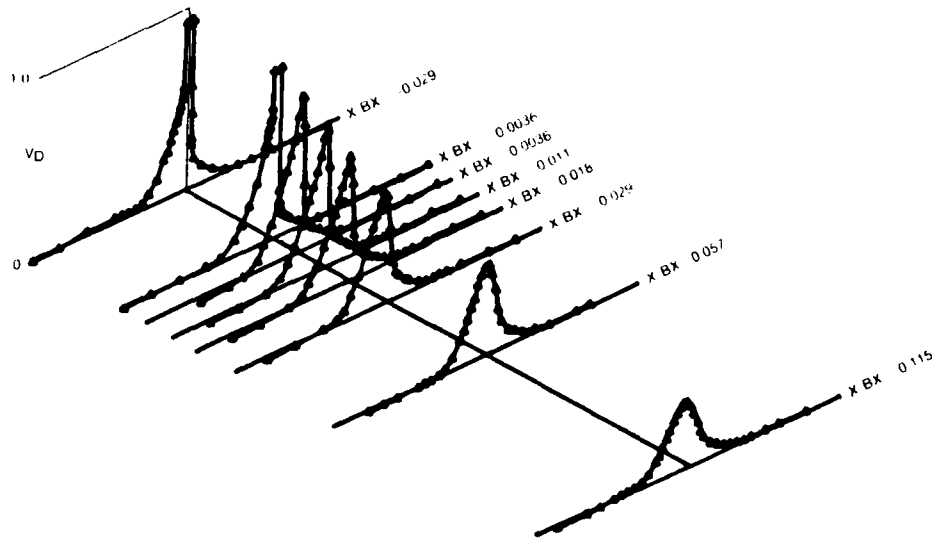
FD 201758

FIGURE 21
BOUNDARY LAYER AND NEAR WAKE VELOCITY PROFILE - BUILDS I AND II

Build I



Build II



FD 201759

FIGURE 22
BOUNDARY LAYER AND NEAR WAKE HOT-FILM VELOCITY DEFICIT -- BUILDS I
AND II

The near wakes of the two builds are different near the trailing edge, but do look very similar further downstream (by $X/BX = 0.032$). The near wakes of both builds strongly resemble the airfoil boundary layers just upstream of their trailing edges. This leads to stronger velocity gradients on the pressure sides of the wakes near the trailing edge than on the suction sides.

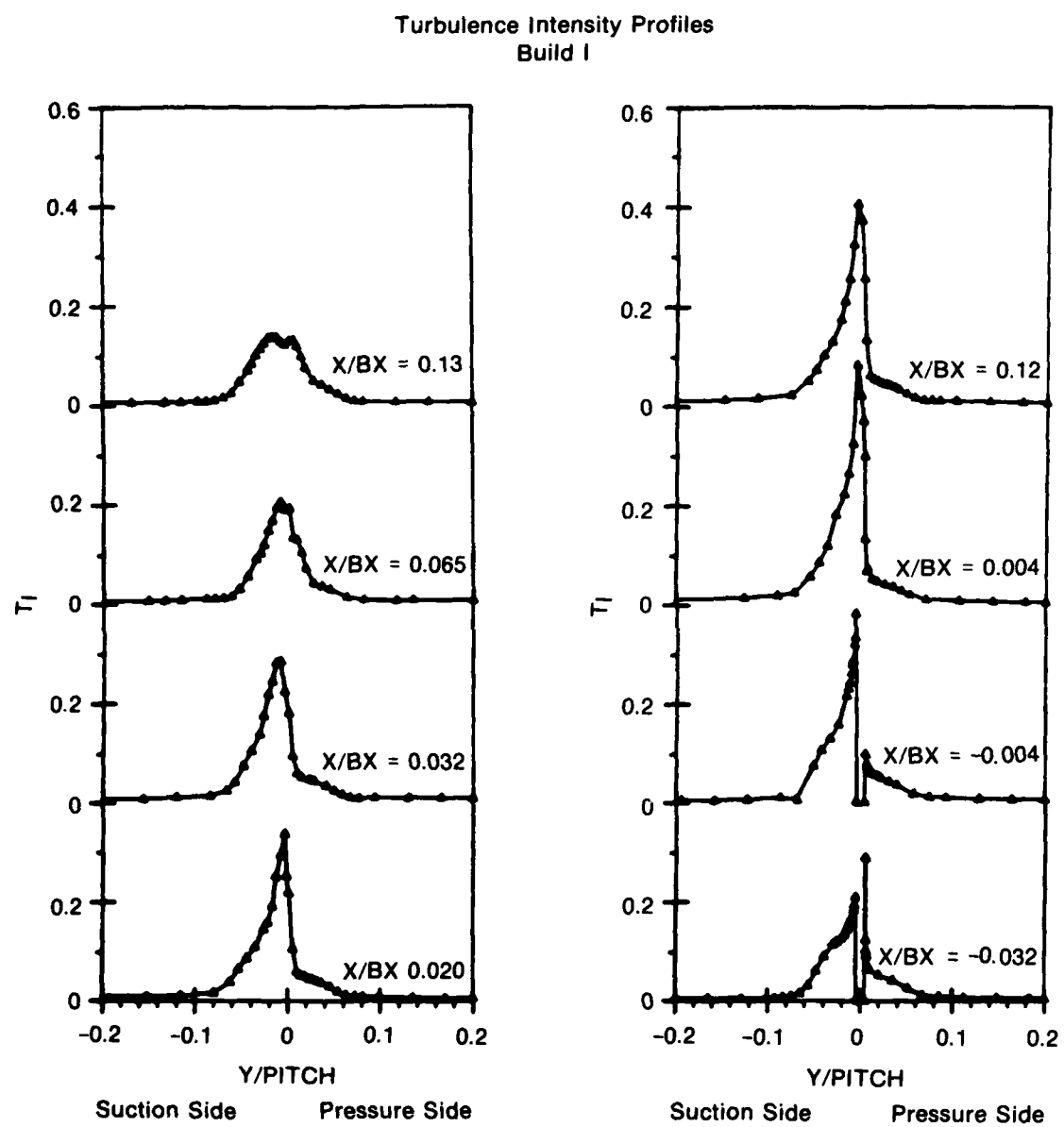
The far downstream wake profile shapes presented are similar to the profile shapes presented by Raj and Lakshminarayana (Reference 19) and also Lakshminarayana and Davino (Reference 20). However, the data shown in Reference 19 at the trailing-edge traverse location does not look like the Build I data at $X/BX = 0.004$, although it is similar to, though not quite as deep as, the Build II data at $X/BX = 0.0036$.

TURBULENCE AND WAKE SHEDDING FREQUENCY

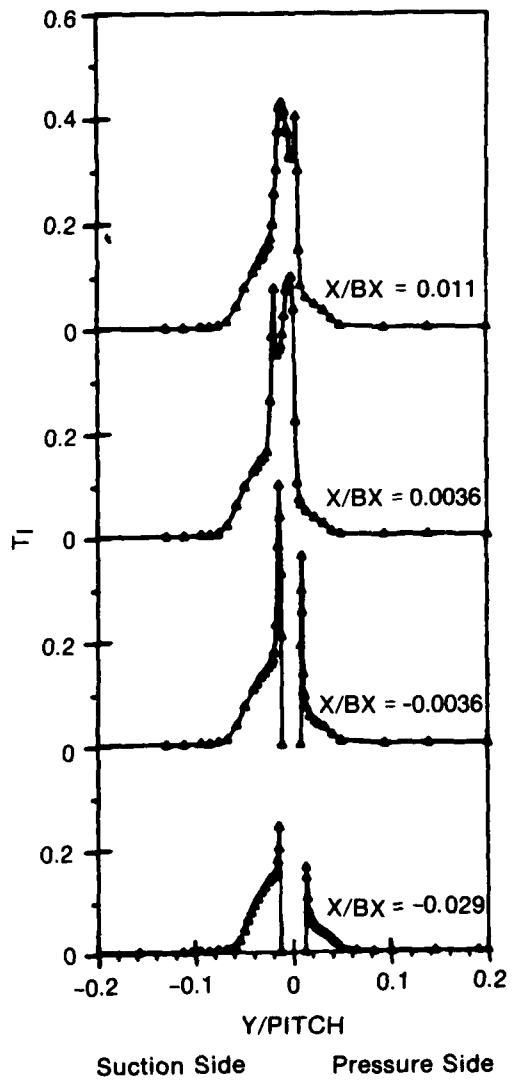
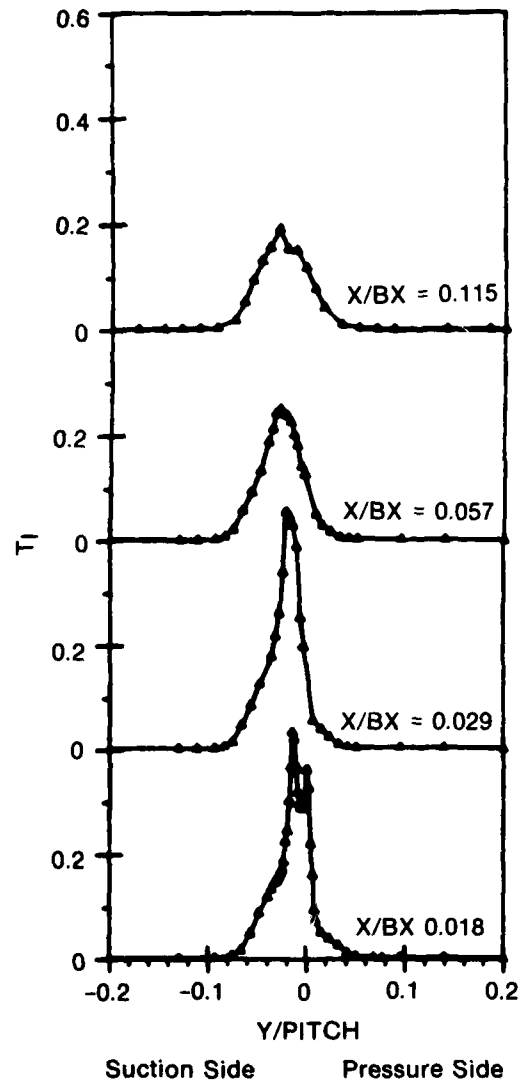
Turbulence intensity in Figures 23 and 24 was derived from measured linearized anemometer voltages. Turbulence intensity in this report is defined as the linearized voltage divided by the local time averaged linearized voltage. Both Builds I and II have turbulence intensities exceeding 40% in the near wake. The inner wake region of Build I near the trailing edge ($X/BX = 0.004, 0.012, 0.020$) has a local minimum in turbulence intensity. This effect was also observed by Lakshminarayana and Davino (Reference 20) who explained this phenomenon as zero turbulence intensities near the surface in the boundary layer profiles "being transformed into a free shear layer" as the flow passes the trailing edge. The Build II data presented here does not support this statement. Even though the closest turbulence intensity profiles in the wake resemble the boundary layer turbulence intensity profiles, only Build I has this decrease in the inner wake.

Caution must be exercised when interpreting turbulence intensities. In the large shear flow gradients at the edge of the wake, the probe remained fixed in space, while a small amount of wake flutter (i.e., Karman vortex strut) produced large variations in velocity and, thus, high readings. If a Lagrangian technique could be used (i.e., the probe follows the fluctuating wake), lower turbulence intensities would be measured because the probe would be in the same location relative to the wake and would not oscillate between high and low velocity regions.

FIGURE 23
TURBULENCE INTENSITY PROFIL



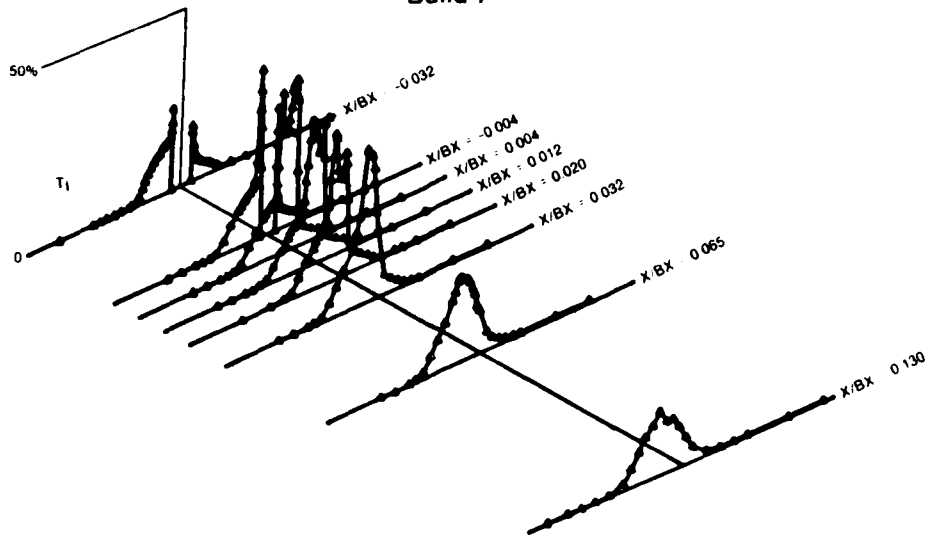
Turbulence Intensity Profiles
Build II



FD 201760

41/42

Build I



Build II

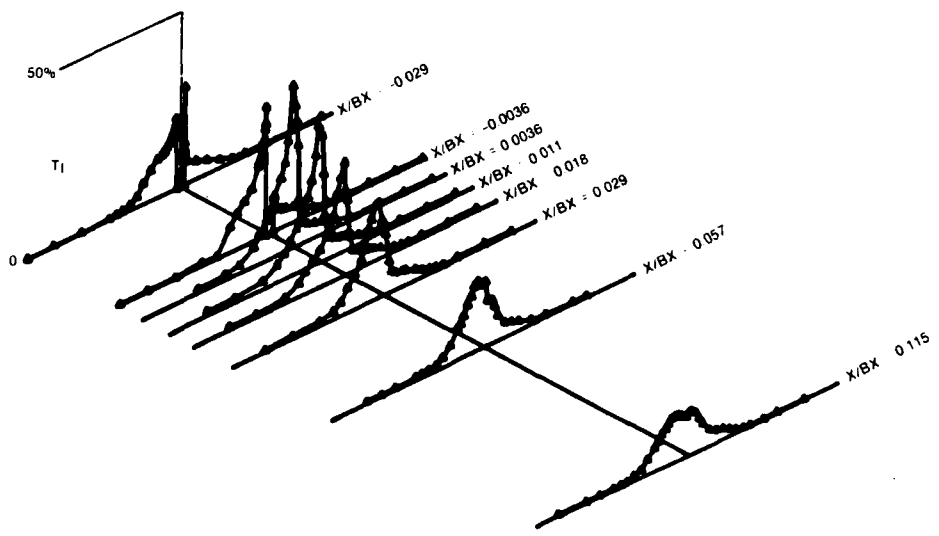


FIGURE 24
NEAR WAKE HOT-FILM LOCAL TURBULENCE INTENSITY - BUILDS I AND II

The amount of time the probe spends in the turbulent wake compared to the time in the laminar outer wake can be referred to as an intermittency factor. This intermittency effect, explained by Lin (Reference 21) was evident on an oscilloscope during data acquisition.

Turbulence spectra were acquired at selected locations to determine the shedding frequency of the trailing edge Karman vortices. Approximate shedding frequencies were determined from the Strouhal number of a circular cylinder and defined using the trailing-edge diameter (TED) as the characteristic length and the free stream velocity (FSV), as follows. FSV is defined in Figure 25.

$$S = \frac{\text{TED}(f)}{\text{FSV}} = 0.21$$

$$f_{\text{BUILD I}} = 1775 \text{ Hz}$$

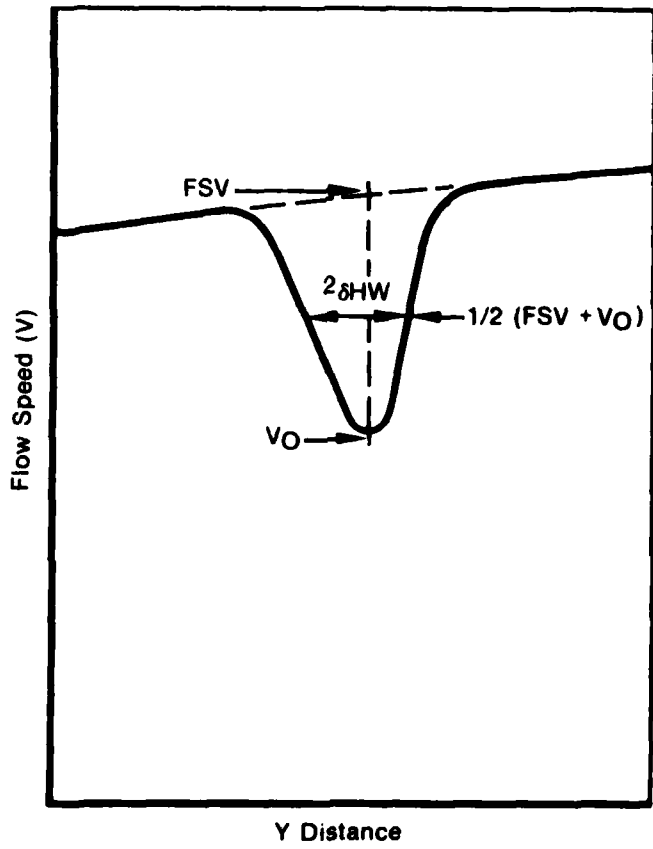
$$f_{\text{BUILD II}} = 4850 \text{ Hz}$$

Two typical plots are shown in Figure 26 for Builds I and II. Both were recorded near the trailing edge on the pressure side of the wake. The Build I spectrum indicates an increase in turbulence level caused by vortex shedding for frequencies between 1500 and 2200 Hz. The vortex shedding in Build I was most prominent in the two traverses made downstream of the low velocity region near trailing edge ($X/BX = 0.032, 0.065$). The Build II turbulence spectra does not indicate that the Karman vortex shedding was occurring.

Vortex shedding has been measured in the wakes of a high-speed turbine plane cascades with thick trailing edges by Lawaczeck (Reference 22), Heinemann (Reference 23), and by Sieverding (Reference 24). The results of the current experiment for Build I are similar. It may be conjectured that the lack of a predominant shedding frequency in Build II is due to the small size of the trailing edge relative to the boundary layer.

WAKE VELOCITY PROFILE SIMILARITY AND INTEGRAL PARAMETERS

Wake velocity shape similarity profiles for the five-hole probe and hot-film traverses are shown in Figures 27 and 28. The profiles



FD 201762

FIGURE 25
WAKE NOMENCLATURE

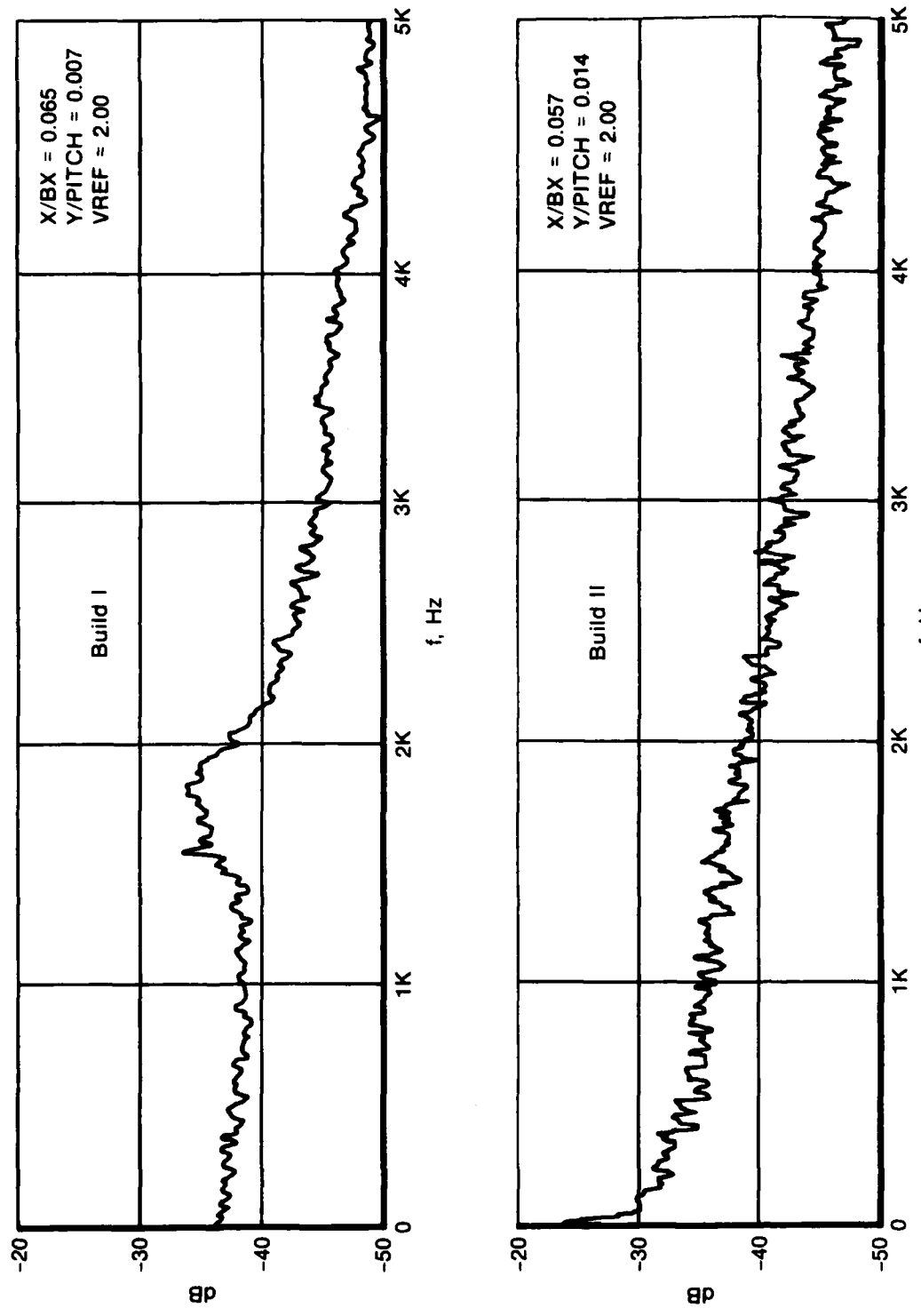


FIGURE 26
FREQUENCY SPECTRUM PROFILES - BUILDS I AND II
Frequency Spectrum Profiles

FD 201763

FIGURE 27
UNIVERSAL WAKE PROFILE (FIVE-HOLE PROBE)

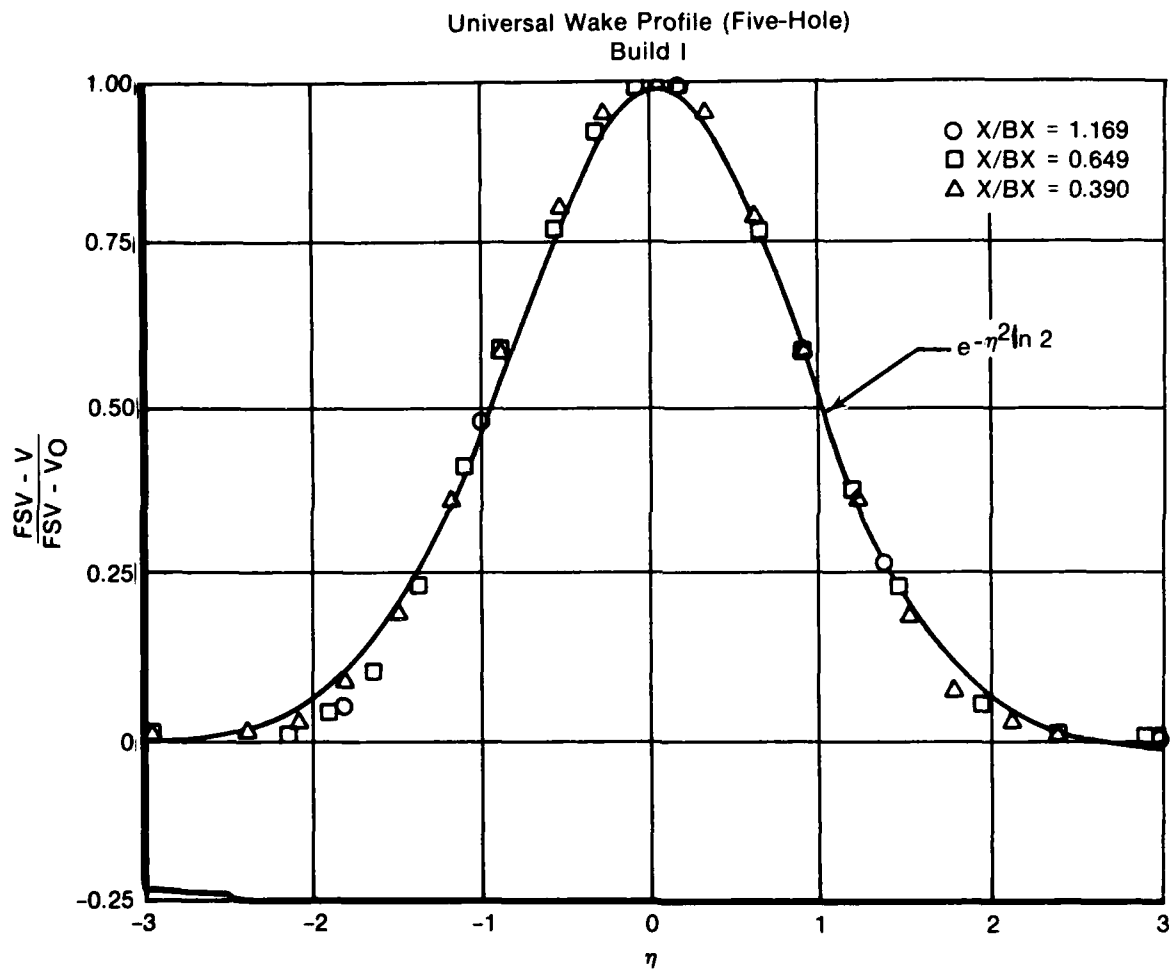
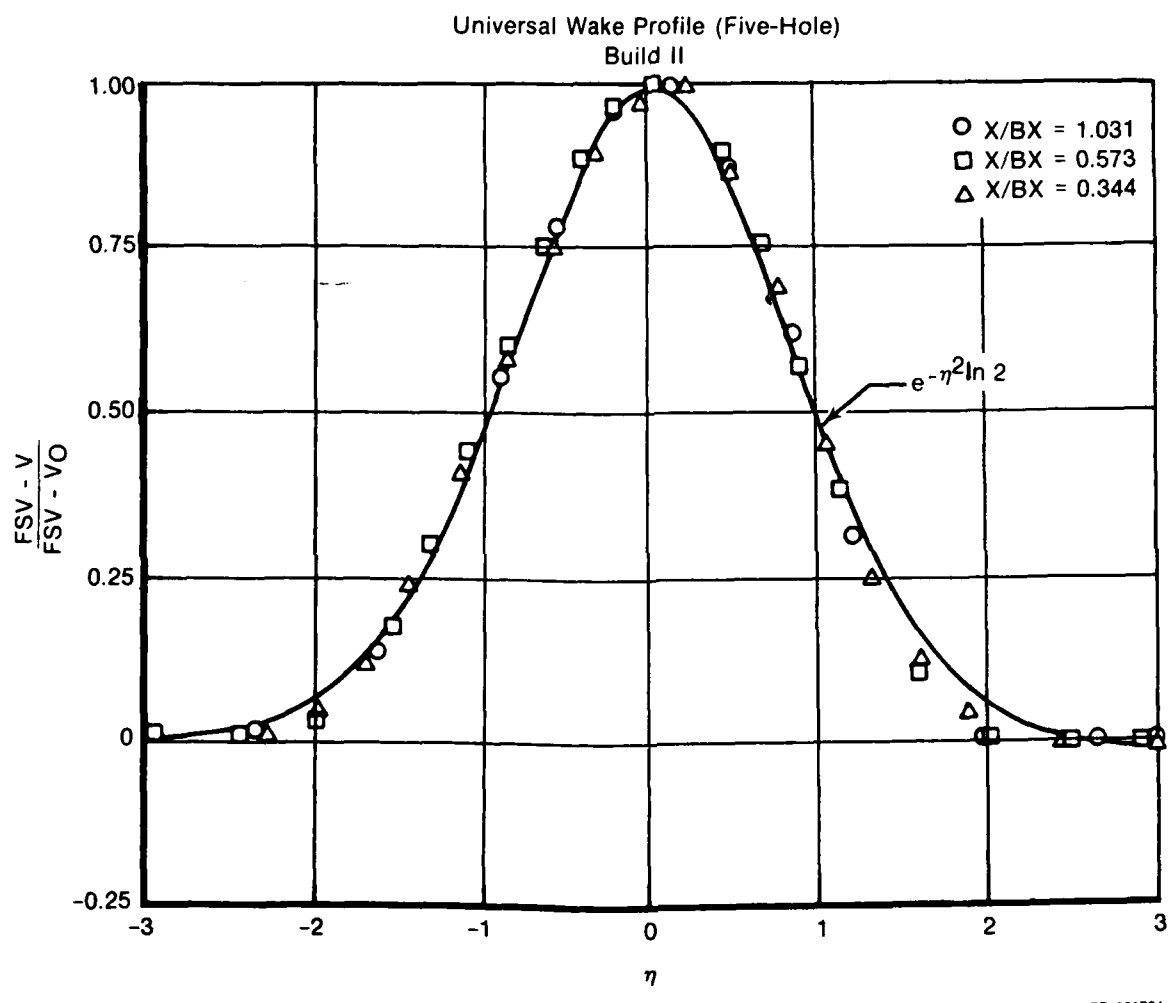


FIGURE 27
WIRE PROBE DATA - BUILDS I AND II



FD 201764

FIGURE 28
UNIVERSAL WAKE PROFILES (HOT-FILM PROBE)

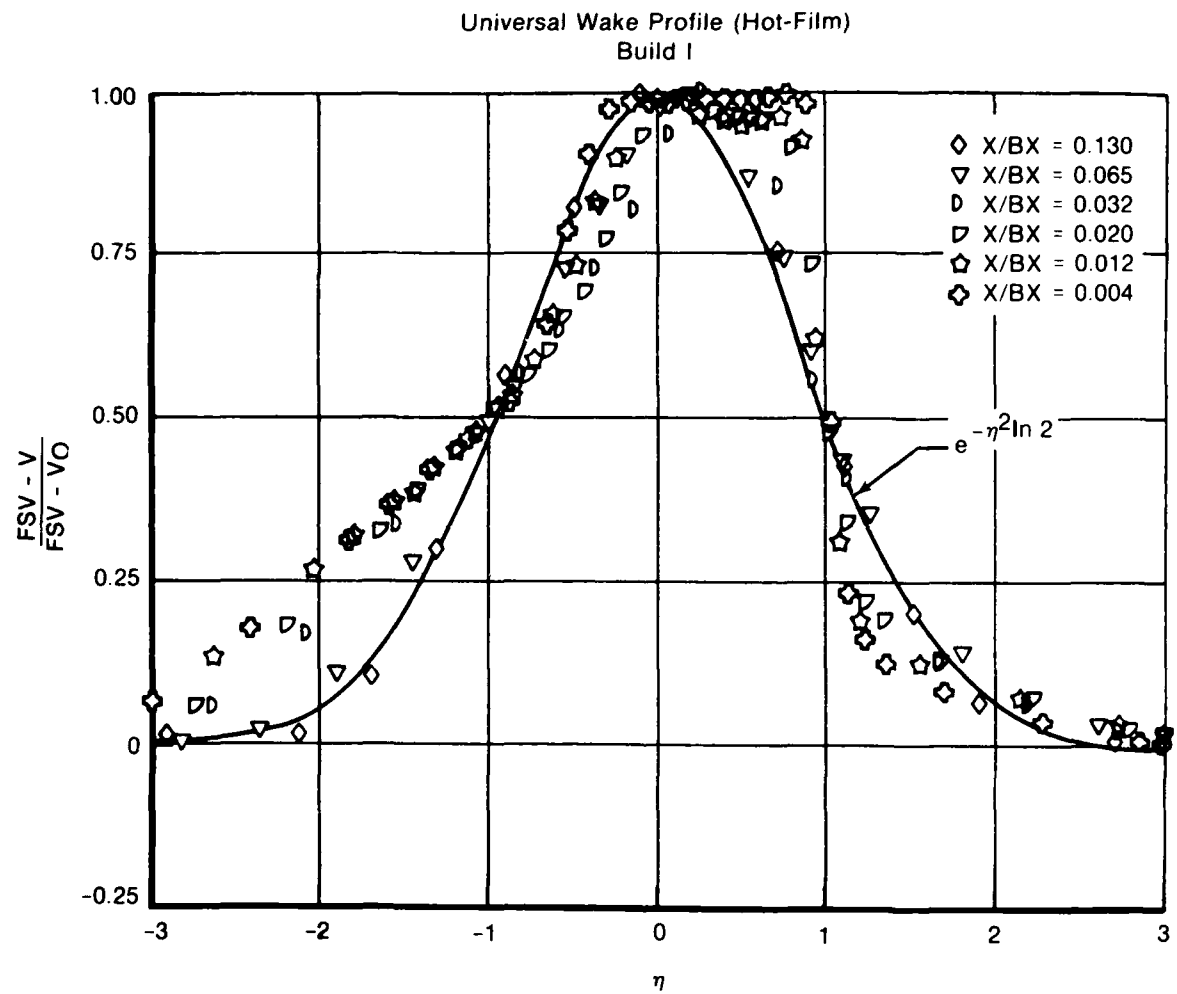
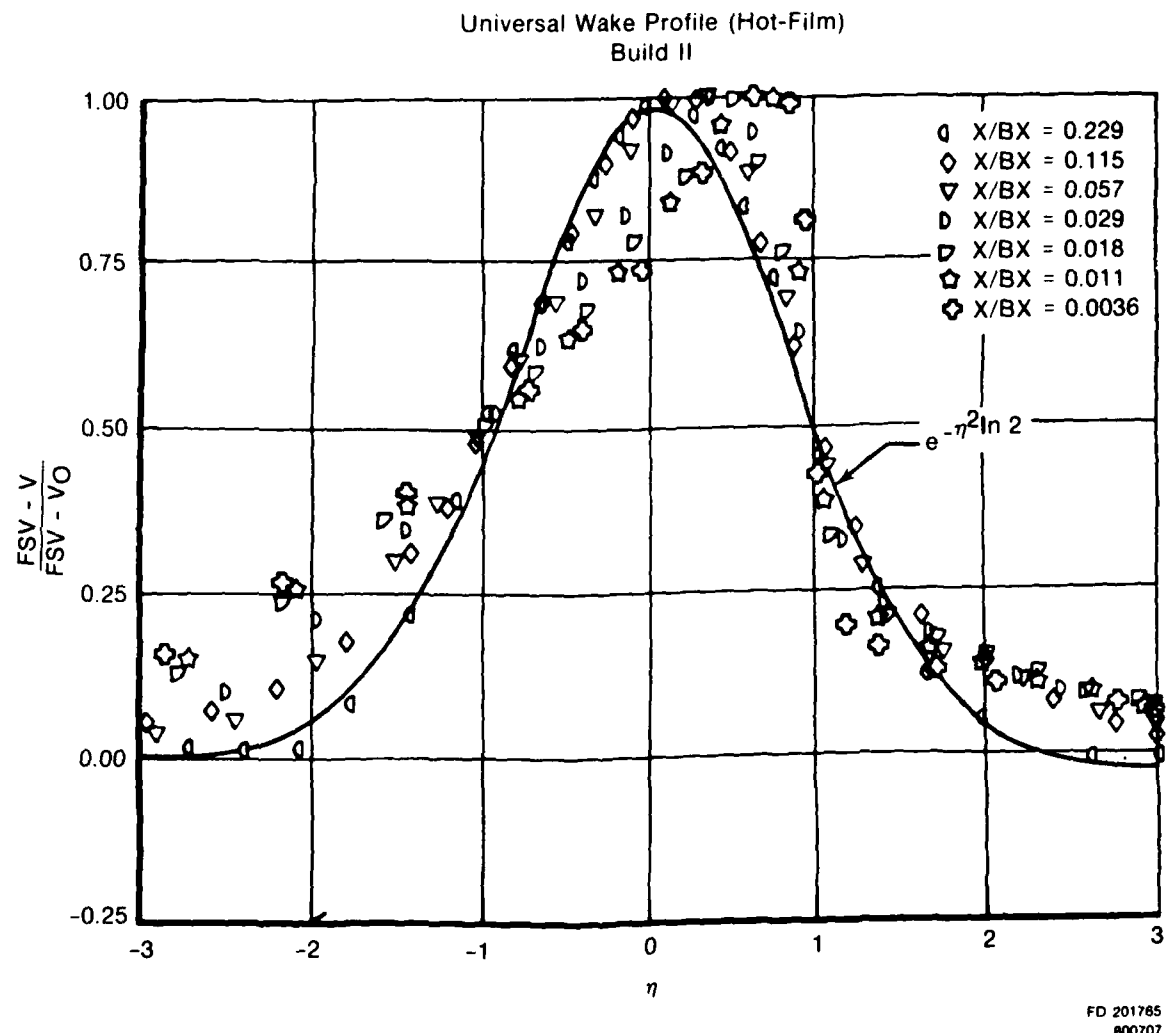


FIGURE 28
HOT-FILM PROBE DATA - BUILDS I AND II



were normalized by the wake half-width. The fit used in Reference 20 ($e^{-n^2 \ln 2}$) is excellent for the far downstream traverses (i.e., $X/BX > 0.057$). As expected, however, the near wake traverses do not fit this universal wake shape.

Wake parameter mass averages performed over a cascade pitch did not indicate any appreciable changes in total pressure loss, static pressure, normalized velocity, or turbulence intensity versus downstream distance.

Wake parameters, including wake half-width (δ_{HW}), displacement thickness (δ^*), momentum thickness (θ), shape factor (δ^*/θ), and wake minimum time average normalized velocity (V_{CL}/FSV) are plotted versus X/BX in Figure 29. Data from the five-hole, Kiel, and hot-film traverses are presented. Velocities from the Kiel results were calculated assuming an atmospheric static pressure. This assumption was justified by the five-hole data.

Both builds have similar wake half-widths near the trailing edge. The build II width increases slightly more rapidly with increasing distance from the trailing edge. If the boundary layer thickness half-widths are summed with the trailing-edge diameter, the result will form a continuous line instead of having a step at $X/BX = 0$.

The Build I displacement thickness in the very near wake is substantially larger than for Build II, due to the low momentum region which acts like an extension of the airfoil's larger trailing edge. Even though Build I has a larger displacement thickness at the trailing edge, both builds are similar at the far downstream positions, asymptotic to almost the same value of $\delta^*/PITCH = 0.01$. Again, if the trailing-edge diameter is added to the boundary layer displacement thickness data, a more continuous function is formed.

The normalized momentum thickness plots for both builds are similar in shape and magnitude. Build II has slightly larger thicknesses in the near wake, but both builds have similar values far downstream.

Shape factor δ^*/θ data for both builds reflect the displacement and momentum thickness data and the decay of the velocity defect. As expected, the value of shape factor decays asymptotically to 1.0 as the wakes mix out.

FIGURE 29
BOUNDARY LAYER AND WAKE INTEGRAL PARAMETERS

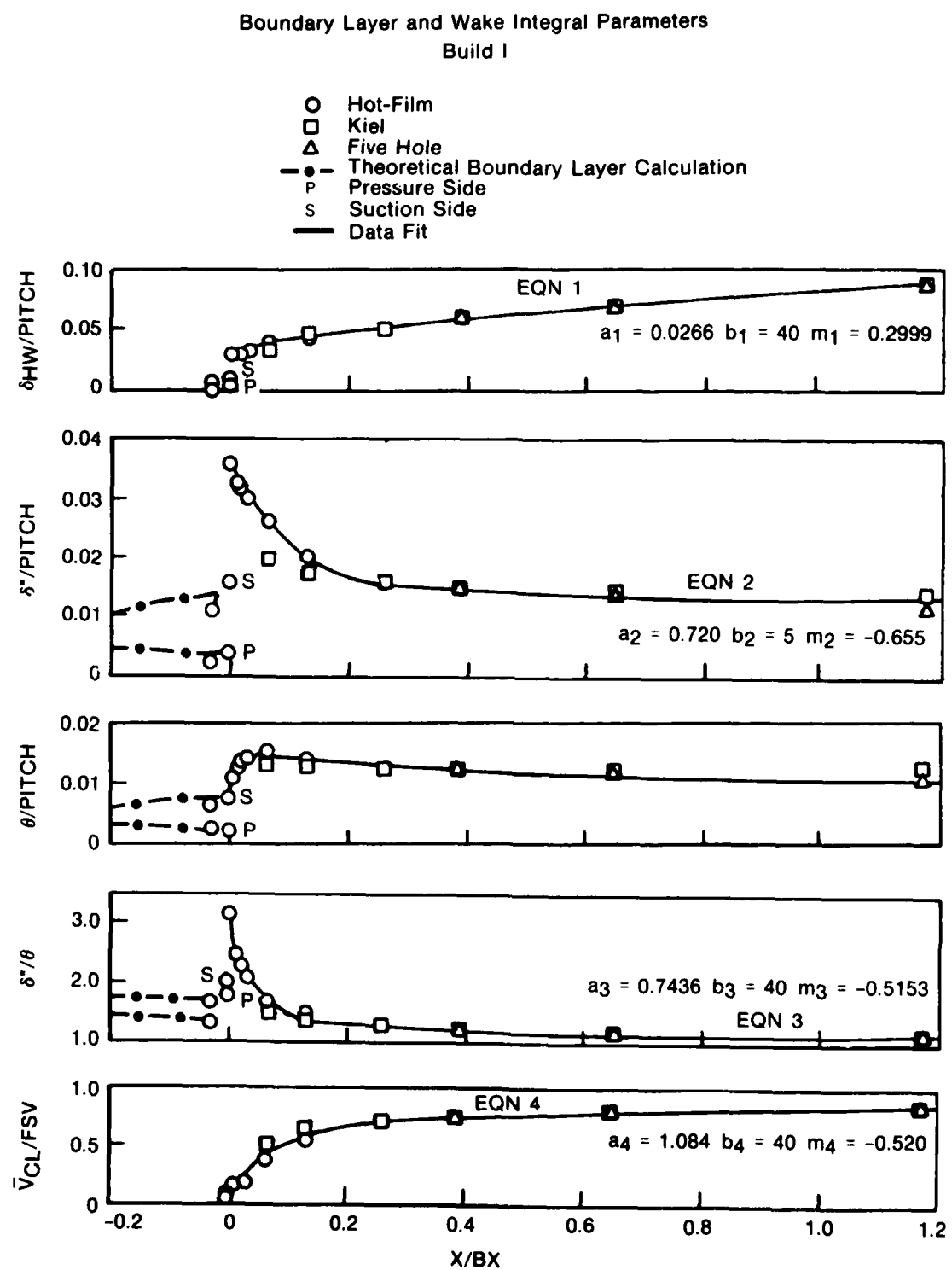
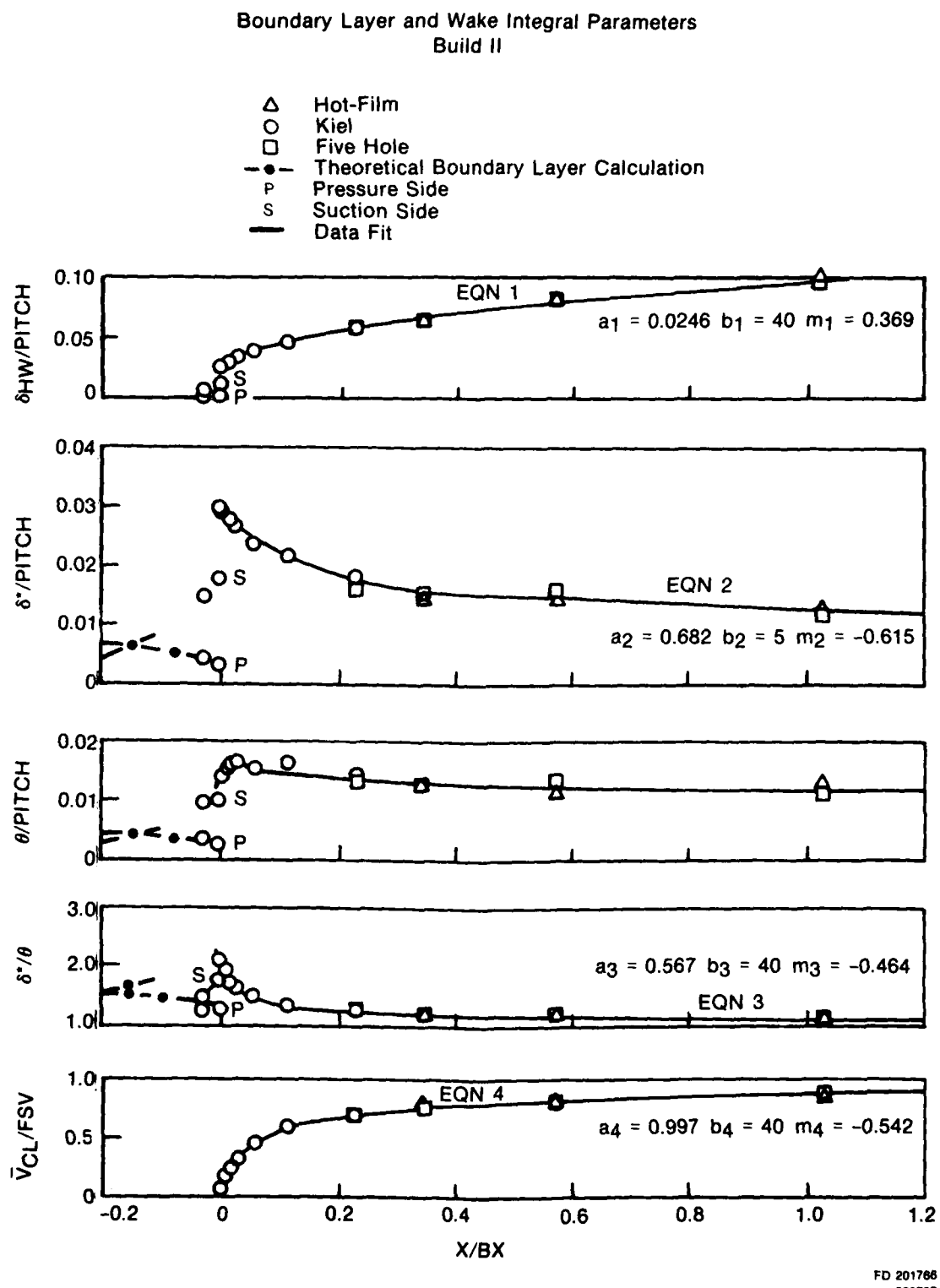


FIGURE 29
INTEGRAL PARAMETERS - BUILDS I AND II



The minimum wake velocity data for Build I, in contrast to the Build II data, shows an apparent shifting of the plotted data in the positive x-direction. The apparent trailing edge has been shifted downstream due to the recirculation region. Also, the Build II data are slightly higher than Build I, indicating Build II wakes mix faster than Build I.

It is believed that the more rapid mixing of the Build II wake is due primarily to the airfoil's thinner trailing-edge diameter. This difference in wake behavior is not a result of the airfoil boundary layers, since they are very similar on an integral thickness basis for the two airfoils. In fact, the total boundary layer momentum thickness (pressure and suction) at the airfoil trailing edge (and even the momentum thickness to chord ratio) is slightly larger for Build II than for Build I. Had the airfoil trailing-edge diameters been the same, one would have expected the Build II wake defect to mix out more slowly. The fact that the opposite occurred must be attributed to the thinner Build II trailing edge.

The computed boundary layer results from Reference 17 generally agree well with measured data. The suction side prediction for Build II did not reach the trailing edge. The calculations were begun as laminar flow from the leading edge. When the skin friction went to zero, the calculation was "tripped" to turbulent flow, holding the boundary layer momentum thickness constant through transition. The suction side calculation predicted separation at the 90% axial chord location for Build II. The trip locations are tabulated as follows:

Boundary Layer Transition Location (X/BX)

	<u>Build I</u>	<u>Build II</u>
Suction Side	0.28	0.56
Pressure Side	0.15	0.24

Each set of wake parameter data was fit to equations listed below. The forms of these equations were derived from those presented in References 19 and 20. The exponents determined for wake centerline velocity and, to a lesser extent, wake width decay rate agree with exact solutions presented in Schlichting (Reference 25) for an isolated two-

dimensional wake.

$$\delta_{HW}/PITCH = a_1(b_1(X/BX) + 1)^{m_1} \quad (1)$$

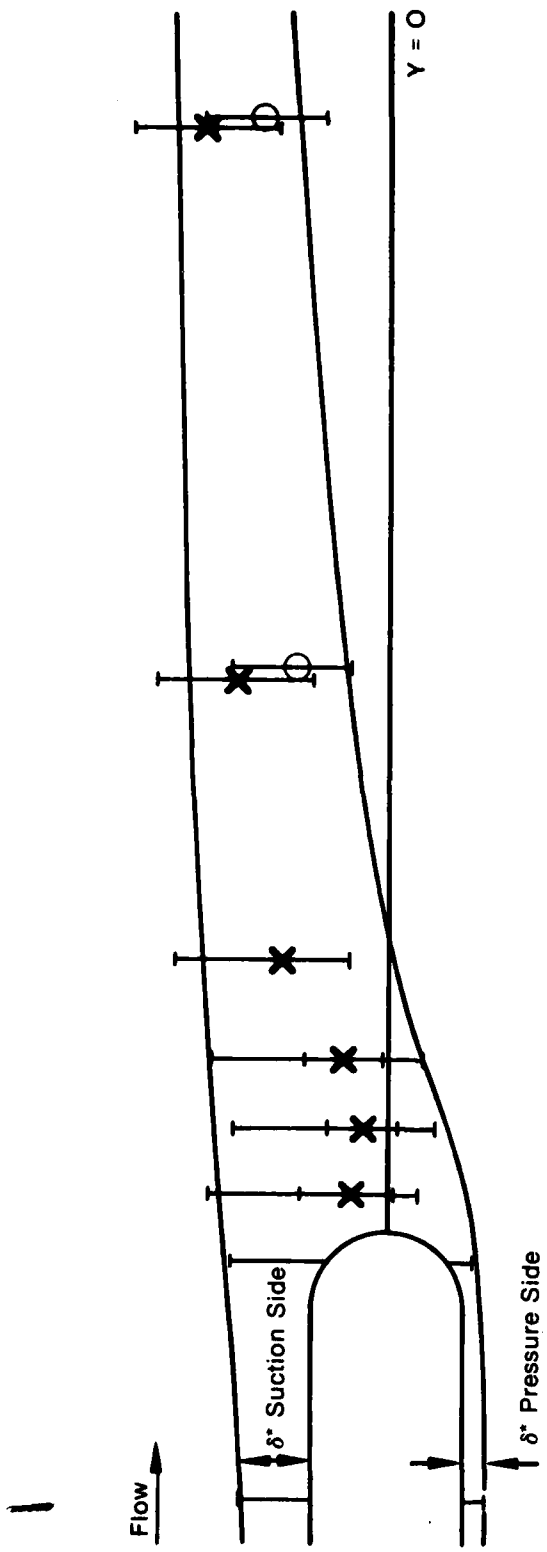
$$1 - \frac{0.01}{(\delta^*/PITCH)} = a_2(b_2(X/BX) + 1)^{m_2} \quad (2)$$

$$1 - \frac{1}{\delta^*/\theta} = a_3(b_3(X/BX) + 1)^{m_3} \quad (3)$$

$$1 - \frac{V_o}{FSV} = a_4(b_4(X/BX) + 1)^{m_4} \quad (4)$$

$\theta/PITCH$ was determined from the δ^*/θ and $\delta^*/PITCH$ fit calculations. Shown in Figure 29 are the fitted curves and the associated constants. When comparing the fit results, it is valuable to realize the constant (a) is an initial value term at $X/BX=0$, and the exponent (m) and constant (b) are related to decay rate. The value of b was chosen and the other constants determined by a least squares fit. The constant (a) can be approximated from the boundary layer prediction calculations to give acceptable results.

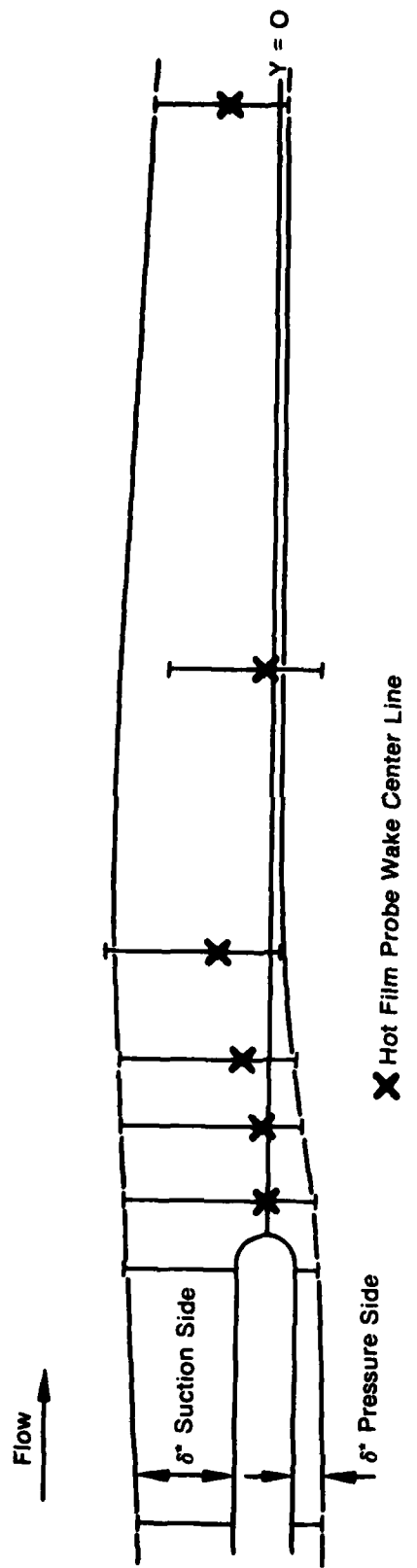
The location of the wake centerline and displacement surface is of particular interest when wake modeling is considered. The location of the far wake was well-defined by these experiments. The far wakes are convected at the mean flow angle which remains nearly constant. The near wake centerline was less well-defined due to the smaller scale in this region relative to the trailing edge. There is considerable scatter, especially in Build II, in the locations of the near wake centerline. Build I had the additional complexity of the wide low-velocity region. An estimate of the locus of wake centerline points is shown in Figures 30 and 31. Adding the boundary layer and wake displacement thickness onto this line provides a continuous displacement body, also shown in Figures 30 and 31. The most notable characteristic of these displacement surfaces in the near wake is the curvature on the pressure side. These displacement surfaces will be used in conjunction with an inviscid analysis and validity of this model will be discussed in the next section.



X Hot Film Probe Wake Center Line
 O Kiel Probe Wake Center Line

FD 19787

FIGURE 30
WAKE LOCATION - BUILD I



FD 19790

FIGURE 31
WAKE LOCATION - BUILD II

SECTION V

ANALYTICAL WAKE MODELS

The major objective of the analytical phases of this program was to model the viscous flow in both the near- and far-wake regions in an inviscid cascade flow calculation. The most efficient cascade flow calculations for transonic flow use the potential flow model. Both Ives (Reference 9) and Caspar (Reference 16) offer computations of this type. Modeling viscous effects and retaining the potential flow model require adjusting the streamlines around the actual body to create a new displacement surface containing the viscous flow blockage and curvature effects. This streamline adjustment can be accomplished by either of two equally accurate methods. First, a non-zero velocity (airfoil surface blowing) boundary conditions may be imposed on the potential solution or, second, a new displacement body may be used with the usual zero normal-velocity boundary conditions. For this study, the second approach was taken.

WAKE MODELS

Two cases were studied for Build I: the first using the experimentally measured wake displacement surface location and a second using a wake displacement surface constructed with some of the experimental information and supplemented with a free shear layer calculation. For both cases, the imposed upstream and downstream conditions were derived from the test data. Upstream conditions were determined from an integration of the five-hole probe traverse data; the downstream angle was taken to be determined by the far wake trajectory.

In the first approach, a displacement body was constructed which had the shape of the combination of the airfoil shape, the computed blade boundary layer, and the measured wake displacement thickness. This body is shown in Figure 32. The pressure distribution for this displacement body was calculated using Caspar, and is plotted in Figure 32. The plot indicates that there is a considerable amount of loading in the wake region, as shown by the shaded area at the trailing edge. This large loading results from the near wake curvature, immediately aft of the trailing edge. It is possible that either the wake displacement surface, as defined by the absolute y-coordinate, is not correct in the

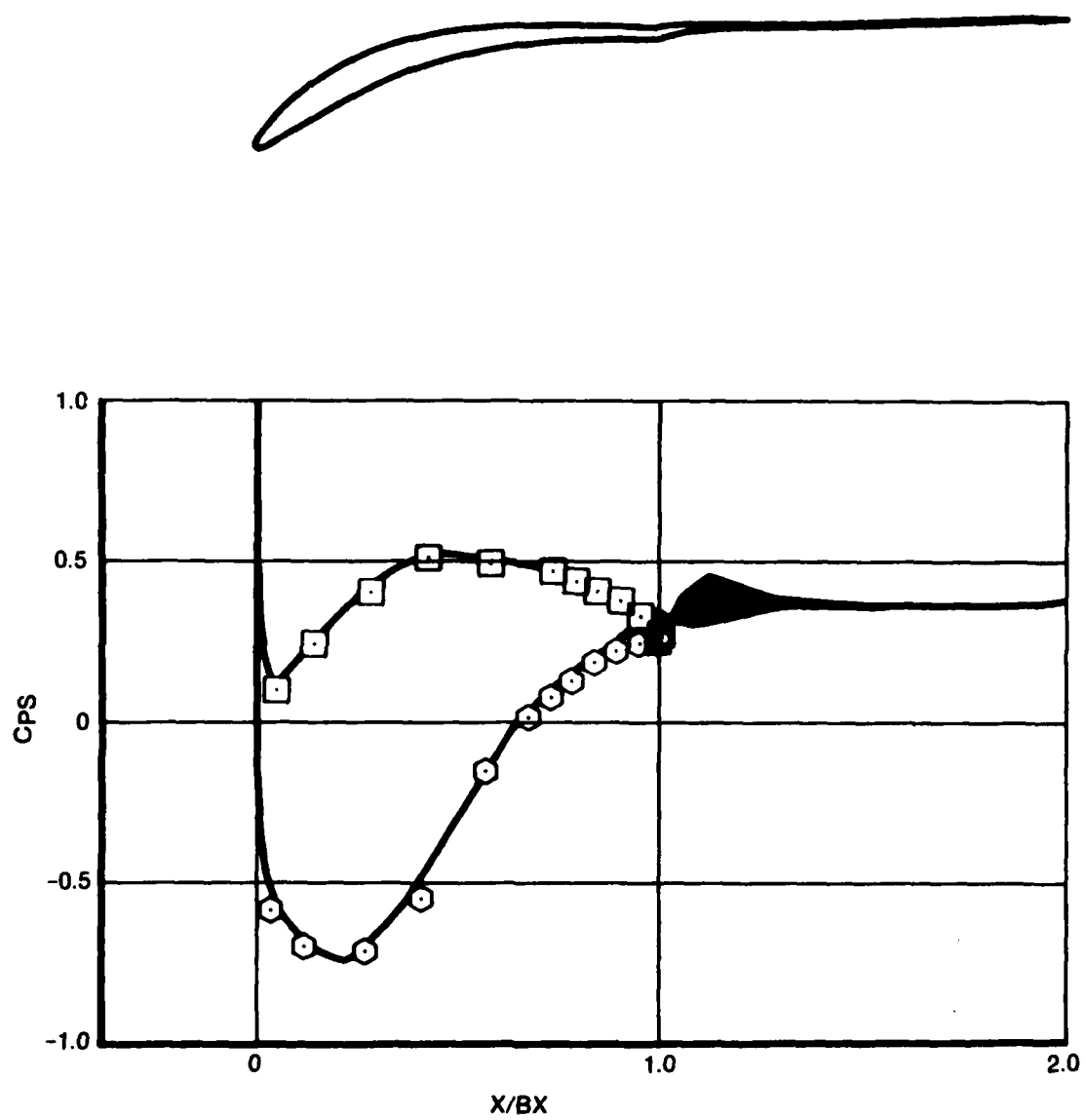


FIGURE 32
MEASURED DATA WAKE MODEL AND PRESSURE DISTRIBUTION

near wake or the model is inadequate. More accurate near wake measurements would be required to resolve this.

In the second approach, an initial displacement body was first constructed which was the combination of the blade shape, the stagnation streamline calculated by analyzing the blade alone, and a cusp-shaped base region which was added symmetrically to the stagnation streamline immediately aft of the blade trailing edge. The resulting body and the computed pressure distribution for this case are shown in Figure 33. This figure indicates that there is nearly no loading in the wake region.

This pressure distribution was then used with very fast integral boundary/shear layer calculation to compute displacement thicknesses. These thicknesses were added to the initial body to construct the final displacement body. The laminar calculation is based upon the method of Gruschwitz (Reference 25); the turbulent solution is the lag-entrainment method of Green, et. al., (Reference 26). The computed results for the displacement and momentum thicknesses, both normalized by cascade pitch, are plotted in Figures 34 and 35, along with the experimentally measured values. As can be seen, there is good agreement both before the trailing edge ($X/BX < 0$) and in the far wake region ($X/BX > 0.1$). There is some disagreement, however, between the measured and predicted variations in the near wake region. The final body and pressure distributions are shown in Figure 36 compared with the measured static pressure data.

PROFILE LOSS

Using the wake integral parameters, the mixed out profile loss was then calculated using the control volume calculation of Stewart (Reference 11). The aerodynamic conditions at various axial chord locations downstream of the actual airfoil were used. In each case, the computed profile loss (ω_2) was 0.017. This is in agreement with the experimentally measured value for the Kiel probe. Angle changes due to mixing for this axial exit angle case are negligible.

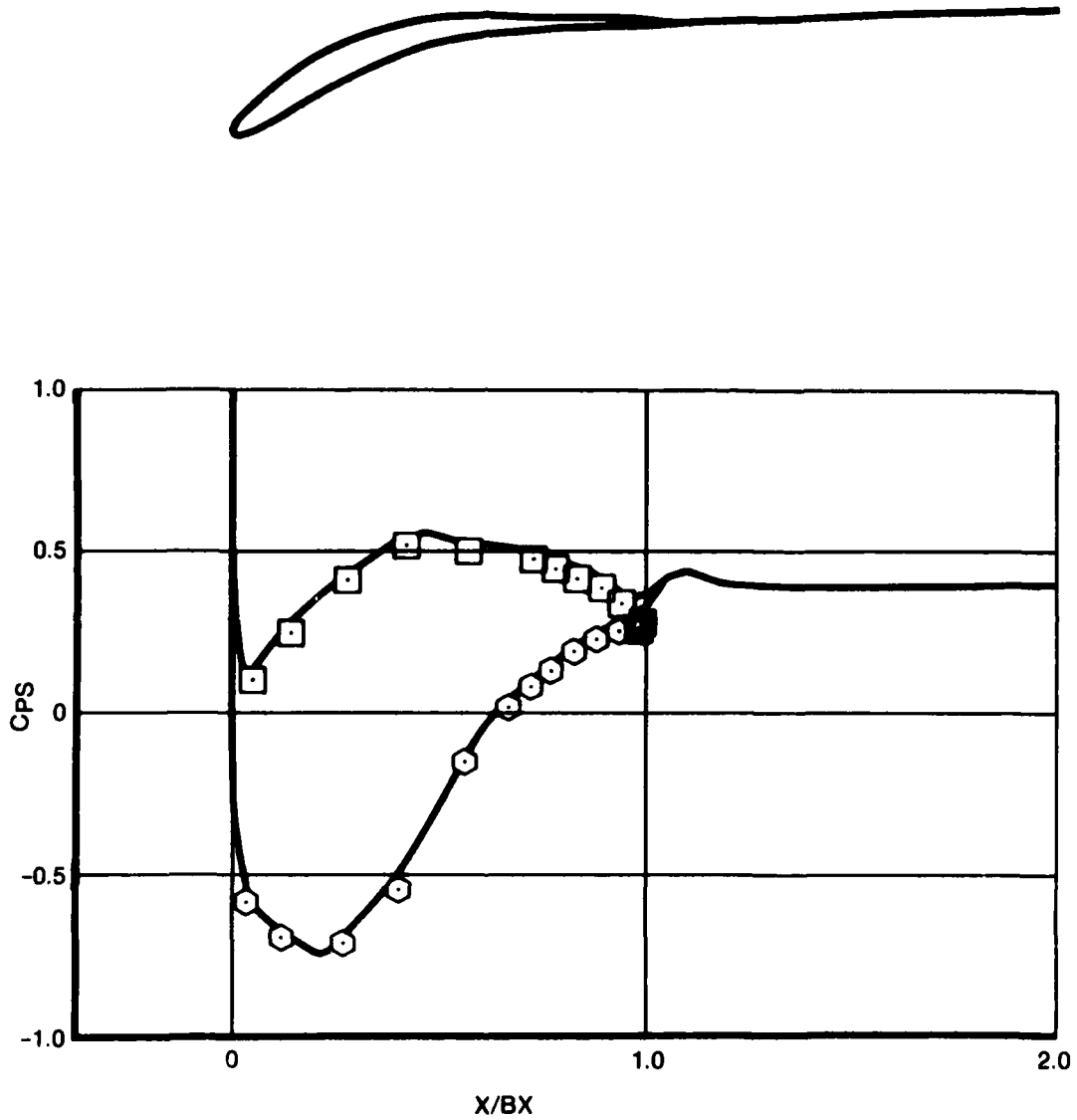


FIGURE 33
CONTRUCTED INITIAL WAKE MODEL AND PRESSURE DISTRIBUTION

FD 197990

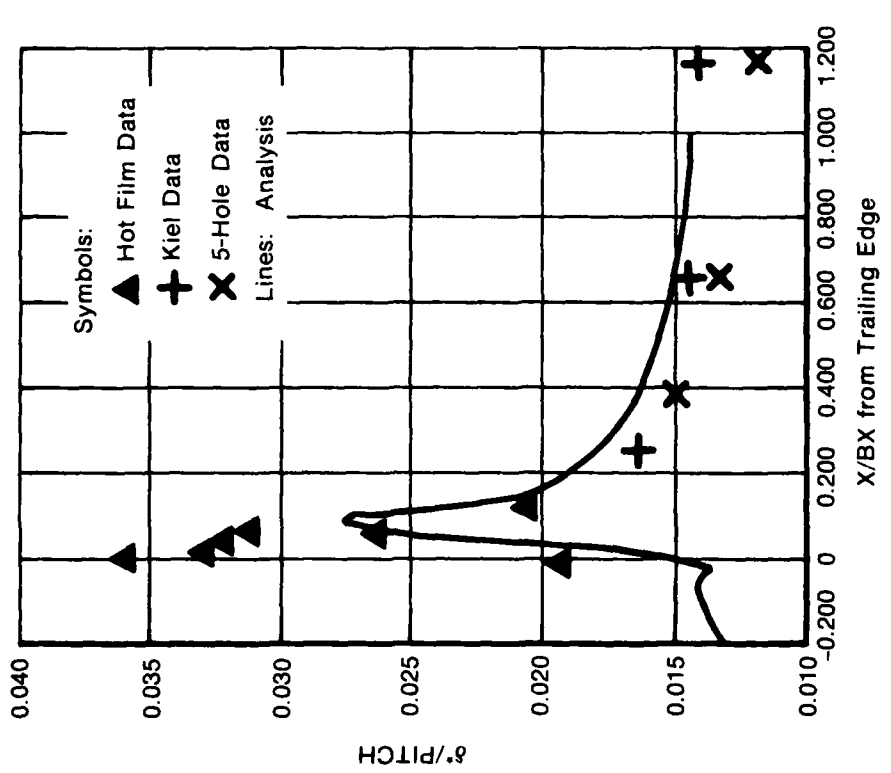


FIGURE 34
COMPUTED DISPLACEMENT THICKNESS
FOR BOUNDARY LAYER AND WAKE

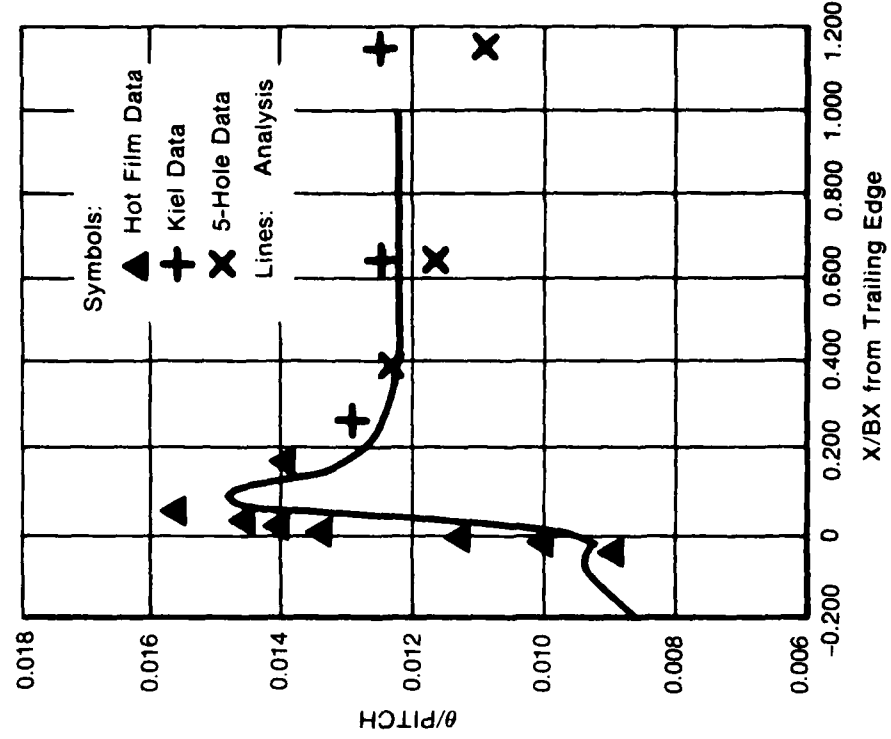
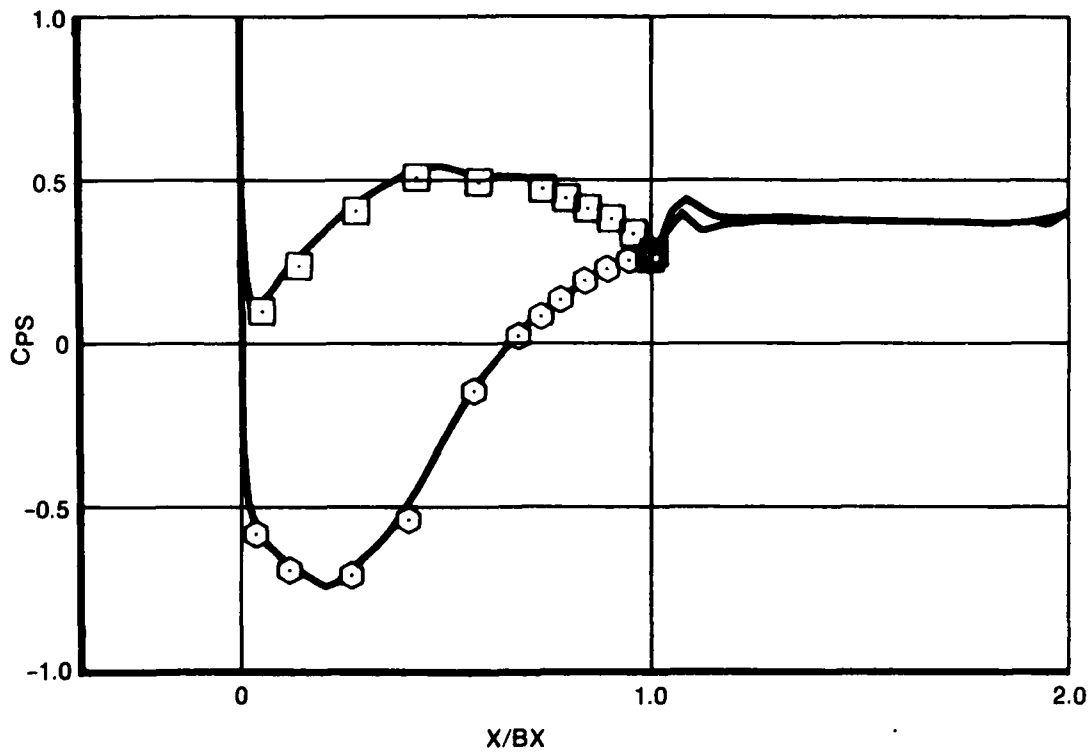


FIGURE 35
COMPUTED MOMENTUM THICKNESS
FOR BOUNDARY LAYER AND WAKE



FD 197993

FIGURE 36
CONTRUCTED FINAL WAKE MODEL AND PRESSURE DISTRIBUTION

FLOW TURNING

As is well known, a potential flow solution about a body is unique only if the circulation is specified. For cascade flows with specified upstream conditions, this implies the imposition of either the downstream conditions or a local trailing-edge condition. As mentioned before, this is more fully discussed in the review by Klein (Reference 13). The local trailing-edge condition which has the most experimental verification is that the static pressures are equal on the suction and pressure sides at the trailing edge prior to separation. The data taken for Builds I and II confirm this equal pressure condition, as shown in Figure 14 and Table 3. It must be emphasized that this is a viscous flow condition. With large, rounded trailing edges, this condition has not been reliably implemented to predict flow turning because the computed inviscid flow is a very inaccurate representation of the true trailing-edge viscous flow. The improvements in accuracy at the trailing edge in the inviscid calculations which include a wake model should improve the accuracy of these turning calculations. More work is required to verify this.

SECTION VI

CONCLUSIONS

- The desired aerodynamic conditions were achieved for the wake experiment. Excellent cascade flow periodicity and two-dimensionality were achieved for both builds. Surface pressure distributions and boundary layer behavior of both airfoils provided the desired airfoil trailing-edge conditions for the wake experiments.
- Profile losses and flow turning computed from far downstream traverses agree well with the high-speed data taken in the DFVLR tunnel. Thus, the low-speed test can be used to model the viscous effects present in shockless high-speed flow.
- Far wake velocity profiles were found to satisfy a universal wake function. Although trailing-edge conditions for each of the airfoils were quite different, the far wakes are very much alike. The cascade airfoil far wake velocity profiles develop in a way similar to those of isolated airfoils.
- Near wake velocity profiles look similar to their respective boundary layer velocity profiles. Therefore, a universal wake function was not found for the near wake velocities.
- Von Karman vortex shedding was found to occur in the near wake of the Build I airfoil, but not for the Build II airfoil. The Strouhal number was approximately 0.21. The reason for this difference may be related to the small size of the Build II trailing-edge relative to the boundary layer.
- The wake flow was highly turbulent with a wide band of frequencies present for both builds. The shedding frequency was not a dominant feature of the flow and appears not to effect the mean velocity profiles in the far wake.
- The viscous flow effects in cascade wakes can be approximately modeled in potential flow calculations with a displacement body. More accurate experimental information is required to gain confidence in the details of the near wake model.

- The use of a wake model eliminates the trailing edge stagnation point in the inviscid calculation and resulted in a considerably more realistic flow in the trailing edge plane. Losses and angles consistent with measured data were computed with a wake mixing calculation.
- The use of a wake model should improve the accuracy of flow turning predictions based on a local trailing edge pressure condition.

APPENDIX
TABLES OF EXPERIMENTAL RESULTS

Tables 4 through 11 detail the data generated in this experimental investigation to analytically model the viscous wake in an inviscid potential flow calculation.

TABLE 4. TABULATION OF FIVE-HOLE TRAVERSE DATA

BUILD I

X/BX = 0.390

Pt	Y/PITCH	CPT	CPS	YAW	PHI	VEL/FSV
1	-.5750	-.001	.330	3.383	-1.639	1.003
2	-.4857	.002	.330	3.295	-1.799	1.005
3	-.3964	.002	.331	3.291	-1.708	1.005
4	-.3518	.001	.333	3.193	-1.633	1.001
5	-.3071	.000	.329	3.032	-2.101	1.003
6	-.2714	-.003	.331	3.008	-1.735	1.000
7	-.2357	-.003	.332	3.010	-1.787	.998
8	-.2000	-.001	.333	3.013	-1.837	.999
9	-.1643	-.001	.330	3.126	-2.088	1.001
10	-.1464	-.009	.333	3.104	-1.777	.997
11	-.1286	-.002	.333	3.009	-1.761	.997
12	-.1107	-.001	.333	2.816	-1.673	.999
**						
13	-.1018	-.008	.331	2.815	-1.664	.995
14	-.0929	-.023	.330	2.342	-1.677	.985
15	-.0839	-.059	.333	2.910	-1.663	.954
16	-.0750	-.110	.334	2.251	-1.760	.913
17	-.0661	-.171	.336	2.355	-1.918	.859
18	-.0571	-.230	.337	2.372	-2.129	.805
19	-.0482	-.267	.336	2.751	-2.138	.771
20	-.0393	-.281	.335	2.841	-2.077	.757
21	-.0304	-.268	.335	3.385	-1.703	.771
22	-.0214	-.228	.336	3.385	-1.702	.809
23	-.0125	-.177	.331	3.663	-1.277	.859
24	-.0036	-.115	.331	3.665	-1.142	.912
25	.0054	-.063	.328	3.763	-.986	.954
26	.0143	-.028	.329	3.765	-.935	.981
27	.0232	-.008	.330	3.667	-1.053	.997
**						
28	.0321	-.002	.331	3.385	-.969	.998
29	.0500	-.002	.331	3.382	-1.089	.998
30	.0679	-.001	.331	3.384	-1.016	.999
31	.1036	-.002	.333	3.382	-1.072	.997
32	.1393	-.003	.331	3.385	-.959	.998
33	.1839	-.006	.330	3.384	-.992	.997
34	.2286	-.008	.327	3.387	-.893	.998
35	.3179	-.006	.329	3.380	-1.189	.997
36	.4071	-.005	.329	3.378	-1.443	.999
37	.5857	-.002	.329	3.284	-1.496	1.001
38	.6750	-.006	.327	3.295	-1.791	1.000

TABLE 4. TABULATION OF FIVE-HOLE TRAVERSE DATA
(Con't)

BUILD I

X/BX = 0.649

Pt	Y/PITCH	CPT	CPS	YAW	PHI	VEL/FSV
1	-.5750	-.002	.334	2.725	-1.756	1.001
2	-.4857	.001	.334	2.724	-1.738	1.002
3	-.3964	.002	.333	2.529	-1.600	1.003
4	-.3518	.000	.334	2.534	-1.720	1.000
5	-.2893	-.003	.336	2.530	-1.636	.998
6	-.2536	-.002	.333	2.535	-1.741	.999
7	-.2179	-.003	.334	2.531	-1.665	.998
8	-.2000	-.002	.335	2.531	-1.663	.998
9	-.1821	-.004	.333	2.534	-1.719	.998
10	-.1643	-.002	.335	2.531	-1.655	.997
11	-.1464	-.003	.332	2.439	-1.716	.998
12	-.1286	-.004	.332	2.434	-1.586	.998
**						
13	-.1196	-.013	.333	2.436	-1.652	.990
14	-.1107	-.033	.331	2.246	-1.633	.975
15	-.1018	-.062	.331	2.060	-1.710	.953
16	-.0929	-.102	.332	2.063	-1.778	.921
17	-.0839	-.144	.333	2.062	-1.763	.885
18	-.0750	-.182	.334	2.066	-1.842	.851
19	-.0661	-.212	.333	2.064	-1.805	.825
20	-.0571	-.229	.334	2.633	-1.811	.809
21	-.0482	-.232	.332	2.626	-1.672	.808
22	-.0304	-.182	.331	2.810	-1.379	.855
23	-.0214	-.141	.330	3.000	-1.269	.890
24	-.0125	-.097	.331	3.002	-1.144	.927
25	-.0036	-.058	.330	3.003	-1.112	.958
26	.0143	-.013	.334	2.814	-1.079	.993
**						
27	.0321	-.002	.330	2.813	-1.106	1.000
28	.0500	-.001	.335	2.814	-1.066	1.000
29	.0679	.001	.332	2.814	-1.083	1.001
30	.0857	-.004	.330	2.814	-1.061	.998
31	.1036	-.001	.330	2.816	-1.007	1.000
32	.1393	-.004	.328	2.817	-.980	.999
33	.1839	-.005	.330	3.008	-.915	.998
34	.2286	-.007	.330	2.818	-.929	.996
35	.3179	-.006	.329	2.717	-1.188	.998
36	.4071	-.004	.329	2.715	-1.327	.999
37	.4964	-.002	.329	2.716	-1.253	1.001
38	.5857	-.004	.329	2.715	-1.418	.999
39	.6750	-.003	.330	2.726	-1.779	.999

TABLE 4. TABULATION OF FIVE-HOLE TRAVERSE DATA
(Con't)

BUILD I

X/BX = 1.169

Pt	Y/PITCH	CPT	CPS	YAW	PHI	VEL/FSV
1	-1.2893	-.006	.328	3.000	-1.286	1.000
2	-1.2891	-.001	.330	3.095	-1.230	1.004
3	-1.2357	-.003	.332	3.003	-1.105	1.000
4	-1.1464	-.055	.327	2.624	-1.102	.964
5	-1.0929	-.175	.331	2.621	-1.314	.861
6	-1.0393	-.086	.331	3.379	-1.257	.936
7	-.9679	-.003	.330	2.905	-1.271	1.001
8	-.8607	.006	.331	2.905	-1.258	1.005
9	-.7536	.000	.329	2.715	-1.339	1.001
10	-.5929	.000	.329	2.822	-1.811	1.003
11	-.3964	.002	.331	2.717	-1.560	1.003
12	-.3250	-.003	.330	2.718	-1.582	1.001
13	-.2357	-.004	.331	2.720	-1.644	.999
**						
14	-.1643	-.015	.329	2.532	-1.682	.991
15	-.1286	-.091	.328	2.535	-1.748	.933
16	-.0750	-.172	.328	2.811	-1.517	.865
17	-.0214	-.052	.328	2.908	-1.120	.965
18	.0500	-.004	.325	2.816	-.990	1.002
**						
19	.1750	-.007	.327	2.913	-.929	.999
20	.3179	-.008	.327	3.000	-1.236	.999
21	.3950	-.004	.329	2.526	-1.265	1.000
22	.5143	-.006	.326	2.715	-1.400	1.000
23	.6750	-.006	.327	2.722	-1.707	.999
24	.7464	-.005	.325	2.719	-1.617	1.001
25	.8714	-.022	.326	2.528	-1.536	.989
26	.9250	-.183	.326	2.528	-1.555	.855
27	.9786	-.064	.325	2.530	-1.089	.957
28	.9964	-.026	.323	2.624	-1.082	.987
29	1.1036	-.003	.329	2.717	-1.167	1.004
30	1.2107	-.001	.324	2.716	-1.215	1.005

TABLE 4. TABULATION OF FIVE-HOLE TRAVERSE DATA

(Con't)

BUILD I

X/BX = -1.260

Pt	Y/PITCH	CPT	CPS	YAW	PHI	VEL/FSV
1	-2.900	-.004	-.069	38.326	-.893	1.000
2	-1.700	-.006	-.060	38.274	-.986	.995
3	-0.580	-.005	-.055	36.947	-.754	.991
4	0.580	-.006	-.034	38.881	-.749	.982
5	1.700	-.004	-.025	37.344	-.850	.978
6	2.900	-.001	-.099	38.408	-.267	1.014

TABLE 5. TABULATION OF KIEL TRAVERSE DATA

BUILD I

	X/BX = 0.065		X/BX = 0.130		
PT	Y/PITCH	CPT	PT	Y/PITCH	CPT
1	-.5750	.003	1	-.5750	-.013
2	-.4857	.005	2	-.4857	-.006
3	-.3964	.013	3	-.4411	-.013
4	-.3071	.003	4	-.3964	-.005
5	-.2179	.000	5	-.3518	-.006
6	-.1286	-.001	6	-.3071	-.005
7	-.1107	-.001	7	-.2179	-.003
8	-.0929	.002	8	-.1732	-.005
**			9	-.1464	-.005
9	-.0839	.001	10	-.1286	-.004
10	-.0750	-.004	11	-.1107	-.002
11	-.0661	-.019	**		
12	-.0571	-.073	12	-.0929	-.001
13	-.0482	-.166	13	-.0750	-.011
14	-.0393	-.248	14	-.0661	-.049
15	-.0357	-.291	15	-.0571	-.139
16	-.0321	-.325	16	-.0482	-.222
17	-.0286	-.361	17	-.0393	-.317
18	-.0250	-.404	18	-.0304	-.383
19	-.0214	-.441	19	-.0214	-.401
20	-.0179	-.463	20	-.0125	-.291
21	-.0143	-.464	21	-.0036	-.189
22	-.0107	-.438	22	.0054	-.094
23	-.0071	-.368	23	.0143	-.045
24	-.0036	-.310	24	.0321	-.013
25	.0000	-.231	**		
26	.0036	-.173	25	.0500	.003
27	.0071	-.115	26	.0857	.000
28	.0107	-.089	27	.1393	-.003
29	.0143	-.069	28	.2286	-.006
30	.0321	-.008	29	.2732	-.005
**			30	.3179	-.004
31	.0500	.001	31	.3625	-.007
32	.0946	.001	32	.4071	-.006
33	.1393	.003	33	.4964	-.006
34	.2286	.000	34	.5411	.000
35	.3179	-.003	35	.5857	.006
36	.4071	-.003	36	.6304	-.002
37	.4964	-.003	37	.6750	-.005
38	.5857	-.001			
39	.6750	-.001			

TABLE 5. TABULATION OF KIEL TRAVERSE DATA

(Con't)

BUILD I

X/BX = 0.260

X/BX = 0.390

PT	Y/PITCH	CPT	PT	Y/PITCH	CPT
1	-.5750	-.001	1	-.5750	-.002
2	-.4857	.004	2	-.4857	.010
3	-.4411	.001	3	-.3964	.004
4	-.3964	-.001	4	-.3518	.003
5	-.3518	.006	5	-.2714	.000
6	-.3071	.000	6	-.2357	.001
7	-.2179	-.006	7	-.2000	-.002
8	-.1732	.000	8	-.1643	-.003
9	-.1464	-.002	9	-.1464	-.005
10	-.1286	-.002	**		
**			10	-.1107	-.010
11	-.1107	-.009	11	-.0929	-.026
12	-.0929	-.007	12	-.0839	-.070
13	-.0750	-.059	13	-.0750	-.130
14	-.0661	-.137	14	-.0661	-.189
15	-.0571	-.210	15	-.0571	-.240
16	-.0482	-.276	16	-.0482	-.270
17	-.0393	-.314	17	-.0393	-.276
18	-.0304	-.312	18	-.0304	-.251
19	-.0214	-.268	19	-.0214	-.200
20	-.0125	-.187	20	-.0125	-.137
21	-.0036	-.116	21	-.0036	-.079
22	.0054	-.054	22	.0054	-.036
23	.0143	-.015	23	.0143	-.014
24	.0321	-.003	**		
25	.0500	.001	24	.0232	-.002
26	.0679	-.001	25	.0321	-.001
27	.0857	.002	26	.0500	-.001
28	.1393	.008	27	.0679	-.001
29	.1839	-.007	28	.1036	.000
30	.2286	-.006	29	.1393	-.002
31	.2732	-.006	30	.1839	-.004
32	.3179	-.007	31	.2286	-.004
33	.3625	-.009	32	.3179	-.007
34	.4071	-.006	33	.4071	-.005
35	.4518	-.003	34	.4964	.000
36	.4964	.005	35	.5857	-.003
37	.5857	-.005	36	.6750	-.003
38	.6750	-.003			

TABLE 5. TABULATION OF KIEL TRAVERSE DATA

(Con't)

BUILD I

X/BX = 0.649

X/BX = 1.169

PT	Y/PITCH	CPT	PT	Y/PITCH	CPT
1	-.5750	.000	1	-.4857	.002
2	-.4857	.001	2	-.3964	.002
3	-.3964	.001	3	-.3071	-.002
4	-.3071	.001	4	-.2179	.000
5	-.2714	.000	5	-.2000	-.004
6	-.2357	-.001	**		
7	-.2000	-.001	6	-.1821	-.007
8	-.1643	-.001	7	-.1643	-.020
9	-.1464	-.002	8	-.1464	-.052
**			9	-.1286	-.104
10	-.1286	-.010	10	-.1107	-.150
11	-.1107	-.044	11	-.1018	-.165
12	-.1018	-.076	12	-.0929	-.175
13	-.0929	-.122	13	-.0839	-.176
14	-.0839	-.160	14	-.0750	-.171
15	-.0750	-.192	15	-.0661	-.152
16	-.0661	-.218	16	-.0571	-.131
17	-.0571	-.229	17	-.0482	-.105
18	-.0482	-.221	18	-.0393	-.081
19	-.0393	-.198	19	-.0304	-.055
20	-.0304	-.157	20	-.0214	-.035
21	-.0214	-.119	21	-.0036	-.012
22	-.0125	-.078	**		
23	-.0036	-.044	22	.0143	-.003
24	.0143	-.008	23	.0321	-.001
**			24	.0500	-.001
25	.0321	-.002	25	.0679	-.003
26	.0500	.000	26	.0857	-.001
27	.0679	-.001	27	.1393	-.005
28	.1036	.001	28	.2286	-.005
29	.2286	-.004	29	.3179	-.009
30	.3179	-.005	30	.4071	-.005
31	.4071	-.004	31	.4964	-.006
32	.4964	-.005	32	.5857	-.005
33	.5857	-.004	33	.6750	-.001
34	.6750	-.004			

TABLE 6. TABULATION OF HOT-FILM TRAVERSE DATA

BUILD I

X/BX = -0.032

SUCTION SIDE

PT	Y/PITCH	TI	V/FSV
1	-.3359	.002	.988
2	-.2466	.002	.988
3	-.2020	.002	.990
4	-.1573	.002	.991
5	-.1127	.002	.994
6	-.1038	.002	.993
7	-.0948	.002	.993
8	-.0859	.002	.995
9	-.0770	.005	.997
10	-.0680	.005	1.000
11	-.0636	.007	1.000
12	-.0591	.011	.998
**			
13	-.0546	.023	.995
14	-.0502	.043	.967
15	-.0466	.063	.933
16	-.0430	.079	.889
17	-.0395	.092	.840
18	-.0359	.105	.791
19	-.0323	.117	.734
20	-.0288	.126	.681
21	-.0252	.138	.622
22	-.0234	.142	.595
23	-.0216	.145	.567
24	-.0198	.148	.536
25	-.0180	.151	.510
26	-.0163	.159	.483
27	-.0154	.176	.448
28	-.0145	.200	.401
29	-.0136	.241	.279
30	-.0127	.000	.000
**			

TABLE 6. TABULATION OF HOT-FILM TRAVERSE DATA

(Con't)

BUILD I

X/BX = -0.032

PRESSURE SIDE

PT	Y/PITCH	TI	V/FSV
1	.0127	.000	.000
2	.0130	.144	.390
3	.0132	.164	.437
4	.0148	.104	.727
5	.0157	.081	.793
6	.0166	.069	.832
7	.0175	.068	.838
8	.0184	.062	.857
9	.0202	.055	.880
10	.0220	.053	.894
11	.0237	.047	.910
12	.0255	.045	.921
13	.0273	.042	.934
14	.0291	.039	.942
15	.0327	.036	.957
16	.0363	.031	.972
17	.0398	.024	.987
18	.0434	.018	.992
**			
19	.0470	.013	1.000
20	.0648	.003	.999
21	.0827	.002	.995
22	.1005	.002	.990
23	.1452	.002	.985
24	.1898	.002	.984
25	.2791	.004	.987
26	.3684	.004	.996

TABLE 6. TABULATION OF HOT-FILM TRAVERSE DATA

(Con't)

BUILD I

X/BX = -0.004

SUCTION SIDE

PT	Y/PITCH	TI	V/FSV
1	-.5000	.002	.983
2	-.3964	.002	.986
3	-.3071	.002	.989
4	-.2179	.002	.992
5	-.1286	.002	.999
6	-.1107	.002	.998
7	-.0929	.003	1.000
8	-.0839	.003	1.000
9	-.0750	.005	1.000
**			
10	-.0661	.011	1.000
11	-.0571	.038	.980
12	-.0482	.076	.894
13	-.0393	.108	.778
14	-.0357	.118	.719
15	-.0321	.131	.675
16	-.0286	.139	.625
17	-.0250	.148	.581
18	-.0214	.157	.526
19	-.0196	.164	.501
20	-.0179	.178	.462
21	-.0161	.230	.393
22	-.0143	.380	.254
23	-.0134	.498	.152
24	-.0125	.436	.052
25	-.0116	.327	.043
26	-.0107	.208	.036
27	-.0104	.000	.000
**			

TABLE 6. TABULATION OF HOT-FILM TRAVERSE DATA

(Con't)

BUILD I

X/BX = -0.004

PRESSURE SIDE

PT	Y/PITCH	TI	V/FSV
**			
1	.0086	.000	.000
2	.0089	.191	.035
3	.0093	.295	.068
4	.0098	.361	.151
5	.0102	.254	.357
6	.0107	.136	.666
7	.0116	.100	.771
8	.0125	.093	.804
9	.0143	.072	.859
10	.0179	.054	.903
11	.0232	.045	.929
12	.0268	.040	.951
13	.0321	.034	.968
14	.0411	.020	.992
**			
15	.0500	.008	1.000
16	.0946	.002	.984
17	.1393	.002	.981
18	.2286	.002	.978
19	.3179	.002	.982
20	.5000	.002	1.000

TABLE 6. TABULATION OF HOT-FILM TRAVERSE DATA

(Con't)

BUILD I

X/BX = 0.004

PT	Y/PITCH	TI	V/FSV
1	-.3964	.002	.990
2	-.3071	.002	.995
3	-.2179	.002	.995
4	-.1286	.002	.992
5	-.1107	.002	.992
6	-.0929	.003	.995
7	-.0834	.004	.994
8	-.0750	.007	.997
**			
9	-.0661	.021	.992
10	-.0571	.061	.936
11	-.0482	.097	.827
12	-.0393	.126	.700
13	-.0357	.136	.653
14	-.0321	.146	.598
15	-.0286	.153	.552
16	-.0250	.163	.503
17	-.0214	.261	.389
18	-.0196	.382	.256
19	-.0179	.474	.144
20	-.0161	.358	.077
21	-.0143	.348	.069
22	-.0125	.357	.070
23	-.0107	.364	.070
24	-.0089	.387	.066
25	-.0071	.422	.062
26	-.0054	.470	.063
27	-.0036	.483	.064
28	-.0016	.481	.063
29	.0000	.496	.056
30	.0018	.434	.076
31	.0036	.221	.526
32	.0054	.103	.776
33	.0071	.072	.846
34	.0089	.061	.878
35	.0143	.048	.921
36	.0232	.036	.962
37	.0321	.024	.991
38	.0411	.009	1.002
**			
39	.0500	.005	.999

TABLE 6. TABULATION OF HOT-FILM TRAVERSE DATA

(Con't)

BUILD I

X/BX = 0.004

PT	Y/PITCH	TI	V/FSV
40	.0946	.003	.987
41	.1393	.003	.982
42	.2286	.003	.981
43	.3179	.003	.982

TABLE 6. TABULATION OF HOT-FILM TRAVERSE DATA

(Con't)

BUILD I

X/BX = 0.012

PT	Y/PITCH	TI	V/FSV
1	-.5000	.002	1.002
2	-.3964	.002	1.022
3	-.3071	.002	1.024
4	-.2179	.002	1.071
5	-.2179	.002	1.017
6	-.1286	.002	1.017
**			
7	-.1107	.002	1.008
8	-.0929	.003	1.005
9	-.0839	.004	1.006
10	-.0750	.007	1.005
11	-.0661	.014	1.002
12	-.0571	.042	.977
13	-.0482	.079	.884
14	-.0393	.109	.767
15	-.0357	.123	.715
16	-.0321	.133	.669
17	-.0304	.137	.657
18	-.0286	.145	.622
19	-.0268	.153	.597
20	-.0250	.154	.575
21	-.0232	.160	.543
22	-.0214	.171	.521
23	-.0196	.199	.478
24	-.0179	.256	.414
25	-.0161	.302	.349
26	-.0143	.373	.260
27	-.0125	.418	.203
28	-.0107	.429	.128
29	-.0089	.403	.110
30	-.0071	.412	.118
31	-.0054	.378	.136
32	-.0036	.371	.146
33	-.0018	.323	.161
34	.0000	.331	.149
35	.0018	.335	.141
36	.0036	.403	.177
37	.0054	.300	.449
38	.0071	.150	.723
39	.0089	.083	.829
40	.0143	.060	.883

TABLE 6. TABULATION OF HOT-FILM TRAVERSE DATA

(Con't)

BUILD I

X/BX = 0.012

PT	Y/PITCH	TI	V/FSV
41	.0232	.046	.928
42	.0321	.035	.965
43	.0411	.018	.987
**			
44	.0500	.007	.992
45	.0946	.002	.984
46	.1393	.002	.979
47	.2286	.002	.973
48	.3179	.002	.981
49	.5000	.002	.995

TABLE 6. TABULATION OF HOT-FILM TRAVERSE DATA

(Con't)

BUILD I

X/BX = 0.020

PT	Y/PITCH	TI	V/FSV
1	-.5000	.002	1.008
2	-.3964	.002	1.016
3	-.3071	.002	1.018
4	-.2179	.002	1.019
5	-.1286	.002	1.018
6	-.0929	.003	1.013
7	-.0750	.007	1.013
**			
8	-.0661	.016	1.009
9	-.0571	.050	.968
10	-.0482	.089	.862
11	-.0393	.120	.738
12	-.0357	.134	.681
13	-.0321	.147	.624
14	-.0304	.151	.609
15	-.0286	.159	.577
16	-.0268	.166	.549
17	-.0250	.172	.533
18	-.0232	.186	.497
19	-.0214	.224	.453
20	-.0196	.245	.422
21	-.0179	.301	.355
22	-.0161	.367	.291
23	-.0143	.432	.216
24	-.0125	.420	.181
25	-.0107	.364	.162
26	-.0089	.318	.172
27	-.0071	.295	.186
28	-.0054	.288	.190
29	-.0036	.288	.189
30	-.0018	.314	.187
31	.0000	.361	.228
32	.0018	.327	.380
33	.0036	.220	.591
34	.0054	.161	.709
35	.0071	.095	.809
36	.0089	.074	.838
37	.0143	.053	.884
38	.0232	.040	.927
39	.0321	.027	.961
40	.0411	.012	.981

TABLE 6. TABULATION OF HOT-FILM TRAVERSE DATA

(Con't)

BUILD I

X/BX = 0.020

PT	Y/PITCH	TI	V/FSV
**			
41	.0500	.005	.983
42	.0679	.004	.981
43	.0768	.004	.981
44	.0946	.004	.980
45	.1393	.003	.975
46	.2286	.002	.972
47	.3179	.002	.975
48	.5000	.002	.987

TABLE 6. TABULATION OF HOT-FILM TRAVERSE DATA

(Con't)

BUILD I

X/BX = 0.032

PT	Y/PITCH	TI	V/FSV
1	-.3964	.003	1.014
2	-.3071	.003	1.015
3	-.2179	.003	1.015
4	-.1286	.003	1.008
5	-.1107	.003	1.008
6	-.0929	.005	1.002
7	-.0839	.007	1.001
**			
8	-.0750	.015	.998
9	-.0661	.048	.961
10	-.0571	.086	.864
11	-.0482	.127	.725
12	-.0357	.179	.537
13	-.0321	.217	.478
14	-.0286	.261	.405
15	-.0250	.339	.332
16	-.0214	.452	.230
17	-.0179	.442	.182
18	-.0143	.428	.208
19	-.0107	.387	.302
20	-.0071	.252	.541
21	-.0036	.198	.666
22	.0054	.057	.893
23	.0143	.040	.939
24	.0232	.024	.973
25	.0321	.011	.988
**			
26	.0411	.006	.993
27	.0500	.005	.991
28	.0946	.004	.989
29	.1393	.004	.981
30	.2286	.003	.982
31	.3179	.003	.985

TABLE 6. TABULATION OF HOT-FILM TRAVERSE DATA

(Con't)

BUILD I

X/BX = 0.065

PT	Y/PITCH	TI	V/FSV
1	-.3964	.003	1.014
2	-.3071	.003	1.013
3	-.2179	.003	1.005
4	-.1286	.004	.993
5	-.1107	.003	.993
6	-.0929	.006	.989
**			
7	-.0839	.010	.987
8	-.0750	.022	.978
9	-.0661	.060	.928
10	-.0571	.096	.827
11	-.0482	.136	.695
12	-.0393	.191	.556
13	-.0357	.215	.495
14	-.0321	.244	.453
15	-.0286	.252	.405
16	-.0250	.243	.392
17	-.0214	.239	.409
18	-.0179	.228	.473
19	-.0143	.204	.548
20	-.0107	.184	.637
21	-.0071	.145	.739
22	-.0036	.130	.787
23	.0071	.054	.918
24	.0143	.033	.959
25	.0232	.020	.985
26	.0321	.011	.993
27	.0411	.009	.998
**			
28	.0500	.008	1.000
29	.0946	.008	1.008
30	.1393	.008	1.008
31	.2286	.008	1.007
32	.3179	.008	1.012

TABLE 6. TABULATION OF HOT-FILM TRAVERSE DATA

(Con't)

BUILD I

X/BX = 0.130

PT	Y/PITCH	TI	V/FSV
1	-.3964	.002	1.010
2	-.3518	.003	1.012
3	-.3071	.003	1.010
4	-.2625	.003	1.008
5	-.2179	.003	1.003
6	-.1732	.003	1.000
7	-.1464	.003	.999
8	-.1286	.003	.998
9	-.1107	.003	.995
10	-.0929	.005	.996
**			
11	-.0750	.019	.994
12	-.0661	.054	.958
13	-.0571	.096	.868
14	-.0482	.132	.754
15	-.0393	.157	.643
16	-.0304	.191	.562
17	-.0214	.153	.571
18	-.0125	.151	.670
19	-.0036	.119	.814
20	.0054	.079	.913
21	.0143	.043	.971
22	.0321	.011	.998
**			
23	.0500	.004	.994
24	.0679	.003	.998
25	.0857	.003	1.000
26	.1393	.003	1.000
27	.1839	.003	1.000
28	.2286	.003	1.003
29	.2732	.002	1.008
30	.3179	.002	1.007

TABLE 7. TABULATION OF FIVE-HOLE TRAVERSE DATA

BUILD II

X/BX = 0.344

PT	Y/PITCH	CPT	CPS	YAW	PHI	V/FSV
1	-.5795	.000	.314	3.174	-1.858	1.003
2	-.4902	.002	.312	3.177	-2.008	1.004
3	-.4009	.003	.315	2.986	-1.909	1.004
4	-.3562	.004	.315	2.985	-1.897	1.007
5	-.3116	.003	.315	2.986	-1.928	1.005
6	-.2759	.005	.318	2.794	-1.776	1.004
7	-.2402	.005	.316	2.794	-1.807	1.004
8	-.2045	.006	.319	2.607	-1.903	1.003
9	-.1688	.008	.319	2.417	-1.863	1.004
10	-.1330	.009	.321	2.035	-1.648	1.003
11	-.1152	.010	.320	2.034	-1.527	1.004
**						
12	-.0884	.006	.322	1.847	-1.260	1.001
13	-.0795	-.004	.320	1.470	-1.145	.993
14	-.0705	-.028	.319	1.470	-1.153	.977
15	-.0616	-.063	.320	1.282	-1.089	.950
16	-.0527	-.101	.325	1.281	-1.138	.913
17	-.0438	-.154	.323	1.088	-1.476	.874
18	-.0348	-.196	.324	1.088	-1.586	.837
19	-.0259	-.232	.325	1.280	-1.842	.804
20	-.0170	-.251	.326	1.282	-1.947	.787
21	-.0080	-.257	.329	1.848	-1.819	.781
22	.0009	-.225	.323	1.848	-1.820	.811
23	.0098	-.184	.323	2.225	-1.733	.848
24	.0188	-.125	.320	2.224	-1.472	.900
25	.0277	-.069	.320	2.417	-1.159	.943
26	.0366	-.034	.319	2.418	-1.062	.970
27	.0455	-.012	.320	2.418	-1.089	.987
**						
28	.0634	.003	.321	2.420	-1.008	.997
29	.0991	.004	.322	2.608	-1.038	.997
30	.1348	.003	.323	2.797	-1.075	.996
31	.1795	.002	.323	3.176	-1.088	.995
32	.2241	-.003	.319	3.178	-.941	.994
33	.3134	.002	.322	3.554	-1.090	.998
34	.4027	-.001	.318	3.554	-1.093	.996
35	.4920	.003	.320	3.553	-1.183	.998
36	.5813	.007	.323	3.551	-1.301	.998
37	.6705	.007	.322	3.550	-1.503	.999

TABLE 7. TABULATION OF FIVE-HOLE TRAVERSE DATA

BUILD II

X/BX = 0.573

PT	Y/PITCH	CPT	CPS	YAW	PHI	V/FSV
1	-.5795	.001	.317	3.171	-1.634	1.002
2	-.4902	.000	.317	3.172	-1.725	1.001
3	-.4009	.005	.319	3.361	-1.676	1.002
4	-.3116	.002	.318	3.171	-1.619	1.000
5	-.2223	.009	.321	2.792	-1.448	1.003
6	-.1866	.007	.321	2.793	-1.395	1.003
7	-.1509	.009	.321	2.415	-1.311	1.003
8	-.1330	.010	.322	2.415	-1.270	1.002
9	-.1152	.009	.320	2.038	-1.132	1.003
**						
10	-.0973	.002	.321	2.039	-1.105	.998
11	-.0795	-.034	.319	1.662	-.986	.973
12	-.0705	-.063	.319	1.662	-1.017	.950
13	-.0616	-.093	.321	1.662	-1.032	.926
14	-.0527	-.127	.322	1.470	-1.125	.897
15	-.0438	-.158	.323	1.468	-1.248	.870
16	-.0348	-.182	.325	1.467	-1.338	.848
17	-.0259	-.202	.323	1.466	-1.449	.832
18	-.0170	-.208	.324	1.846	-1.383	.826
19	-.0080	-.208	.323	1.845	-1.507	.826
20	.0009	-.190	.322	1.845	-1.550	.844
21	.0098	-.162	.321	2.224	-1.609	.868
22	.0188	-.124	.321	2.413	-1.492	.900
23	.0277	-.085	.318	2.415	-1.314	.932
24	.0455	-.022	.318	2.418	-1.096	.980
25	.0634	-.001	.319	2.419	-1.047	.997
**						
26	.0813	.004	.320	2.418	-1.099	.997
27	.0991	.003	.321	2.797	-1.091	.996
28	.1348	.002	.320	2.798	-1.041	.995
29	.1705	.002	.322	2.988	-.966	.995
30	.2241	.003	.322	3.178	-.955	.996
31	.3134	.001	.322	3.368	-.939	.994
32	.4920	.004	.323	3.745	-1.011	.995
33	.5813	.005	.324	3.743	-1.118	.994
34	.6705	.009	.325	3.741	-1.271	.996

TABLE 7. TABULATION OF FIVE-HOLE TRAVERSE DATA

BUILD II

X/BX = 1.031

PT	Y/PITCH	CPT	CPS	YAW	PHI	V/FSV
1	-1.2937	.000	.312	2.984	-1.241	1.003
2	-1.2045	-.002	.314	2.604	-1.312	1.001
3	-1.1330	-.002	.313	2.036	-1.336	1.000
4	-1.0973	-.021	.311	1.658	-1.271	.988
5	-1.0616	-.085	.311	1.471	-1.100	.939
6	-1.0437	-.124	.314	1.472	-1.045	.906
7	-1.0259	-.153	.315	1.663	-.977	.822
8	-1.0080	-.159	.314	2.045	-.772	.877
9	-.9902	-.134	.313	2.237	-.443	.897
10	-.9545	-.044	.312	2.614	-.252	.969
11	-.9187	.004	.314	2.426	-.563	1.002
12	-.8473	-.005	.313	2.797	-1.053	.996
13	-.7580	-.004	.313	3.173	-1.222	.996
14	-.6687	.001	.317	3.172	-1.355	.998
15	-.5795	-.002	.315	3.361	-1.416	.996
16	-.4902	.001	.315	3.361	-1.339	.999
17	-.4009	.003	.317	3.171	-1.404	.999
18	-.3116	.008	.319	3.173	-1.258	1.001
19	-.2223	.007	.318	2.797	-1.089	1.002
**						
20	-.1509	.004	.317	2.422	-.864	.999
21	-.1152	-.016	.318	2.235	-.732	.983
22	-.0795	-.087	.319	2.045	-.782	.928
23	-.0616	-.128	.318	2.043	-.905	.897
24	-.0438	-.154	.321	2.044	-.823	.874
25	-.0259	-.163	.319	2.040	-1.035	.868
26	-.0080	-.144	.317	2.420	-.993	.885
27	.0098	-.106	.315	2.797	-1.072	.917
28	.0277	-.055	.314	2.800	-.938	.958
29	.0634	.000	.316	2.992	-.740	.998
**						
30	.0991	.005	.319	3.182	-.717	.999
31	.1884	.003	.318	3.373	-.593	.997
32	.2777	.002	.319	3.373	-.572	.997
33	.3670	.003	.320	3.751	-.605	.997
34	.4563	.005	.321	3.751	-.667	.998
35	.5455	.005	.319	3.939	-.751	.998
36	.6348	.007	.322	3.937	-.877	.998
37	.7241	.007	.322	3.938	-.846	.998
38	.7777	.004	.322	3.938	-.807	.997
39	.8134	-.016	.320	3.748	-.841	.983
40	.8491	-.067	.319	3.557	-.944	.944
41	.8670	-.102	.320	3.748	-.839	.916
42	.8848	-.133	.321	3.748	-.842	.891

AD-A091 378

PRATT AND WHITNEY AIRCRAFT GROUP WEST PALM BEACH FL G--ETC F/G 20/4
SUPERCRITICAL AIRFOIL TECHNOLOGY PROGRAM WAKE EXPERIMENTS AND M--ETC(U)
SEP 80 D E HOBBS, J H WAGNER
N00019-79-C-0229
PWA-FR-13514 NL

UNCLASSIFIED

2 M 2
42-430

- END
DATE FILMED
42-430
DTIC

TABLE 7. TABULATION OF FIVE-HOLE TRAVERSE DATA

BUILD II

X/BX = 1.031

PT	Y/PITCH	CPT	CPS	YAW	PHI	V/FSV
43	.9027	-.155	.320	3.750	-.728	.873
44	.9205	-.161	.321	4.130	-.573	.867
45	.9562	-.124	.322	4.130	-.551	.897
46	.9920	-.046	.323	4.319	-.320	.954
47	1.0277	-.007	.321	3.937	-.114	.988
48	1.1170	.006	.324	3.938	-.127	.996
49	1.2063	.008	.323	3.937	-.082	.997

TABLE 7. TABULATION OF FIVE-HOLE TRAVERSE DATA

BUILD II

X/BX = 1.229

PT	Y/PITCH	CPT	CPS	YAW	PHI	V/FSV
1	-2.900	-.004	-.125	39.397	-.667	1.000
2	-2.200	-.002	-.011	38.593	-.948	.949
3	-1.500	-.009	-.121	39.996	-.777	.995
4	-0.700	.001	-.045	38.898	-.629	.964
5	0.000	-.001	-.100	40.898	-.621	.989
6	0.700	.004	-.083	40.198	-.363	.982
7	1.500	.002	-.033	41.898	-.340	.959
8	2.200	.007	-.101	40.098	-.363	.990
9	2.900	.008	-.015	41.395	-.113	.951

TABLE 8. TABULATION OF KIEL TRAVERSE DATA

BUILD II

X/BX = 0.229

X/BX = 0.344

PT	Y/PITCH	CPT	PT	Y/PITCH	CPT
1	-.5795	-.003	1	-.5795	-.006
2	-.5348	-.002	2	-.4902	-.003
3	-.4902	-.001	3	-.4009	-.004
4	-.4455	.000	4	-.3116	-.002
5	-.4009	.000	5	-.2402	.001
6	-.3562	-.001	6	-.1688	.002
7	-.3116	.001	7	-.1330	.003
8	-.2670	.000	8	-.0973	.003
9	-.2223	.000	**		
10	-.1688	.003	9	-.0884	-.005
11	-.1330	.007	10	-.0795	-.020
12	-.1152	.006	11	-.0705	-.053
13	-.0973	.006	12	-.0616	-.101
14	-.0884	.004	13	-.0527	-.157
**			14	-.0438	-.204
15	-.0795	.000	15	-.0348	-.244
16	-.0705	-.023	16	-.0259	-.268
17	-.0616	-.072	17	-.0170	-.268
18	-.0527	-.131	18	-.0080	-.246
19	-.0438	-.204	19	.0009	-.194
20	-.0348	-.265	20	.0098	-.144
21	-.0259	-.303	21	.0188	-.086
22	-.0170	-.319	22	.0277	-.040
23	-.0080	-.292	23	.0366	-.015
24	.0009	-.225	24	.0455	-.004
25	.0098	-.144	**		
26	.0188	-.080	25	.0634	.003
27	.0277	-.037	26	.0991	.013
28	.0366	-.012	27	.1348	.002
29	.0455	-.005	28	.2241	.004
**			29	.3134	.002
30	.0634	.002	30	.4027	.002
31	.0991	.005	31	.4920	.006
32	.1348	-.002	32	.5813	.006
33	.1795	.002	33	.6705	.013
34	.2241	.003			
35	.3134	.004			
36	.3580	.004			
37	.4027	.005			
38	.4473	.003			
39	.4920	.005			
40	.5366	.005			
41	.5813	.004			
42	.6705	.006			

TABLE 8. TABULATION OF KIEL TRAVERSE DATA

BUILD II

X/BX = 0.573

X/BX = 1.031

PT	Y/PITCH	CPT	PT	Y/PITCH	CPT
1	-.5795	.000	1	-1.2937	-.004
2	-.4902	.001	2	-1.2045	.005
3	-.4009	-.001	3	-1.1330	-.004
4	-.3116	.002	4	-1.0973	-.039
5	-.2223	.003	5	-1.0616	-.111
6	-.1866	.003	6	-1.0437	-.147
7	-.1509	.000	7	-1.0259	-.169
8	-.1330	.007	8	-1.0080	-.164
**			9	-.9902	-.132
9	-.1152	.004	10	-.9545	-.042
10	-.0973	-.011	11	-.9187	-.002
11	-.0795	-.055	12	-.8473	-.002
12	-.0705	-.090	13	-.7580	.001
13	-.0616	-.119	14	-.6687	.001
14	-.0527	-.154	15	-.5795	-.001
15	-.0438	-.180	16	-.4902	.001
16	-.0348	-.203	17	-.4009	-.001
17	-.0259	-.217	18	-.3116	.005
18	-.0170	-.223	19	-.2223	.001
19	-.0080	-.210	**		
20	.0098	-.161	20	-.1509	.003
21	.0188	-.123	21	-.1152	-.028
22	.0277	-.086	22	-.0795	-.099
23	.0455	-.025	23	-.0616	-.133
24	.0634	.002	24	-.0438	-.150
**			25	-.0259	-.142
25	.0991	.005	26	-.0080	-.108
26	.1705	.003	27	.0098	-.064
27	.2241	.002	28	.0277	-.026
28	.3134	.001	29	.0634	.001
29	.4027	.004	**		
30	.4920	.003	30	.0991	.001
31	.5813	.004	31	.1884	.001
32	.6705	.003	32	.2777	.001
			33	.3670	.004
			34	.4563	.004
			35	.5455	.005
			36	.6348	.008
			37	.7241	.005
			38	.7777	.002
			39	.8134	-.013
			40	.8491	-.063
			41	.8670	-.093
			42	.8848	-.127

TABLE 8. TABULATION OF KIEL TRAVERSE DATA

BUILD II

X/BX = 1.031

PT	Y/PITCH	CPT
43	.9027	-.156
44	.9205	-.164
45	.9562	-.129
46	.9920	-.058
47	1.0277	-.008
48	1.1170	.010
49	1.2063	.010

TABLE 9. TABULATION OF HOT-FILM TRAVERSE DATA

BUILD II

X/BX = -0.0287	SUCTION SIDE

PT	Y/PITCH	TI	V/FSV
1	-.5564	.004	.983
2	-.4671	.004	.985
3	-.3779	.007	.988
4	-.2886	.004	.993
5	-.1993	.004	1.007
**			
6	-.1636	.005	1.000
7	-.1279	.005	.977
8	-.0921	.006	.975
9	-.0832	.007	.973
10	-.0743	.010	.983
11	-.0654	.016	.981
12	-.0564	.031	.968
13	-.0475	.062	.926
14	-.0386	.092	.861
15	-.0296	.115	.762
16	-.0252	.121	.725
17	-.0207	.128	.668
18	-.0171	.135	.620
19	-.0145	.145	.580
20	-.0127	.153	.555
21	-.0109	.161	.522
22	-.0091	.169	.490
23	-.0073	.183	.451
24	-.0064	.194	.427
25	-.0055	.210	.390
26	-.0046	.000	.000

**

TABLE 9. TABULATION OF HOT-FILM TRAVERSE DATA

BUILD II

X/BX = -0.0287		PRESSURE SIDE	
PT	Y/PITCH	TI	V/FSV
**			
1	.0046	.000	.000
2	.0050	.289	.398
3	.0055	.124	.564
4	.0059	.103	.708
5	.0064	.092	.749
6	.0104	.065	.840
7	.0202	.054	.899
8	.0345	.043	.948
9	.0514	.026	.985
10	.0675	.012	1.000
**			
11	.0854	.008	1.000
12	.1121	.007	1.004
13	.1479	.006	1.009
14	.1836	.006	1.013
15	.2193	.005	1.020
16	.3086	.004	1.032
17	.3979	.004	1.047
18	.4871	.003	1.061
19	.5764	.004	1.079

TABLE 9. TABULATION OF HOT-FILM TRAVERSE DATA

BUILD II

X/BX = -0.0036

SUCTION SIDE

PT	Y/PITCH	TI	V/FSV
1	-.5511	.003	.982
2	-.4618	.003	.989
3	-.3725	.003	.994
4	-.2832	.004	.995
5	-.1939	.005	1.007
6	-.1582	.005	1.000
**			
7	-.1225	.006	.996
8	-.0868	.010	.989
9	-.0689	.007	.976
10	-.0511	.075	.907
11	-.0421	.107	.840
12	-.0332	.131	.742
13	-.0243	.159	.626
14	-.0154	.216	.470
15	-.0136	.230	.436
16	-.0118	.243	.412
17	-.0100	.261	.372
18	-.0091	.279	.341
19	-.0082	.285	.329
20	-.0073	.319	.293
21	-.0064	.333	.275
22	-.0055	.381	.225
23	-.0046	.000	.000
**			

TABLE 9. TABULATION OF HOT-FILM TRAVERSE DATA

BUILD II

X/BX = -0.0036		PRESSURE SIDE	
PT	Y/PITCH	TI	V/FSV
**			
1	.0046	.000	.000
2	.0055	.098	.736
3	.0064	.077	.817
4	.0073	.071	.836
5	.0091	.065	.860
6	.0109	.062	.879
7	.0127	.059	.890
8	.0145	.057	.901
9	.0180	.055	.915
10	.0216	.051	.932
11	.0305	.044	.958
12	.0395	.036	.977
13	.0573	.018	1.000
**			
14	.0752	.010	.993
15	.0930	.009	.990
16	.1287	.007	.992
17	.1645	.007	.992
18	.2002	.006	1.000
19	.2895	.005	1.003
20	.3788	.005	1.020
21	.4680	.004	1.036
22	.5573	.004	1.057

TABLE 9. TABULATION OF HOT-FILM TRAVERSE DATA

BUILD II

X/BX = 0.0036

PT	Y/PITCH	TI	V/FSV
1	-.5723	.006	1.037
2	-.4830	.007	1.040
3	-.3937	.008	1.045
4	-.3045	.009	1.046
5	-.2152	.010	1.049
**			
6	-.1259	.014	1.032
7	-.0902	.018	1.015
8	-.0723	.025	1.000
9	-.0545	.058	.941
10	-.0455	.087	.865
11	-.0366	.121	.764
12	-.0277	.183	.638
13	-.0188	.224	.486
14	-.0143	.265	.402
15	-.0098	.325	.323
16	-.0054	.483	.189
17	-.0009	.421	.081
18	.0014	.371	.089
19	.0025	.300	.256
20	.0036	.135	.607
21	.0059	.070	.814
22	.0080	.074	.848
23	.0125	.054	.875
24	.0170	.050	.893
25	.0259	.044	.921
26	.0348	.038	.952
27	.0438	.031	.969
28	.0527	.023	.980
**			
29	.0705	.012	.986
30	.1063	.009	.985
31	.1420	.008	.991
32	.1777	.008	.989
33	.2313	.007	.994
34	.3205	.007	1.003
35	.4098	.005	1.013
36	.4991	.005	1.025
37	.5884	.005	1.038

TABLE 9. TABULATION OF HOT-FILM TRAVERSE DATA

BUILD II

X/BX = 0.011

PT	Y/PITCH	TI	V/FSV
1	-.5762	.006	1.017
2	-.4870	.007	1.022
3	-.3977	.008	1.029
4	-.3084	.010	1.034
5	-.2191	.011	1.031
6	-.1477	.012	1.021
**			
7	-.1120	.014	1.019
8	-.0763	.022	1.006
9	-.0584	.050	.952
10	-.0495	.074	.888
11	-.0405	.103	.800
12	-.0316	.130	.697
13	-.0227	.173	.568
14	-.0182	.209	.495
15	-.0137	.254	.413
16	-.0093	.322	.330
17	-.0048	.404	.236
18	-.0004	.371	.202
19	.0020	.255	.415
20	.0041	.133	.691
21	.0086	.061	.833
22	.0130	.054	.865
23	.0175	.051	.883
24	.0220	.047	.904
25	.0264	.045	.915
26	.0309	.041	.938
27	.0354	.038	.951
28	.0398	.034	.958
29	.0488	.025	.975
30	.0577	.016	.984
**			
31	.0666	.012	.988
32	.0755	.011	.988
33	.0845	.010	.989
34	.1023	.010	.986
35	.1380	.009	.986
36	.1738	.008	.986
37	.2273	.007	1.000
38	.3166	.007	1.009
39	.4059	.006	1.018
40	.4952	.005	1.032
41	.5845	.005	1.041

TABLE 9. TABULATION OF HOT-FILM TRAVERSE DATA

BUILD II

X/BX = 0.018

PT	Y/PITCH	TI	V/FSV
1	-.5798	.009	1.015
2	-.4905	.005	1.025
3	-.4012	.006	1.030
4	-.3120	.007	1.036
5	-.2227	.008	1.036
6	-.1512	.010	1.028
**			
7	-.1155	.010	1.019
8	-.0798	.016	1.001
9	-.0620	.039	.967
10	-.0530	.065	.911
11	-.0441	.088	.834
12	-.0352	.110	.736
13	-.0263	.146	.628
14	-.0218	.159	.567
15	-.0173	.192	.496
16	-.0129	.252	.420
17	-.0084	.295	.349
18	-.0039	.337	.261
19	-.0018	.253	.331
20	.0005	.218	.432
21	.0050	.105	.744
22	.0095	.060	.834
23	.0139	.054	.860
24	.0184	.052	.883
25	.0229	.046	.901
26	.0273	.044	.918
27	.0318	.041	.929
28	.0363	.038	.942
29	.0452	.030	.963
30	.0541	.019	.978
**			
31	.0630	.013	.983
32	.0720	.011	.984
33	.0809	.009	.985
34	.0987	.008	.985
35	.1345	.007	.984
36	.1702	.007	.986
37	.2238	.007	.993
38	.3130	.006	1.002
39	.4023	.005	1.011
40	.4916	.005	1.021
41	.5809	.005	1.033

TABLE 9. TABULATION OF HOT-FILM TRAVERSE DATA

BUILD II

 $X/BX = 0.029$

PT	Y/PITCH	TI	V/FSV
1	-.5846	.005	1.006
2	-.4954	.005	1.013
3	-.4061	.005	1.020
4	-.3168	.007	1.021
5	-.2275	.007	1.030
**			
6	-.1561	.009	1.019
7	-.1204	.011	1.007
8	-.0846	.013	.991
9	-.0668	.024	.973
10	-.0579	.042	.940
11	-.0489	.074	.864
12	-.0400	.105	.773
13	-.0311	.138	.657
14	-.0266	.176	.588
15	-.0221	.218	.524
16	-.0177	.244	.460
17	-.0132	.281	.398
18	-.0088	.284	.341
19	-.0043	.223	.376
20	.0002	.180	.574
21	.0046	.094	.785
22	.0091	.059	.852
23	.0136	.052	.874
24	.0225	.047	.918
25	.0270	.044	.933
26	.0404	.033	.967
27	.0493	.023	.980
28	.0582	.015	.989
**			
29	.0671	.010	.990
30	.0761	.007	.992
31	.0939	.007	.990
32	.1296	.007	.992
33	.1654	.007	.996
34	.2189	.006	1.002
35	.3082	.006	1.008
36	.3975	.006	1.016
37	.4868	.005	1.027
38	.5761	.005	1.039

TABLE 9. TABULATION OF HOT-FILM TRAVERSE DATA

BUILD II

X/BX = 0.057

PT	Y/PITCH	TI	V/FSV
1	-.5795	.003	1.007
2	-.4902	.003	1.013
3	-.4009	.003	1.017
4	-.3116	.004	1.016
5	-.2223	.005	1.015
6	-.1509	.006	1.011
7	-.1330	.007	1.010
8	-.1152	.007	1.006
**			
9	-.0884	.009	1.002
10	-.0795	.010	.999
11	-.0705	.011	.996
12	-.0616	.014	.990
13	-.0527	.028	.977
14	-.0438	.054	.929
15	-.0348	.091	.846
16	-.0304	.101	.799
17	-.0259	.119	.746
18	-.0214	.148	.687
19	-.0170	.167	.683
20	-.0125	.193	.567
21	-.0080	.203	.518
22	-.0036	.188	.481
23	.0009	.191	.473
24	.0054	.132	.536
25	.0098	.128	.635
26	.0143	.103	.767
27	.0188	.071	.846
28	.0277	.041	.913
29	.0366	.034	.937
30	.0455	.028	.961
31	.0634	.012	.986
**			
32	.0813	.006	.992
33	.1170	.004	.994
34	.1348	.004	.993
35	.2241	.003	.994
36	.3134	.003	1.000
37	.4027	.002	1.005
38	.4920	.003	1.013
39	.5813	.003	1.018
40	.6705	.003	1.021

TABLE 9. TABULATION OF HOT-FILM TRAVERSE DATA

BUILD II

 $X/BX = 0.115$

PT	Y/PITCH	TI	V/FSV
1	-.5973	.003	1.016
2	-.5080	.003	1.018
3	-.4188	.004	1.019
4	-.3295	.005	1.019
5	-.2402	.005	1.020
6	-.1687	.007	1.015
**			
7	-.1330	.007	1.009
8	-.1152	.007	1.003
9	-.0973	.008	.995
10	-.0884	.008	.990
11	-.0795	.010	.988
12	-.0705	.015	.982
13	-.0616	.024	.966
14	-.0527	.047	.938
15	-.0438	.071	.881
16	-.0393	.084	.856
17	-.0348	.102	.816
18	-.0304	.114	.772
19	-.0259	.125	.734
20	-.0214	.136	.693
21	-.0170	.138	.653
22	-.0125	.136	.625
23	-.0080	.127	.609
24	-.0036	.122	.614
25	.0009	.129	.644
26	.0054	.130	.697
27	.0098	.119	.757
28	.0143	.099	.819
29	.0188	.075	.865
30	.0277	.049	.915
31	.0366	.040	.941
32	.0455	.031	.965
33	.0545	.022	.978
34	.0634	.013	.986
**			
35	.0723	.008	.990
36	.0812	.005	.992
37	.0991	.004	.991
38	.1170	.004	.991
39	.1527	.004	.991
40	.2062	.003	.992

TABLE 9. TABULATION OF HOT-FILM TRAVERSE DATA

BUILD II

X/BX = 0.115

PT	Y/PITCH	TI	V/FSV
41	.2955	.003	.998
42	.3848	.003	1.002
43	.4741	.003	1.008
44	.5634	.003	1.015

TABLE 9. TABULATION OF HOT-FILM TRAVERSE DATA

BUILD II

X/BX = 0.229

PT	Y/PITCH	TI	V/FSV
1	-.5795	.004	1.010
2	-.4902	.004	1.007
3	-.4009	.004	1.007
4	-.3116	.004	1.007
5	-.2223	.005	1.005
6	-.1688	.005	1.006
7	-.1330	.006	1.005
8	-.1152	.007	1.002
9	-.0973	.008	1.001
10	-.0884	.010	1.002
11	-.0795	.014	1.003
**			
12	-.0705	.027	1.000
13	-.0616	.052	.976
14	-.0527	.077	.933
15	-.0438	.103	.877
16	-.0393	.112	.842
17	-.0348	.118	.810
18	-.0304	.123	.785
19	-.0259	.126	.756
20	-.0214	.123	.728
21	-.0170	.120	.708
22	-.0125	.114	.694
23	-.0080	.109	.690
24	-.0036	.108	.697
25	.0009	.114	.714
26	.0054	.112	.741
27	.0098	.113	.774
28	.0188	.094	.856
29	.0277	.068	.918
30	.0366	.045	.956
31	.0455	.029	.976
32	.0634	.011	.993
**			
33	.0813	.006	.993
34	.0991	.005	.991
35	.1348	.004	.989
36	.1795	.005	.989
37	.2241	.004	.990
38	.3134	.004	.991
39	.4027	.004	.994
40	.4920	.004	.996
41	.5813	.004	.998
42	.6705	.003	.997

TABLE 10. WAKE AND BOUNDARY LAYER INTEGRAL PARAMETERS

BUILD I

X/BX	HW/PITCH	δ^*/PITCH	θ/PITCH	δ^*/θ	V _o /FSV
Hot-Film					
-.032 (S)	.00469	.01116	.00663	1.684	
-.032 (P)	.00088	.00310	.00229	1.355	
-.032 (S+P)	.00557	.01426	.00892		
-.032 (*)	.03092	.03961			
-.004 (S)	.00925	.01582	.00777	2.037	
-.004 (P)	.00186	.00391	.00219	1.783	
-.004 (S+P)	.01111	.01973	.00996		
-.004 (*)	.03210	.04062			
.004 (S)	.01150	.01523	.00787	1.936	
.004 (P)	.00187	.00369	.00238	1.550	
.004 (S+P)	.01337	.01892	.01025	1.846	
.004 (*)	.03043	.03565	.01131	3.151	.056
.012 (S)	.01365	.01617	.00867	1.865	
.012 (P)	.00610	.00751	.00339	2.216	
.012 (S+P)	.01976	.02368	.01206	1.963	
.012 (*)	.02995	.03297	.01332	2.475	.141
.020 (S)	.01696	.01620	.00860	1.885	
.020 (P)	.00539	.00688	.00383	1.798	
.020 (S+P)	.02234	.02308	.01242	1.858	
.020 (*)	.03228	.03184	.01398	2.279	.162
.032 (S)	.02143	.01897	.00923	2.055	
.032 (P)	.01215	.01197	.00529	2.262	
.032 (S+P)	.03358	.03094	.01452	2.130	.1.82
.065 (S)	.02331	.01462	.00845	1.729	
.065 (P)	.01635	.01186	.00714	1.661	
.065 (S+P)	.03966	.02648	.01560	1.698	.392
.130 (S)	.02000	.00892	.00626	1.426	
.130 (P)	.02477	.01140	.00757	1.506	
.130 (S+P)	.04476	.02032	.01382	1.470	.562

TABLE 10. WAKE AND BOUNDARY LAYER INTEGRAL PARAMETERS

BUILD I

X/BX	HW/PITCH	$\delta^*/PITCH$	$\theta/PITCH$	δ^*/θ	V_o/FSV
Kiel					
.065 (?)	.03594	.01991	.01349	1.476	.504
.130 (?)	.04650	.01731	.01294	1.338	.624
.260	.05276	.01609	.01265	1.272	.705
.390	.05909	.01506	.01230	1.224	.750
.649	.07107	.01461	.01248	1.171	.796
1.169	.09042	.01400	.01246	1.124	.850
Five Hole					
.390	.06022	.01497	.01230	1.216	.757
.649	.07072	.01378	.01184	1.164	.808
1.169	.08955	.01176	.01077	1.092	.855

Notes:

- S = Suction surface boundary layer
 P = Pressure surface boundary layer
 (*) = Sum of boundary layers + (airfoil thickness or constant velocity region)
 (?) = Data of questionable accuracy due to probe size
 BX = 195.707mm (7.705 in.)
 Pitch = 142.240mm (5.6 in.)
 TED = 3.6068 mm (0.142 in.)

TABLE 11. WAKE AND BOUNDARY LAYER INTEGRAL PARAMETERS

BUILD II

X/BX	$\delta_{HW}/PITCH$	$\delta^*/PITCH$	$\theta/PITCH$	δ^*/θ	V_o/FSV
Hot-Film					
-.029 (S)	.00504	.01514	.01029	1.471	
-.029 (P)	.00061	.00460	.00369	1.246	
-.029 (S+P)	.00565	.01974	.01398		
-.029 (*)	.01494	.02903			
-.0036 (S)	.01242	.01803	.01020	1.768	
-.0036 (P)	.00061	.00331	.00263	1.261	
-.0036 (S+P)	.01303	.02113	.01283		
-.0036 (*)	.02230	.03042			
.0036 (S)	.02106	.02279	.01081	2.108	
.0036 (P)	.00426	.00744	.00372	2.002	
.0036 (S+P)	.02532	.03023	.01453	2.081	.081
.011 (S)	.02462	.02220	.01096	2.024	
.011 (P)	.00377	.00663	.00449	1.474	
.011 (S+P)	.02839	.02882	.01546	1.865	.202
.018 (S)	.02255	.01968	.01129	1.743	
.018 (P)	.00731	.00864	.00540	1.602	
.018 (S+P)	.02986	.02833	.01669	1.698	.262
.029 (S)	.02335	.01774	.01070	1.659	
.029 (P)	.01098	.01003	.00604	1.659	
.029 (S+P)	.03432	.02777	.01674	1.659	.341
.057 (S)	.02607	.01508	.00966	1.561	
.057 (P)	.01236	.00859	.00594	1.446	
.057 (S+P)	.03843	.02367	.01560	1.517	.473
.115	.02562	.01198	.00909	1.317	
.115	.02127	.00986	.00726	1.357	
.115	.04689	.02184	.01636	1.335	.609
.229	.03169	.00998	.00774	1.290	
.229	.02562	.00845	.00658	1.283	
.229	.05731	.01843	.01432	1.287	.690

TABLE 11. WAKE AND BOUNDARY LAYER INTEGRAL PARAMETERS

BUILD II

X/BX	HW/PITCH	$\delta^*/PITCH$	$\theta/PITCH$	δ^*/θ	V_o/FSV
Kiel					
.229	.05506	.01650	.01313	1.256	.713
.344	.06613	.01575	.01371	1.209	.765
.573	.08360	.01588	.01371	1.158	.813
1.031	.09600	.01217	.01111	1.096	.877
Five Hole					
.344	.06473	.01454	.01223	1.188	.781
.573	.08001	.01418	.01234	1.149	.826
1.031	.10010	.01351	.01223	1.105	.867

Notes:

- (S) = Suction side boundary layer
 (P) = Pressure side boundary layer
 (*) = Sum of boundary layers + TED
 BX = 221.539mm (8.722 in.)
 Pitch = 142.240mm (5.60 in.)
 TED = 1.3208mm (0.052 in.)

REFERENCES

1. Dunavant, J.C., et, al, "High Speed Cascade Tests of the NACA 65-(12A₁₀) 10 and NACA 65-(12A₂I_{8b}) 10 Compressor Blade Sections", NACA RML55, p. 108.
2. Whitcomb, R.T., and L.R. Clark, "An Airfoil Shape for Efficient Flight at Supercritical Mach Numbers," NASA TMX-1109, May 1965.
3. Bauer, F., P. Garabedian, and D. Korn, "Supercritical Wing Sections," Lecture Notes in Economics and Mathematical Systems, Vol. 66, Springer-Verlag, New York, 1972.
4. Bauer, F., P. Garabedian, and D. Korn, "Supercritical Wing Sections IV," Lecture Notes in Economic and Mathematical Systems, Vol. 150, Springer-Verlag, New York, 1977.
5. Korn, D., "Numerical Design of Transonic Cascades," ERDA Research and Development Report COO-3077-72, Courant Institute of Mathematical Sciences, New York University, January 1975.
7. Stephens, H.E., "Supercritical Airfoil Technology in Compressor Cascades: Comparison of Theoretical and Experimental Results," AIAA Journal, Vol. 17, No. 6, June 1979, pp. 594-600.
8. Ives, D.C. and J.F. Liutermozza, "Analysis of Transonic Cascade Flow Using Conformal Mapping and Relaxation Techniques," AIAA Journal, Vol. 15, No. 5, May 1977, pp. 647-652.
9. Ives, D.C. and J.F. Liutermozza, "Second Order Accurate Calculation of Transonic Flow Over Turbomachinery Cascades," AIAA Paper 78-1149, AIAA 11th Fluid and Plasma Dynamics Conference, Seattle, Washington, July 1978.
10. Stephens, H.E. and D.E. Hobbs, "Design and Performance Evaluation of Supercritical Airfoils for Axial Flow Compressors," Final Report, Naval Air Systems Command, Contract N00019-77-C-0546, February 1979.
11. Stewart, W.L., "Analysis of Two-Dimensional Compressible-Flow Loss Characteristics Downstream of Turbomachine Blade Rows in Terms of Basic Boundary Layer Characteristics," NACA TN-3515, July 1955.
12. Hansen, E.C., G.K. Serovy, and P.M. Sockol, "Axial-Flow Compressor Turning Angle and Loss by Inviscid-Viscous Interaction Blade-to-Blade Comparison," ASME Paper 79-GT-5, Gas Turbine Conference, San Diego, California, March 12-15, 1979.
13. Klein, A., "Aerodynamics of Cascades," AGARDograph No. 220, 1977, pp. 438-442.

14. Peacock, R.E., "Boundary-Layer Suction to Eliminate Corner Separation in Cascade Airfoils," Aeronautical Research Council, R&M No. 3663, London, 1971.
15. Thermo-Systems, Incorporated, "General System Information for 1050 Series Anemometry," St. Paul, Minnesota.
16. Caspar, J.R., D.E. Hobbs, and R.L. Davis, "Calculation of Two-Dimensional Potential Cascade Flow Using Finite Area Methods," AIAA Journal, Vol. 18, No. 1, January 1980, pp. 103-109.
17. McDonald, H. and R.W. Fish, "Practical Calculations of Transitional Boundary Layers," International Journal of Heat and Mass Transfer, 16(9), 1973, pp. 1729-1744.
18. Scharnhrost, R.K., J.O.A. Walker, and D.E. Abbott, "Comparisons of Theoretical Profiles for a Two-Dimensional Time-Mean Turbulent Boundary Layer with Experimental Data," AFOSR TR-TI-0877.
19. Raj, R. and B. Lakshminarayana, "On the Investigation of Cascade and Turbomachinery Rotor Wake Characteristics," NASA CR-134680, 1975.
20. Lakshminarayana, B. and R. Davino, "Mean Velocity and Decay Characteristics of the Guide Vane and Stator Blade Wake of an Axial Flow Compressor," ASME 79-GP-9, March 1979.
21. Lin, C.C., Turbulent Flows and Heat Transfer, Princeton University Press, Princeton, New Jersey, Vol. 5, 1959, pp. 163+.
22. Lawaczeck, O. and H.J. Heinemann, "Von Karman Vortex Streets in the Wakes of Subsonic and Transonic Cascades," 46th AGARD-PEP Meeting, Monterey, California.
23. Heinemann, H.J., O. Lawaczeck, and K.A. Butefisch, "Von Karman Vortices and their Frequency Determination in the Wakes of Profiles in Sub- and Transonic Regimes," IUTAM Symposium, Gottingen, 1975. Edit.: K. Oswaltitsch and R. Russ, Springer-Verlag, New York
24. Sieverding, C.H. "Unsteady Flow Measurements in Straight Cascades," from "Measuring Techniques in Transonic and Subsonic Cascades and Turbomachines", Lausanne, November 1976. Edit.: A. Boles and T. Franson, Juris-Verlag, Zurich.
25. Schlichting, H., "Boundary Layer Theory", McGraw-Hill, New York, Fourth Edition, 1960, pp. 590-613.
26. Ibid, pp. 355-363.
27. Green, J.E., D.J. Weeks, and J.W.F. Brooman, "Prediction of Turbulent Layers and Wakes in Compressible Flow by a Lag-Entrainment Method," ARC R&M No. 3791, 1977.

LIST OF SYMBOLS

AVDR	Axial velocity density ratio = streamtube inlet height/exit height, H_1/H_2
a, b, m	Constants in data fit equations
BX	Airfoil axial chord
C	Airfoil chord
c_f	Skin friction coefficient
c_{PS}	Static pressure coefficient = $P-P_{S0}/Q_0$
c_{PT}	Total pressure coefficient = $P-P_{T0}/Q_0$
dB	Decibels = 20 LOG (E/VREF)
f	Frequency Hz (1/sec)
FSV	Free stream velocity
E	Linearizer voltage
H	Spanwise streamtube height
M	Mach number
P	Pressure
PITCH,	Cascade pitch
q	Local dynamic head, P_T-P_S
Q_0	Inlet dynamic head = $P_{T0}-P_{S0}$
Re	Reynolds number = $\frac{V_0 C}{\nu}$
S	Strouhal number = $\frac{\text{TED}(f)}{\text{FSV}}$
TED	Trailing edge diameter
TI	Turbulence intensity
U^+	Velocity to friction velocity ratio
U	Friction velocity = <u>wall shear stress</u> / density
V	Velocity

v_D	Velocity deficit = $\frac{FSV - V}{FSV}$
V_{REF}	Reference voltage
x	Axial coordinate, defined in text
y	Pitchwise coordinate, defined in text
y^+	Nondimensional pitchwise distance = $\frac{Y \cdot U^+}{\eta}$
a_{CD}	chord angle
β	Cascade flow angle
δ	Boundary layer or wake thickness parameter
δ^*	Displacement thickness
θ	Spanwise flow angle (degrees)
Θ	Yaw angle (degrees) defined in text
Θ_{THETA}, YAW	Momentum thickness
θ	Normalized pitchwise distance = Y / δ_{HW}
η	Kinematic viscosity
ν	Cascade loss coefficient, $(P_{T1} - P_{T2}) / (P_{T1} - P_{S1})$
ω	

Subscripts

CL	Wake center line
HW	Half width (see wake nomenclature)
U	Upstream cascade reference position or minimum wake velocity
0	Upstream of cascade
1	Downstream of cascade
2	Static
S	Total
T	

Superscripts

- Time average.

DISTRIBUTION LIST

<u>No. of Copies</u>	<u>To</u>
5	Department of the Navy, Naval Air Systems Command, Attn: AIR 310, Washington, D.C. 20361
14	Department of the Navy, Naval Air Systems Command, Attn: AIR 954, Washington, D.C. 20361
2	Office of Naval Research, Code 473, Attn: Mr. Patton 800 North Quincy Street, Arlington, VA 22217
1	Commander, Naval Air Systems Command Washington, D.C. 20361, Attn: AIR-330
1	Commander, Naval Air Systems Command Washington, D.C. 20361, Attn: AIR 330B
1	Commander, Naval Air Systems Command Washington, D.C. 20361, Attn: AIR-330C
1	Commander, Naval Air Systems Command Washington, D.C. 20361, Attn: AIR-03PA1
1	Commander, Naval Air Systems Command Washington, D.C. 20361, Attn: AIR-03PA3
1	Commander, Naval Air Systems Command Washington, D.C. 20361, Attn: AIR-530
1	Commander, Naval Air Systems Command Washington, D.C. 20361, Attn: AIR-5360
1	Commander, Naval Air Systems Command Washington, D.C. 20361, Attn: AIR-5361
1	Commanding Officer, Naval Air Propulsion Test Center Trenton, New Jersey 16828
1	Commanding Officer, Naval Air Development Center Warminster, PA 19112, Attn: AVTD
1	Melvin J. Hartmann, Chief, Compressor Design Section NASA Lewis Research Center Cleveland, OH 44135
Remaining Copies	Prof. M.F. Platzer, Chairman Department of Aeronautics Naval Post Graduate School Monterey, CA 93940

